Ministry of Higher Education and Scientific Research

Hassiba Benbouali University of Chlef

Faculty of Technology

Department of Electrical Engineering

THESIS

Submitted in fulfillment of the requirements for the degree of

DOCTORATE (LMD)

Field: Electrotechnics

Specialty: Electrical networks

By

FATIHA BOUHADJI

Theme:

Commande Avancée d'un Filtre Actif de Puissance à Structure Multi-Niveaux

“Advanced Control of a Multi-Level Structure Active Power Filter”

Soutenue le 25/04/2026, devant le jury composé de :

BOUDJEMA Zinelabidine	Prof	Université Hassiba Benbouali de Chlef	President
BOUYAKOUB Ismail	MCA	Université Hassiba Benbouali de Chlef	Supervisor
DJAHBAR Abdelkader	Prof	Université Hassiba Benbouali de Chlef	Examiner
BOT Youcef	Prof	Université de khemis miliana	Examiner
YOUSFI Abdelkader	MCA	Université de khemis miliana	Examiner
MEHEDI Fayçal	MCA	Université Hassiba Benbouali de Chlef	Guest
BESSAAD Taieb	MCA	Université Hassiba Benbouali de Chlef	Guest

Acknowledgments

First and foremost, I thank Allah Almighty, the Most Gracious and the Most Merciful, for granting me the strength, patience, and determination to complete this thesis. Without His guidance and blessings, this work would not have been possible.

I would like to express my deepest gratitude to my supervisor, **Dr.Ismail BOUYAKOUB**, for his invaluable guidance, constant encouragement, and constructive feedback throughout the course of this research. His expertise and support were essential in every stage of this work.

I am also sincerely thankful to my co-supervisor, **Dr.Fayçal MEHEDI**, for his continuous assistance, insightful suggestions, and availability, which greatly contributed to the successful completion of this thesis.

My appreciation extends to the members of the Laboratoire Génie Electrique et Energies Renouvelables (LGEER), Faculty of Technology, Hassiba Benbouali University of Chlef, Algeria ,for their collaboration, technical support, and for providing a stimulating research environment.

I would like to express my sincere and respectful gratitude to the distinguished members of my thesis committee. I am deeply honoured by the presence of **Prof. Boudjema Zinelabidine**, president of the jury. I also thank the examiners, **Prof. Djahbar Abdelkader**, **Prof. Bot Youcef**, and **Dr. Yousfi Abdelkader**, for their insightful comments and constructive evaluation. My sincere thanks are also addressed to the invited member, **Prof.Bessaad Taieb**, for their kind participation despite their professional commitments. I am truly grateful to all of them for their time, expertise, and meaningful contribution to the assessment and improvement of this work.

Finally, I would like to express my heartfelt gratitude to my family for their unconditional love, patience, and unwavering support, and to my friends, whose encouragement and companionship have been a great source of motivation throughout this journey.

Dedication

To my beloved parents, whose endless love, sacrifices, and prayers have always been my greatest source of strength,
and to my grandparents, whose wisdom and blessings have guided me throughout my journey.

To my brothers, for their support and encouragement.

To my friends and my relatives, for their kindness and motivation.

To my faithful cats, for their companionship and the comfort they brought me during this work.

And to all who know me, with gratitude and respect.

I dedicate this work to you all

Abstract

Harmonic distortion caused by nonlinear loads remains a major challenge for modern electrical networks, as it degrades power quality, increases system losses, and accelerates the aging of grid components. Conventional passive filters provide only partial mitigation and lack adaptability under varying operating conditions. To overcome these limitations, active power filters have emerged as an effective solution for harmonic suppression and reactive power compensation. This thesis focuses on the design and control of a parallel active power filter based on a three-level Neutral Point Clamped (NPC) inverter. The Direct Current Control (DCC) method is employed for harmonic current detection, while an advanced Third-Order Sliding Mode Control (TOSMC) strategy is adopted to overcome the drawbacks of conventional controllers, such as sensitivity to parameter variations, steady-state errors, and limited dynamic performance. TOSMC offers improved stability, high tracking precision, and reduced chattering, making it particularly well-suited for power quality applications.In addition, a photovoltaic generator is integrated through the DC link, enabling the system not only to compensate harmonics but also to inject renewable active power into the grid. Simulation results demonstrate significant improvements in harmonic reduction, reactive power compensation, and overall system stability, confirming the effectiveness of the proposed approach.

Keywords Power quality; Harmonic distortion; Parallel active filter; Multilevel inverter; Sliding mode control; Photovoltaic systems.

Résumé

La distorsion harmonique engendrée par les charges non linéaires constitue un défi majeur pour les réseaux électriques modernes, car elle dégrade la qualité de l'énergie, augmente les pertes du système et accélère le vieillissement des composants du réseau. Les filtres passifs classiques n'apportent qu'une atténuation partielle et manquent de flexibilité face aux conditions de fonctionnement variables. Pour surmonter ces limitations, les filtres actifs de puissance se sont imposés comme une solution efficace pour la compensation des harmoniques et de la puissance réactive. Ce travail de thèse porte sur la conception et la commande d'un filtre actif parallèle basé sur un onduleur multiniveau à trois niveaux de type Neutral Point Clamped (NPC). La méthode Direct Current Control (DCC) est utilisée pour l'identification des courants harmoniques, tandis qu'une stratégie avancée de commande par modes glissants d'ordre 3 (TOSMC) est adoptée afin de dépasser les inconvénients des régulateurs conventionnels, tels que la sensibilité aux variations de paramètres, les erreurs en régime permanent et la lenteur de la réponse dynamique. Cette approche assure une meilleure stabilité, une précision de suivi élevée et une réduction significative du phénomène de « chattering ».De plus, un générateur photovoltaïque est intégré au niveau du bus continu, permettant au système non seulement de compenser les harmoniques, mais aussi d'injecter une puissance active renouvelable dans le réseau. Les résultats de simulation confirment des améliorations notables en termes de réduction harmonique, de compensation de la puissance réactive et de stabilité globale du système, validant ainsi l'efficacité de la méthode proposée.

Mots-clés Qualité de l'énergie ; Distorsion harmonique ; Filtre actif parallèle ;NPC Onduleur multiniveaux ; Commande par modes glissants ; Systèmes photovoltaïques.

ملخص

تُعد التشوهات التوافقية الناتجة عن الأحمال غير الخطية من أهم التحديات التي تواجه الشبكات الكهربائية الحديثة، حيث تؤدي إلى تدهور جودة الطاقة، وزيادة خسائر النظام، وتسريع تقادم مكونات الشبكة. إن المرشحات السلبية التقليدية لا تحقق سوى تعويض جزئي وتفتقر إلى المرونة في ظل تغير ظروف التشغيل. ولتجاوز هذه المحدوديات، برزت المرشحات الفعالة كحل فعّال لتعويض التوافقيات والقدرة غير الفعالة.يركّز هذا العمل البحثي على تصميم والتحكم في مرشح فعال متوازي يعتمد على محول متعدد المستويات ثلاثي الدرجات من نوع Neutral Point Clamped (NPC). حيث تُستَخدم طريقة **التحكم المباشر بالتيار (DCC) للتعرف على التيارات التوافقية، بينما تم اعتماد إستراتيجية متقدمة للتحكم بالانزلاق من الرتبة الثالثة (TOSMC) لمعالجة أوجه القصور في المنظمات التقليدية، مثل الحساسية لتغير المعاملات، والأخطاء في الحالة المستقرة، وبطء الاستجابة الديناميكية. هذا الأسلوب يحقق استقراراً أفضل، ودقة عالية في التتبع، مع تقليل واضح لظاهرة الاهتزازات.(Chattering) بالإضافة إلى ذلك، تم دمج مولد كهرضوئي على مستوى خط الجهد المستمر، مما يتيح للنظام ليس فقط تعويض التوافقيات، بل أيضاً حقن طاقة نشطة نظيفة في الشبكة. وقد أكدت نتائج المحاكاة تحسناً ملحوظاً في تقليل التوافقيات، وتعويض القدرة غير الفعالة، وتحقيق استقرار أكبر للنظام، مما يثبت فعالية المنهجية المقترحة

الكلمات المفتاحية جودة القدرة؛ التشوّهات التوافقية؛ المرشّح الفعّال المتوازي؛ محوّل متعدد المستويات؛ التحكّم بالانزلاق؛ الأنظمة الكهروضوئية

Table of Contents

Chapter II Multilevel Active Power Filter

Chapter III Photovoltaic-Supported Three-Level Active Power Filter

Chapter IV Third Order Sliding Mode Control Strategy for a Multilevel Active Power Filter in Grid-Connected PV Systems

Nomenclature

Acronyms

PV	Photovoltaic
PQ	Power Quality
APF	Active Power Filter
NL	Nonlinear Loads
THD	Total Harmonic Distortion
PI	Proportional-Integral
STA	Super-Twisting Algorithm
SMC	Sliding Mode Control
TOSMC	Third-Order Sliding Mode Control
RES	Renewable energy systems
PWM	Pulse-Width Modulation
PCC	Point of Common Connection
STF	Self-Tuning Filter
NN	Neural network
FLC	Fuzzy logic control
MVSI	Multifunctional voltage source inverter
MPPT	Maximum Power Point Tracking
PLL	Phase-Locked Loop
DCC	Direct Current Control

ICC	Indirect Current Control
NPC	Neutral-Point-Clamped
MLI	Multilevel Inverter

NOTATIONS

$\mathbf{I_{cc}}$: Short-circuit current

$\mathbf{V_{co}}$: Open-circuit voltage

MPP : Maximum Power Point (MPP)

$\mathbf{T_s}$: Sampling time

$\mathbf{I_{opt}}$, $\mathbf{V_{opt}}$: Optimal current and voltage at MPP

a : Duty ratio (modulation index)

P : Active power

Q : Reactive power

D : Distorting power

S : Apparent power

$\mathbf{V_s}$: Source voltage

FAP : Shunt Active Power Filter

UPQC : Unified Power Quality Conditioner

$\mathbf{U_d}$: DC voltage at rectifier output

$\mathbf{i_d}$: DC current supplied by rectifier

$\mathbf{i_f}$: RMS current of active filter

$\mathbf{i_c}$: RMS current of nonlinear load

$\mathbf{i_{c\text{-}h}}$: Harmonic current of nonlinear load

$\mathbf{i_s}$: RMS source current

$\mathbf{V_f}$: Voltage of the active filter

PF : Power factor

THDi : Total Harmonic Distortion of current

THDv : Total Harmonic Distortion of voltage

ω : Angular frequency of the grid

fc : Switching frequency

R_d, L_d : Resistance and inductance (DC side)

R_s, L_s : Resistance and inductance of source

R_{cc}, L_{cc} : Short-circuit resistance and inductance

R_f, L_f : Resistance and inductance of active filter

R_c, L_c : Load resistance and inductance (AC side)

I_{ref} : Reference current

V_{dc} : DC-link voltage (capacitor voltage)

$V_{dc.ref}$: Reference DC-link voltage

C_{dc} : DC-link capacitor

S_{cc} : Grid short-circuit apparent power

S_{ch} : Apparent power of nonlinear load

p(t) : Instantaneous real power

p^- : DC component of fundamental active power

q^- : DC component of fundamental reactive power

p~, q~ : Oscillating power components from harmonics

i_α, i_β : Disturbance currents in α–β frame

$i_{d\text{-}q}$: Alternating components in d–q frame

i_d, i_q : DC components in d–q frame

V_α, V_β : Disturbance voltages in α–β frame

θn : Source voltage vector

S_p, S_q : Digital power signals (DPC method)

e_p, e_q : Instantaneous active and reactive power errors

LPF : Low-pass filter

HPF : High-pass filter

I_{sp} : Peak current at DC bus regulator output

I_{sm} : Maximum source current

I_{sl} : Inverter loss current (switching losses)

List of Figures

Chapter I State of the Art on Power Quality and Electrical Disturbances

Chapter II Multilevel Active Power Filter

Chapter III Photovoltaic-Supported Three-Level Active Power Filter

Chapter IV Third Order Sliding Mode Control Strategy for a Multilevel Active Power Filter in Grid-Connected PV Systems

List of Tables

Chapter I State of the Art on Power Quality and Electrical Disturbances

Chapter II Multilevel Active Power Filter

Chapter IV Third Order Sliding Mode Control Strategy for a Multilevel Active Power Filter in Grid-Connected PV Systems

General Introduction

Ensuring high power quality has become a major challenge in modern electrical networks, which are increasingly dominated by nonlinear loads based on power electronic devices These loads draw distorted, non-sinusoidal currents from the grid, injecting significant harmonic components and consuming reactive power [1]. Such distortions degrade voltage waveforms, reduce equipment lifetime, cause overheating of transformers and cables, and disturb the operation of sensitive devices such as medical instruments, PLCs, and communication systems. To guarantee grid reliability, international standards such as IEEE-519 impose strict limits on current and voltage distortion, highlighting the need for effective harmonic mitigation solutions [2].

Historically, passive filters were the first tools developed to address harmonic pollution. Although inexpensive and simple to implement, their performance deteriorates in the presence of variable loads, and they may introduce unwanted resonances with the grid, These limitations have encouraged researchers to explore more flexible and intelligent solutions, leading to the development of active power filters (APFs), Among APF configurations, the shunt active power filter (SAPF) has proven particularly effective, as it injects compensating currents to restore the source current to a nearly sinusoidal form [3].

However, the performance of a SAPF depends strongly on the inverter topology and the control strategy employed. Conventional two-level voltage source inverters remain widely used but show clear limitations in medium- and high-power applications, especially regarding switching losses, electromagnetic compatibility, and output voltage quality. This has motivated the adoption of multilevel inverter topologies, notably the three-level Neutral Point Clamped (NPC) inverter, which offers reduced harmonic distortion, lower dv/dt stress, and increased efficiency [4]. Nevertheless, multilevel structures introduce additional control challenges, such as neutral point balancing and precise current regulation under dynamic grid and load conditions.

Parallel to active filtering, the integration of photovoltaic (PV) generation into the DC bus of active filters has attracted increasing attention. Equipping the SAPF with a PV source allows simultaneous harmonic mitigation, reactive power compensation, and renewable energy injection into the grid [5]. With a DC/DC boost converter and an MPPT controller, the PV generator can supply part of the active power demand while improving energy sustainability. Yet, this hybrid configuration increases system complexity and requires fast, robust, and coordinated control of both the inverter and the PV system [5].

Over the last decade, numerous control strategies have been proposed to improve the performance of SAPFs and PV systems. These include PI controllers, hysteresis control, fuzzy

logic, neural networks, fractional-order controllers, Model Predictive Control (MPC), and simplified sliding mode algorithms [6]. Although each technique offers advantages, all present limitations in dynamic performance, robustness, switching frequency, computational complexity, or residual chattering.

A common observation in the literature is that most studies remain restricted to two-level inverters and classical or early-generation control techniques [7]. For example, several contributions in this area demonstrate the feasibility of active filtering but rely on traditional inverter topologies and conventional control architectures. While these works have significantly advanced the understanding of SAPFs, they do not fully address the more complex challenges associated with multilevel converters or higher-order robust control techniques

This gap clearly shows that multilevel parallel active power filters combined with renewable sources and controlled using advanced nonlinear algorithms remain underexplored. Very few works propose an integrated solution capable of managing:

- harmonic suppression,
- reactive power compensation,
- renewable energy injection,
- neutral point voltage balancing, and
- robust current regulation under grid and load disturbances.

To address these limitations, this thesis proposes a parallel active power filter based on a three-level NPC multilevel inverter powered by a photovoltaic generator, controlled using a modern Third-Order Sliding Mode Control (TOSMC) strategy. Unlike classical SMC or the Super-Twisting Algorithm, TOSMC achieves high robustness while significantly reducing chattering and improving tracking accuracy. The proposed control is applied both to the SAPF (for harmonic identification and current compensation) and the PV generator (for maximum power extraction). This dual application represents a significant advancement compared with existing approaches based on two-level inverters, PI regulators, or predictive control.

The main objective of this research is to design, model, control, and optimize a multifunctional NPC-based PV-SAPF system, capable of improving overall power quality while enhancing energy efficiency and system robustness.

This work is organized into four chapters.

- **Chapter I:** introduces the concept of power quality, identifies the harmonic sources in electrical networks, and reviews the limitations of conventional passive filters that justify the need for active solutions.

- **Chapter II:** entitled *Multilevel Active Power Filter*, presents the modeling of the parallel active filter using a three-level NPC topology. The chapter covers both the power stage and the control stage, including the Direct Current Control (DCC) technique used for harmonic current identification and reference generation.
- **Chapter III:** focuses on the integration of the photovoltaic generator with the active filter. The modeling of the PV array, the DC/DC boost converter, and the implementation of MPPT algorithms are presented. The combined behavior of the PV system, nonlinear loads, the grid, and the SAPF is analyzed to highlight the benefits of this hybrid architecture.
- **Chapter IV** : introduces advanced control strategies and develops the proposed TOSMC-based control framework for both the inverter and the PV system. Simulation results validate the effectiveness of the proposed solution in reducing THD, ensuring fast dynamic response, and providing stable power injection under various operating conditions.

By combining multilevel inverter technology, reliable harmonic identification methods such as DCC, and the robustness of Third-Order Sliding Mode Control, this thesis proposes a comprehensive and efficient strategy for improving power quality in grid-connected renewable energy systems. The results obtained demonstrate the viability of the proposed approach in achieving accurate harmonic mitigation, reactive power compensation, and efficient renewable energy integration, contributing to the development of cleaner and more reliable electrical networks, Figure 1 summarizes the structural organization of the thesis.

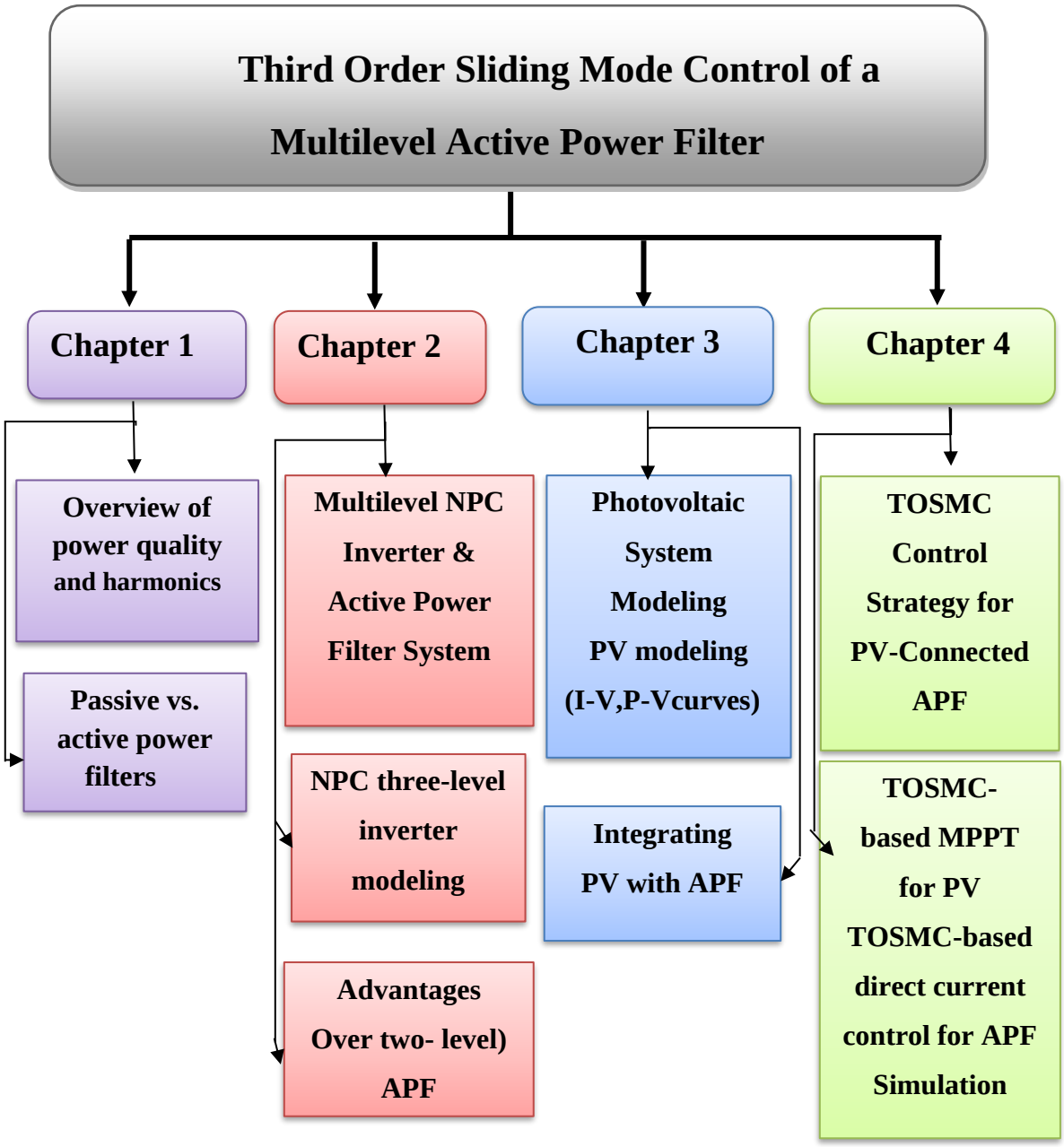

Figure 1 Schematic overview and structural framework of the thesis

Chapter I

State of the Art on Power Quality and Electrical Disturbances

I.1 Introduction

Power quality is a key indicator of the operational integrity and efficiency of electrical equipment connected to the power grid. The performance, reliability, and lifespan of such equipment are directly influenced by the nature of the current it absorbs from the network. Distorted or non-sinusoidal currents can lead to malfunctions, overheating, and accelerated aging of devices. Ensuring high quality electrical energy is therefore not only a technical necessity but also an environmental imperative, since it reduces losses and prevents energy-related pollution [8].

The widespread integration of power electronic devices such as diodes, thyristors, and transistors in rectifiers, inverters, and other converters has enabled more efficient and flexible control of power flow to electrical loads. However, these nonlinear devices inherently draw non-sinusoidal currents rich in harmonics, and they frequently exchange reactive power with the supply. In three-phase systems, harmonic distortion can further cause voltage unbalances and excessive neutral currents, leading to reduced power quality and compromised grid stability [9].

Historically, the mitigation of harmonics was addressed using passive filters, composed of tuned LC circuits. These filters provided a simple and cost-effective solution but suffered from drawbacks such as large size, resonance problems, and poor adaptability to dynamic load variations. To overcome these limitations, the concept of the Shunt Active Power Filter (SAPF) was introduced [9]. SAPFs are based on voltage-source inverters (VSIs) controlled to inject compensating currents into the grid, thereby cancelling harmonics and reactive power components drawn by nonlinear loads. Over time, significant research has focused on improving SAPF performance. Early studies used two-level inverters with conventional current control methods, but these systems often required high switching frequencies and generated considerable losses [10]. The development of multilevel inverters, particularly the Neutral Point Clamped (NPC) topology, provided a more efficient alternative by reducing voltage stress on semiconductor devices, lowering switching losses, and improving output waveform quality. This made NPC-based SAPFs a promising solution for medium and high-power applications. Recent works have further explored advanced control strategies to enhance SAPF performance. Techniques such as predictive control, sliding mode control, fuzzy logic and neural network-based methods, and model predictive control have been proposed to improve dynamic response, stability, and robustness against grid disturbances. In parallel, photovoltaic (PV) systems integrated with SAPFs have attracted growing interest. In such configurations, the PV generator not only supplies active power to the grid but also contributes to harmonic compensation, thereby increasing the overall efficiency and sustainability of the system. Despite these advances, challenges remain in terms of achieving high-quality current compensation under rapidly changing load conditions, maintaining DC-link voltage stability in NPC structures, and designing controllers that balance performance, complexity, and implementation cost. These research gaps motivate the present work, which focuses on the modeling, control, and

dimensioning of parallel active filters based on NPC multilevel inverters, with particular emphasis on their integration into PV-based energy systems [11].

I.2 Quality of Electrical Energy

The quality of electrical energy refers to the extent to which the voltage, current, and frequency of a power system remain stable and within standard limits. The quality of electrical energy encompasses all situations in which the waveform of the supply voltage (voltage quality) or the load current (current quality) deviates from the ideal sinusoidal form. Good power quality ensures the reliable operation of electrical devices without disruptions, overheating, or premature wear. However, various factors such as harmonics, voltage sags or swells, transients, and imbalances can degrade this quality. These disturbances are often caused by non-linear loads like power electronic converters and industrial machinery. Ensuring high-quality electrical energy is essential for improving the performance and lifespan of equipment, reducing energy losses, and maintaining the overall stability of the electrical grid [11].

I.2.1 Voltage Quality

The quality of alternating voltage is closely related to the characteristics of its components represented in:

- The frequency.
- The waveform, which must be sinusoidal: without distortions, peaks, troughs...
- The amplitude of the three tensions.
- The symmetry of the three-phase system, characterized by the equality of the magnitudes of the three voltages and of their relative phase shift.

The quality of the voltage can be affected, either due to certain incidents inherent to nature physical and the constraints related to network operation, either due to certain receivers. Thes defects manifest themselves in the form of various disturbances affecting one or more of the four parameters previously defined [12]. We therefore have four distinct possibilities of disturbances:

- **The fluctuations of the frequency at 50 Hz:** they are rare and are only observed during exceptional circumstances, for example certain serious network faults, at the level of the
  production or transportation.
- **The modification of the waveform of the voltage**: this wave is no longer sinusoidal, and can be considered as representable by a fundamental wave at 50 Hz, associated either with harmonics of integer multiples of 50 Hz frequency, sometimes even to waves of any frequency.

- **The variations in amplitude:** these are not the slow voltage variations that are corrected by load tap changers, but rather rapid voltage variations or voltage dips that often appear as sudden jolts. Voltage dips can be either isolated, or more or less repetitive, in regular or irregular form.
- **The asymmetry of the three-phase system**: which is called imbalance.

We can also mention a specific type of disturbance that is difficult to classify, as it affects both the amplitude and the waveform: transient amplitude variations lasting less than 10ms.Voltage disturbances such as sags, imbalances, and harmonics generally originate from the electrical network itself, although they may also be caused by certain loads. These types of disturbances can have highly detrimental effects on electrical equipment, ranging from overheating or shutdown of rotating machines to the complete destruction of the equipment[13].

I.2.2 Quality of the current

Disturbing currents such as harmonic currents, unbalanced currents, and reactive power are predominantly emitted by non-linear loads, based on power electronics, and/or unbalanced. Reactive power can also be consumed by linear inductive loads such as asynchronous motors, which are widely present in industrial sites [14].

I.3 Harmonic Disturbances in Current and Voltage

I.3.1 Origin of Harmonics

The widespread use of electrical equipment employing static converters has, in recent years, significantly increased harmonic pollution in electrical networks. These devices function as nonlinear loads, generating harmonic currents whose frequencies are integer multiples of the fundamental frequency—or, in some cases, at non-harmonic frequencies. When these harmonic currents pass through the network's impedances, they generate harmonic voltages at connection points, thereby polluting the voltage supplied to other consumers connected to the same network [15].

This issue affects various sectors, including:

- Industrial: with the use of dimmers, rectifiers, and variable speed drives,
- Commercial: such as computer systems and lighting in offices or shops,
- Residential: involving a high concentration of devices like televisions and household appliances.

I.3.2 Characterizations of harmonics

To measure these disruptions, many metrics are established. The most popular ones among them are:

I.3.2.1 Harmonic Rank

The harmonic rank (or harmonic order) is defined as the ratio between the frequency of a harmonic component f_n and the frequency of the fundamental component (usually 50 Hz or 60 Hz in industrial systems) [16]. It is expressed as:

$$h=f_n/f_1 \quad \text{(I.1)}$$

Where:

- h is the harmonic rank (an integer),
- f_n is the frequency of the harmonic,
- f_1 is the fundamental frequency.

I.3.2.2 The Total Harmonic Distortion Rate (THD)

The Total Harmonic Distortion (THD) is a key metric used to quantify the distortion of an electrical signal voltage or current compared to an ideal sinusoidal waveform. It represents the ratio between the root mean square (RMS) value of all harmonic components (excluding the fundamental) and the RMS value of the fundamental frequency component[17].

- The THD is calculated using the formula:

$$THD = \frac{\sqrt{f_2{}^2+f_3{}^2+\cdots}}{f_1} \quad \text{(I.2)}$$

Throughout our study, we will focus on calculating the THDi in current, which can be expressed as follows:

$$THD_i = \frac{\sqrt{i_2{}^2+i_3{}^2+\cdots}}{i_1} = \sqrt{\sum_2^n i_h/i_1} \quad \text{(I.3)}$$

Another characteristic that allows the identification of a distorted signal is its crest factor Fc, in the case of an undistorted sinusoidal signal, it corresponds to:

$$F_c = \frac{I_{max}}{I_{eff}} = \sqrt{2} \quad \text{(I.4)}$$

When the current is distorted, the factor becomes different at this value.

I.3.2.3 Power factor

Any electrical load operating under alternating current such as motors and transformers requires two forms of energy: active energy and reactive energy.

- **Active energy** (measured in kWh) is the energy actually consumed to perform useful work. It is associated with active power P (in kW), which is fully converted into mechanical work or heat losses. It is expressed by:

$$P=\sqrt{3}.UI.cos(\varphi) \quad \text{(I.5)}$$

- **Reactive energy** (measured in kVARh) is necessary to establish and maintain the magnetic fields in inductive machines. It corresponds to reactive power Q (in kVAR), defined by:

$Q=\sqrt{3}.U.I.sin(\varphi)=3.v.i\ sin(\varphi)$ (I.6)

- **Apparent energy** (measured in kVAh) is the vector sum of active and reactive energies. It corresponds to the apparent power S (in kVA), representing the total power supplied to the load:

$S=\sqrt{3}.U.I=3.v.i$ (I.7)

Each of these energy types is associated with a corresponding current:

- The active current is in phase with the voltage,
- The reactive current is phase-shifted by 90°, either lagging (for inductive loads) or leading (for capacitive loads).

In addition, due to waveform distortions (non-sinusoidal currents and/or voltages), another component known as deforming power D (in kVAD) arises [18]. It accounts for the increase in apparent power caused by harmonic distortion. This is defined by:

$D=\sqrt{S^2-P^2-Q^2}$ (I.8)

The power factor is a key parameter representing the efficiency of power usage in the system. It is defined as the ratio of active power to apparent power:

$F_p=\frac{P}{S}=\cos(\varphi)$ (I.9)

To better understand the relationships between these different types of power, a vector (phasor) diagram can be used, as illustrated in Figure I.1 [19].

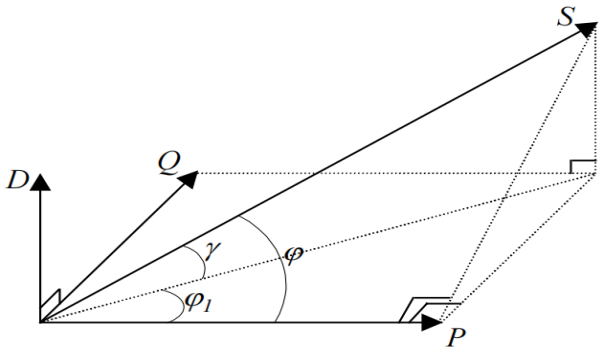

Figure .I.1 Fresnel Power Diagram

I.3.2.4 Effects and consequences of harmonics

There are several ways that harmonics can affect electrical systems and equipment. Heating, disruption of telecommunications networks, failure of certain electrical equipment, and the possibility of resonance excitation are the most significant effects [19]:

Heating: The total losses due to the Joule effect are the sum of those of the fundamental and the harmonics:

$I^2.R=\sum_{h=1}^{\infty} I_h^2.R$ (I.10)

with I the total current, I_h the harmonic current of rank h which represents the fundamental for $h=1$,

and *R* the resistance crossed by the current *I*. Harmonics also increase iron losses (losses due to eddy currents). They take the importance in equipment using magnetic circuits (motors, transformers...). The aging of insulators is often due to a tensile stress resulting from the presence of harmonic voltage, and thus a local increase in leakage current, or still to the exaggerated warm-up in the drivers [12].

- **Interference with telecommunications networks:** Electromagnetic coupling between electrical and telecommunications networks can induce significant noise in the latter. In the case of resonances, part of the telecommunications networks can become unusable [10].
- **The malfunctions of certain electrical equipment:** In the presence of harmonics, the voltage (or current) can change sign several times in half period; therefore, any device whose operation is based on zero crossing electrical quantities (devices using voltage as a reference) can be disturbed [12].
- **The risk of resonance excitation:** The resonance frequencies of the circuits formed by the transformer inductances and cables are normally high. This is not the case when capacitor banks are connected to the grid to improve the power factor; the resonance frequencies can become quite low, thus coinciding with those of the harmonics generated by static converters. In this case, there will be phenomena of harmonic amplification [20].

According to the effect, two types of disturbance are distinguished:

- Instantaneous effects, they create disturbances in the operation of protection and switching devices.
- Medium and long-term effects, they cause the overheating of electrical equipment and lead to its premature aging.

Table I.1 summarizes some examples of electrical equipment susceptible to disruption by hamonic pollution.

Table I.1 Effects of Harmonic Pollution on Equipment

Type of Electrical Equipment	**Effects of Harmonic Pollution**
Rotating Machines Three-phase motors, alternators	- Additional heating (Joule effect) in stator windings. Oscillating torques. - Increased noise.

Transformers	- Additional losses in the iron (due to eddy currents) and in the windings (due to Joule effect). - Risk of saturation in the presence of even harmonics.
Cables	Increased losses, especially in the neutral cable, where 3rd harmonics and multiples of 3 are added. Additional dielectric losses.
Power Electronics (thyristor rectifiers, transistors, etc.)	Functional problems related to the waveform (commutation, synchronization).
Power Capacitors	Additional dielectric losses leading to premature aging of capacitors.
Discharge Lamps	Risk of flickering
Protective Devices (Fuses, Circuit Breakers, etc.)	Premature operation
Computer	Malfunction related to pulsating torques of the motors driving the magnetic supports
Energy meter	Measurement errors
Televisions	Image distortion

I.3.2.5 Regulations and requirements

In order to limit the influence of a polluting load on the other connected loads to the network and at the same time avoid modifying their characteristics, the electricity distributors have been prompted to issue recommendations. These recommendations concern the requirements at the user's connection point on the electrical grid.

The two main international standardization organizations in the field electrotechnics are:

1- CEI (Commission Électrotechnique Internationale).

2- IEEE (Institute of Electrical and Electronics Engineers).

These two organizations carry out the main standardization activities in the field of electrical disturbances worldwide but do not have uniform criteria regarding the definition of interactions between the grid and connected loads.

In order to appreciate the impact of this IEEE document, it is important to understand the meaning of the terms used in Table I.2.

Table I. 2 Limit of Harmonic Current Components (IEEE 519, 1992.)

Maximum Harmonic Current Distortion as a Percentage of IL						
Individual Harmonic Order (Odd Harmonics)						
Isc / IL	**11**	**11 ≤ h < 17**	**17 ≤ h < 23**	**23 ≤ h < 35**	**35 ≤ h**	**THD**
< 20	4.0	2.0	1.5	0.6	0.3	**5.0**
20–50	7.0	3.5	2.5	1.0	0.5	8.0
50–100	10.0	4.5	4.0	1.5	0.7	12.0
100–1000	12.0	5.5	5.0	2.0	1.0	15.0
> 1000	15.0	7.0	6.0	2.5	1.4	20.0

Legend:

- **IL**: Maximum demand load current
- **Isc**: Maximum short-circuit current
- **THD**: Total Harmonic Distortion of the current

We find that the limits are stricter (THD < 5%) for a short circuit ratio (SCR) less than 20.

I.4 Imbalance of current and voltage

The phenomenon of voltage imbalance can be defined as the measurement of voltage differences between the phases of a three-phase system. The impact of this phenomenon is very severe; it degrades performance, causes overheating, and shortens the lifespan of connected loads. A current imbalance will occur when three-phase loads are not evenly distributed across the three phases of the electrical network. Indeed, any three-phase load must draw an identical current on each phase[23].

I.4.1 Origin of the imbalances

An unbalanced three-phase electrical load, even when supplied by a balanced three-phase network, can lead to voltage imbalances. This occurs due to the flow of unbalanced currents through the network impedances, resulting in unequal voltage drops across the phases. This phenomenon is illustrated in Figure I.2.

Voltage imbalance is commonly observed in low-voltage systems, especially where numerous single-phase loads are distributed unevenly across the phases. However, it can also occur in medium- and high-voltage networks, caused by the operation of welding machines, arc furnaces, or railway traction systems, all of which can introduce significant asymmetrical load conditions.

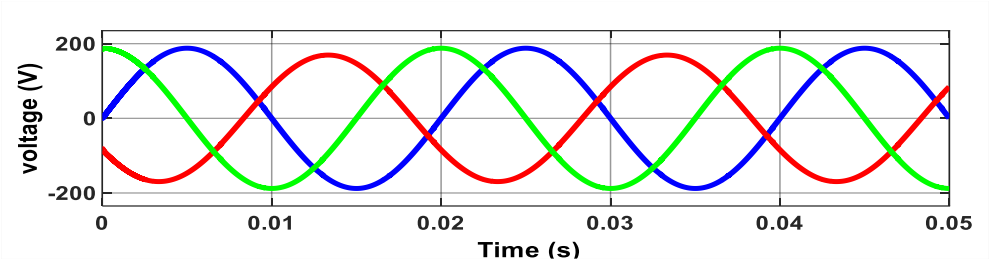

Figure.I.2 Imbalance of the three-phase voltage system

I.4.2 Consequences of the imbalance

It is more appropriate to analyze the consequences of imbalance based on the type of equipment and the voltage level involved. Imbalance can lead to a range of malfunctions, particularly in low-voltage systems, including:

- Risk of damage to single-phase equipment subjected to overvoltage on certain phases
- Malfunctioning of single-phase devices powered by low voltage, such as incandescent lamps, resulting in poor lighting quality.
- Braking torque in rotating machines, caused by negative-sequence components and the formation of a reverse rotating magnetic field, reducing motor efficiency and stability
- Generation of harmonic components, especially third-order harmonics, in three-phase power electronic equipment, which can cause waveform distortion and equipment stress.
- Overheating of the neutral conductor, with a risk of neutral wire failure, especially in low-voltage networks where the neutral conductor has a relatively small cross-section.
- Degradation of electrical insulators due to the thermal and electrical stresses caused by persistent imbalance.

I.4.3 Regulations and requirements

To support both electricity distributors and end users in monitoring and improving the quality of electrical networks, the NF EN 50160 standard was established. It defines the characteristics of the voltage supplied at the customer delivery point, focusing on aspects such as:

- Waveform quality
- Voltage level and its allowable variations
- Frequency stability (typically centered around 50 Hz)
- Three-phase system imbalance

The standard lists different types of voltage disturbances that might occur at the delivery point, and it specifies both which parameters should be monitored and the duration of this monitoring typically over a one-week period. In short, it helps create a clear framework for evaluating power quality, ensuring that what's delivered matches expected performance standards [24].

I.4.4 Tension dip

A voltage dip is defined as a sudden decrease in the supply voltage U_f, typically ranging between 90% and 10% of the nominal voltage U_n, followed by the restoration of voltage after a short period of time. The duration of a voltage dip can vary from 10 milliseconds to 3 minutes [25].

Most electrical devices are designed to tolerate brief interruptions of power lasting less than 10 *ms* without performance degradation. Voltage dips are mainly characterized by two parameters: amplitude and phase angle. These can be graphically represented using phasor diagrams, where the combined relationship of these parameters is referred to as the dip signature or dip type [26]. Figure.I.3 illustrates a simplified representation of this type of electrical disturbance.

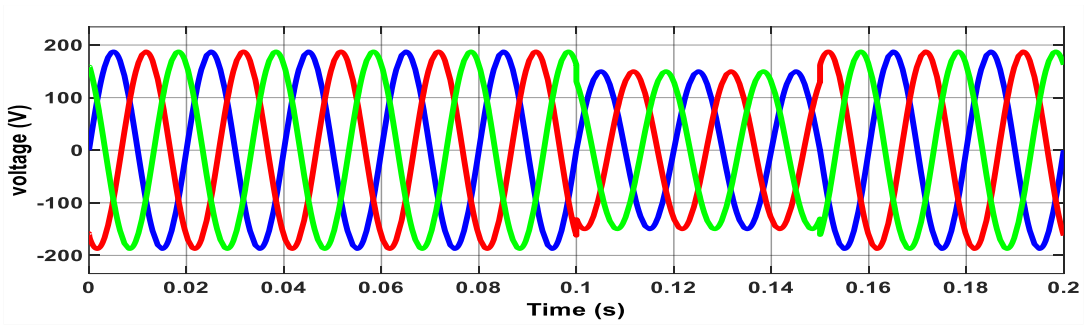

Figure. I.3 Voltage Dip Phenomenon

I.4.4.1 Origin of voltage dips

Voltage dips generally arise from two types of phenomena:

1. Operational causes, such as the switching of equipment with fluctuating loads or the startup of devices that draw high inrush current, like motors and transformers.
2. Random or accidental events, including lightning strikes, short circuits on public distribution networks or internal customer networks, insulation failures, cable damage, or tree branches contacting overhead lines.

I.4.4.2 Consequences of voltage dips

Voltage dips can significantly disrupt the operation of certain industrial and commercial (tertiary) installations [27]. These disturbances may lead to malfunctions in electrical equipment and, in severe cases, can result in complete equipment failure or destruction. Several adverse effects can be observed, including:

- Unexpected shutdown of sensitive equipment,

- Slowdowns, stalling, or overcurrent in asynchronous motors,
- Reduced brightness, extinction, and re-ignition of arc-based lighting systems,
- Loss of synchronization and tripping of asynchronous motors.

I.4.4.3 Regulation of voltage dips

Some distribution service providers define their commitment to power quality through specific thresholds, where voltage dips are characterized by their depth and duration typically with limits such as a 30% voltage drop lasting up to 600 ms [28].

In general, Table I.3 summarizes the main standards related to electrical power quality.

Table I. 3 Main Standards for Electrical Energy Quality

Type of Disturbance	Standards
Harmonics	CEI 61000-2-1:1990 CEI 61000-2-2 CEI 61000-3-2 CEI 61000-4-7: 1991 IEEE 519: 1992
Creux/Surtension/Interruptions	CEI 61009-2-1:1990 IEEE 1159: 1995
Transients	CEI 61000-2-1:1990 CEI 816: 1984 IEEE 1159: 1995
Flicker de tension	CEI 61009-4-15:1997

I.5 Solutions for the depollution of electrical networks

To reduce the spread of harmonics in electrical distribution networks, several solutions are being considered. There are many techniques for mitigating harmonics within the system or by using an external device. All of these pollution reduction solutions have advantages and disadvantages, and all involve additional costs. The best solution will depend on the total load, the power supply to the facility, and the acceptable level of distortion.

I.5.1 Traditional depollution solutions

These are techniques that every electrician should know. They offer a simple and quick solution to certain cases of well-localized faults, using passive components (inductors, capacitors, transformers) and/or connections that modify the installation's schematic**.**

I.5.1.1 Act on the structure of the installation

It is advisable to supply a large polluter with a separate transformer in order to separate it from a

sensitive receiver. In the case of a medium polluter, it is preferable to supply power through separate cables instead of connecting them in parallel. A star distribution allows decoupling through natural and/or additional impedances. [29]

I.5.1.2 Oversizing or downgrading of the electrical installation

We generally proceed with the oversizing of equipment to ensure their resilience to harmonic overloads. This solution does not address the harmonics that do not undergo any corrective action from the user. With this approach, the problems related to harmonic pollution are resolved for a limited duration. The decommissioning of electrical distribution equipment subjected to harmonics is used in the case of existing installations. This method causes a production cost increase and does not take advantage of the installation's real potential. [30]

I.5.1.3 Rebalancing Currents and Voltages

In a three-phase electrical system, an imbalance can occur when the loads connected to each phase are not equal. This leads to unequal phase currents and voltages, which may cause equipment overheating, reduced efficiency, and increased energy losses. Rebalancing refers to the process of redistributing electrical loads or using power electronic devices (such as phase balancers) to ensure that:

- Currents in each phase are equal or close to balanced.
- Phase voltages (tensions) remain symmetrical in amplitude and 120° phase-shifted from each other.

This improves power quality, ensures the proper functioning of sensitive equipment, and extends the lifespan of system components[31].

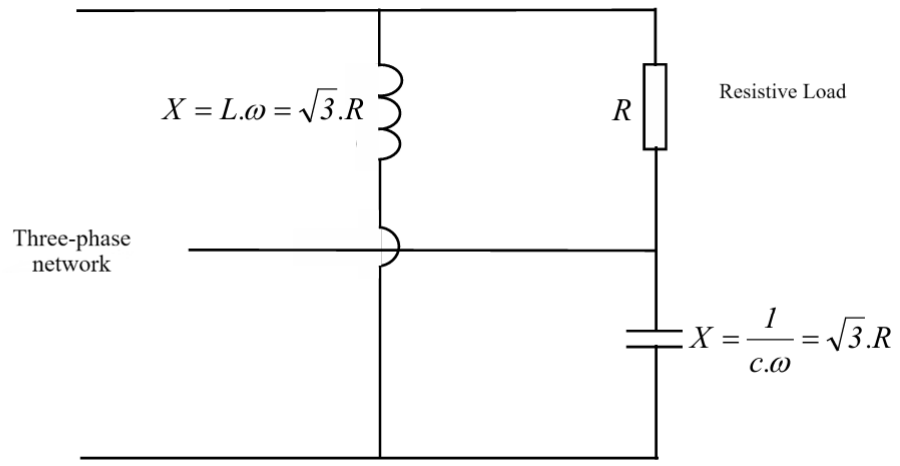

Figure. I.4 Steinmetz assembly for rebalancing

I.5.1.4 Increase in short-circuit power

Another harmonic pollution mitigation solution involves modifying the short-circuit power electric network circuit. The overall harmonic disturbance increases when the short-circuit power of the

network is increased relative to the power of the generator. Indeed, the short-circuit impedance at a point in the network is inversely proportional to the available short-circuit power at that point. Therefore, the impact of harmonics will be all the more reduced if the short-circuit power is high [32].

I.5.1.5 Current smoothing inductor

A current smoothing inductor is an inductive component added in series with the current path (often between the inverter and the grid or load) to reduce the ripple in current and smooth the waveform. It acts as a low-pass filter, limiting high-frequency components and sudden changes in current.

I.5.1.6 Special coupling transformer

The choice of appropriate transformer couplings helps limit the circulation of harmonic currents. The use of an isolation transformer, with a 1:1 ratio and delta-star or delta-zigzag coupling, prevents the propagation of currents. third-order harmonics and their multiples circulating in the neutral. This process has no effect on the other harmonic orders. This solution, on the contrary, limits the available power of the source and increases the line impedance. This results in an increase in voltage distortion due to other harmonic orders. [12]

I.5.1.7 Passive filter

Parallel and series passive filters have been implemented since the mid-1920s, mainly to compensate for the harmonics created by loads, provide the required reactive power, and increase the transport capacity of networks. The principle of passive filtering consists of inserting one or more circuits tuned to the harmonics to be rejected upstream of the load. Thus, to filter a current at a particular frequency. A series resonant filter is placed in parallel on the network. This type of filter is very selective. For to attenuate an entire frequency band, a second-order passive damped filter is preferable. The sizing of these filters depends on the harmonics to be eliminated, the required performance, the network structure, and the nature of the receivers. With this technique, it is generally easier to reject higher-order harmonics than lower-order ones. [33]. Passive filters can be divided into two families, parallel filters and series filters. Depending on the type of filtering chosen, the harmonics can literally be blocked by a high series impedance between the converter and the network, diverted by a low impedance in parallel or a combination of both [34].

I.5.1.7.1 Passive Series Filter

A passive series filter is a type of electrical filter composed of passive components typically inductors and capacitors connected in series with a load or a power line. Its main purpose is to present high impedance at specific harmonic frequencies, thereby blocking or attenuating harmonic currents from entering the protected load or propagating into the power system.

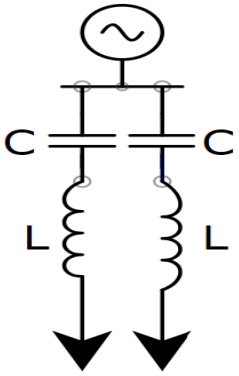

Figure. I.5 Series passive filter

I.5.1.7.2 Parallel passive filter

The parallel passive filter, illustrated in Figure I.6, consists of an inductor connected in parallel with a capacitor. When properly dimensioned to operate under resonance conditions, this configuration presents low impedance at harmonic frequencies and high impedance at the fundamental frequency, effectively preventing the propagation of harmonic currents into the power grid.

The filter behaves inductively for frequencies below the fundamental and capacitively for frequencies above it, which is a significant advantage for controlling current through the inductor. This type of filter is particularly suitable for disturbing loads that generate harmonic currents[26].

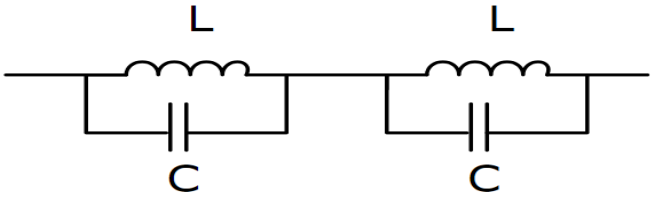

Figure. I.6 Parallel passive filter

There are two kinds of parallel passive filters that are often used: the resonant passive filter and the damped passive filter [35].

I.5.1.7.2.1 Resonant filter

It is a very selective filter consisting of an RLC series circuit, see figure .I.7, and it is tuned to a specific frequency. Its performance is characterized by the reduction of the harmonic voltage across its terminals. This solution also involves offer the harmonic current that one wishes to eliminate, a path with less resistance than the line. It exploits the series resonance of circuits formed by the association of inductive and capacitive elements; these circuits, for each pair (L, C), have a so-called resonance frequency where the circuit impedance is very low. [26]

Figure. I.7 Resonant filter

I.5.1.7.2.2 Damped Passive Filter

A damped passive filter is a type of harmonic filtering device designed to attenuate a wide range of harmonic frequencies, rather than targeting a single one. It consists of an LC network combined with a damping resistor, which serves to flatten the impedance curve and prevent sharp resonance peaks that could otherwise lead to system instability. This configuration allows the filter to present low impedance over a broader frequency band, effectively absorbing multiple harmonic components. Damped filters are particularly suitable for electrical networks where harmonic content is variable or spread across different orders, such as in systems with nonlinear or fluctuating loads. Compared to single-tuned filters, damped filters offer enhanced robustness and operational stability, though they may introduce slight additional losses due to the resistive component. These filters are often used in combination with other passive or active filtering techniques to improve overall power quality.

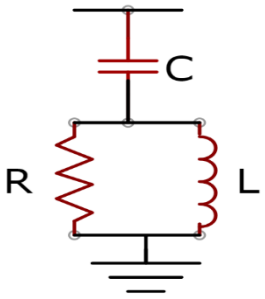

Figure. I.8 Damped filter

I.6 Modern solutions

The study of active power filters for harmonic compensation in electrical networks began in 1970 with the compensation principle proposed by T. Machida and H. Sasaki. Initially, advancements in power semiconductor technology accelerated research, leading to the practical realization of active filters in the early 1990s . Theoretical developments and Pulse Width Modulation (PWM) control techniques enabled active filters to surpass conventional LC passive filters in harmonic compensation performance. Today, active filters have reached an unprecedented level of technological maturity, significantly enhancing their ability to compensate both harmonic currents and reactive power in modern power systems.[26]

I.6.1 Active Filters

Active filters are composed of inverters, which are static power converters. Powered by a direct current or voltage source, the inverter can deliver a current (shunt structure) or a voltage (series structure) whose harmonic content d pends solely on the switching control law of the switches. Active filters therefore act as a source of harmonic voltage or current in opposition to those of the grid in order to restore a quasi-sinusoidal source current. The active filter can be connected to the network in series or in parallel, depending on whether it is designed to compensate for voltage or current harmonics. [22]

In this part of the chapter, we will introduce the main structures proposed in the literature, namely parallel active filters, series filters, combined parallel-series filters, and hybrid structures. active-passive.

I.6.2 Active Series Filter (ASF)

The series active filter is connected in series between the power source and the nonlinear load, with the main objective of ensuring that the source voltage remains sinusoidal. This method relies on isolating harmonics by actively controlling the output voltage of the series active filter (SAF). In essence, the SAF presents a high impedance to harmonic currents, thereby acting as a controllable voltage source. It is particularly effective for filtering harmonics produced by loads that generate harmonic voltages [12].

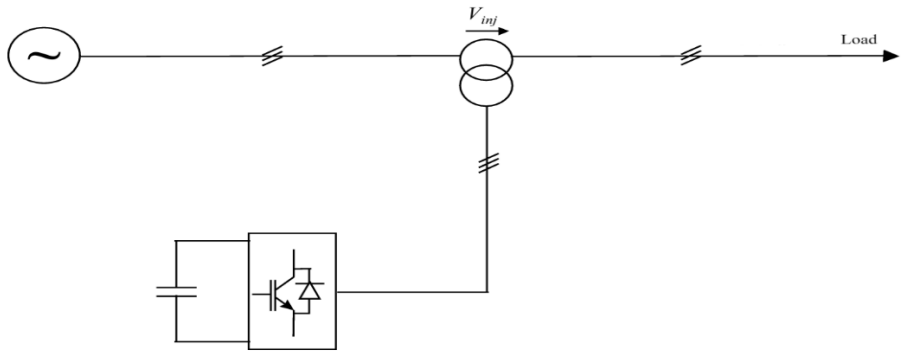

Figure. I.9 Series Active Filter.

I.6.3 Parallel Active Filter (PAF)

Also called a shunt compensator, the parallel active filter is connected in parallel to the distribution network and is most often controlled as a current generator. The parallel active filter is an inverter controlled by several methods, the most well-known being PWM or hysteresis. It injects into the electrical grid harmonic currents i_{inj} equal in amplitude but opposite in phase to those absorbed by the nonlinear load, so that the current drawn from the network remains sinusoidal and in phase with the corresponding phase voltage. Its independence from both the source and the load ensures self-adaptability, reliability, and high performance [37]. The parallel active filter also prevents harmonic, reactive, and unbalanced currents from flowing through the network impedance, thereby improving current and voltage distortion levels.

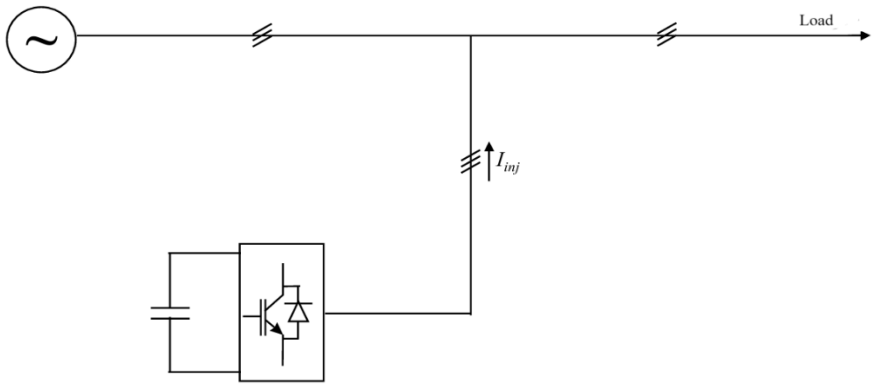

Figure. I.10 Parallel Active Filter.

I.6.4 Active Series Parallel Filter UPQC

The UPQC (Unified Power Quality Conditioner) is primarily the combination of two series and parallel active filters (Figure I.11) that share the same capacity on the DC bus. This type of device is capable of both regulating the network voltage and eliminating harmonics. It is considered the most powerful device and it is capable of performing efficiently all power conditioning tasks.

However, its significant cost and the complexity of controlling numerous switches limit its use to critical applications such as medical equipment. [26]

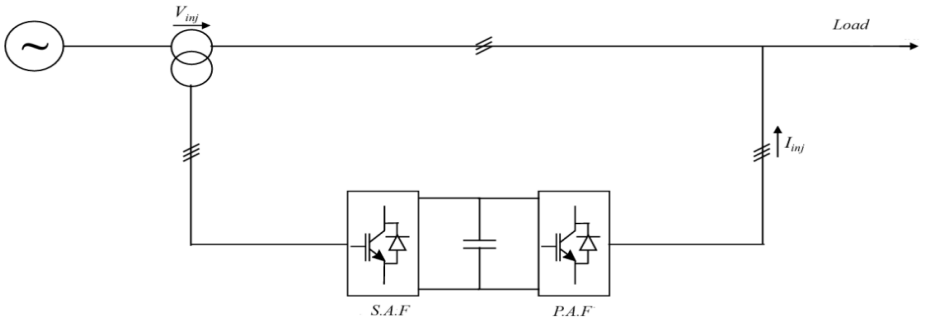

Figure. I.11 Combined Parallel-Series Filter (UPQC).

I.6.5 Active and passive hybrid combination

Despite the great attention given to active filters, their industrial application remains limited to certain countries where traditional solutions are ineffective in the face of proliferation of high-power polluting equipment on a network that is not powerful enough everywhere. The industrial application of these new filtering devices is hindered by their cost. In order to reduce the sizing and consequently the price active filters and thus increase their potential for application, the combination of filters low-power active components to passive filters seems to be a promising solution [38]. Various hybrid topologies have been proposed in the literature, with the most commonly studied configurations including:

- Series active filter combined with parallel passive filters
- Series-connected active filter with parallel passive filters
- Parallel active filter combined with a parallel passive filter

I.6.5.1 Series active filter with parallel passive filters

The role of the series active filter in this case is to prevent harmonic currents from flowing into the grid and to force them to pass through the passive filters connected to their frequencies as shown in Figure. I.12 [40].

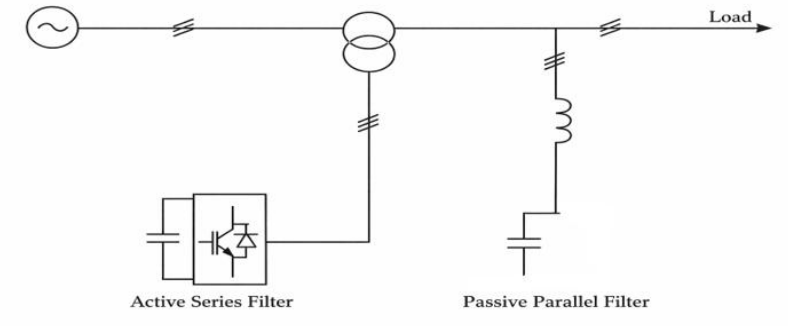

Figure.I.12 Series Active Filter and Parallel Passive Filter.

I.6.5.2 Series-connected active filter with parallel passive filters

In this configuration, the compensator only acts on the harmonic currents, and improves the efficiency of passive filters: it prevents the amplification of harmonic voltages upstream at the anti-resonance frequencies of passive filters, it significantly attenuates harmonic currents between load and source by "lowering" the overall impedance (passive filters plus active compensator). Since the active compensator is not traversed by the entire network current, its sizing (and in particular that of the magnetic coupler) can be reduced.This structure is therefore well-suited to handling power and voltage networks. elevated, while ensuring the re-phasing of the fundamental components. His main disadvantage is that passive filters are defined according to the nature of each charge: a preliminary study is imperative. Finally, almost all the tensions pre-existing harmonics (on the source) are present on the load side. In this sense, this configuration can be likened to a "shunt" type active compensator [41].

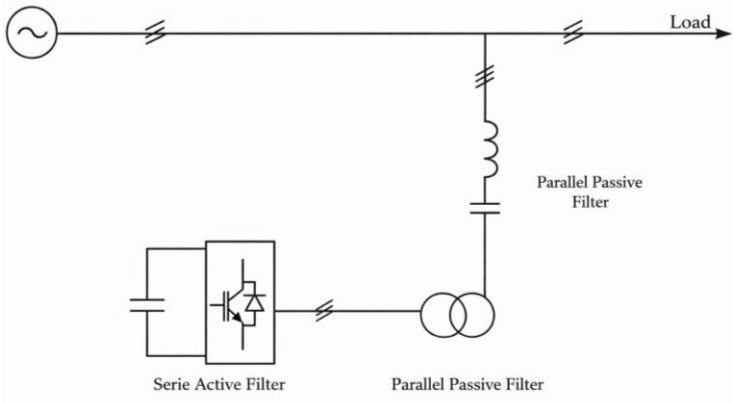

Figure. I.13 Series active filter connected in series with a parallel passive filter.

I.7 Parallel active filter combined with a parallel passive filter

The role of the parallel active filter in this configuration, shown in Fig. I.14, is to compensate for the low-frequency harmonic currents emitted by the polluting load. The filtertuned passive at a high frequency, eliminates high-frequency harmonics including those created by the parallel active filter. This type of filtering has already been applied to the compensation of harmonic currents emitted by a high-power cycloconverter [40].

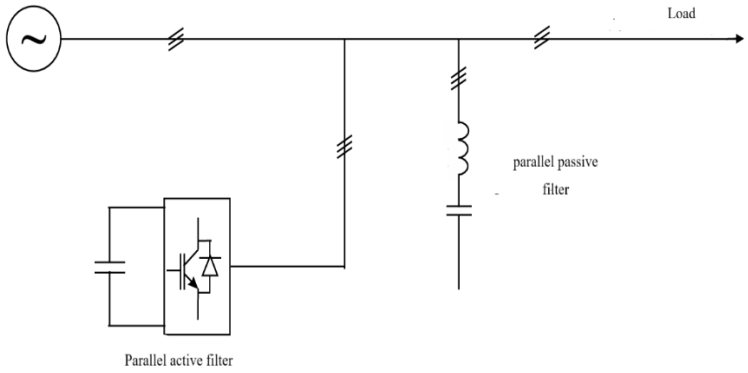

Figure. I.14 Parallel active filter with a parallel passive filter

I.7.1 Advantages of active filters

- Only one filter can eliminate all the unwanted harmonics.
- The resonance state is absent, thus increasing the stability of the power system;
- Flexibility and adaptability with the variation of the load.

I.7.2 Disadvantages of active filters

- The high cost has limited implementation in the industry.
- The losses are higher.
- Improvement of the shape of the tension is not always obvious.

I.7.3 Selection of types of active filtering

Table I.4 below shows a summary of the advantages and disadvantages of the different types and structures of filtering [28]. For the continuation of our work, we have chosen the topology of a parallel active filter due to numerous advantages such as:

- A good attenuation of current-type harmonics.
- Automatic adaptation with the variation of loads connected to the electrical network.
- Reactive power compensation is possible.

Table I. 4 Advantages and Disadvantages of Different Combinations of Active Filtering

Principles	**Advantages**	**Disadvantages**
Passive Filtering	Improvement of current waveform	Risk of resonance, no adaptability
Active Series Filtering (FAS)	Improvement of voltage waveform Adaptability to load and network variations	No improvement of current waveform
Active Parallel Filtering (FAP)	Improvement of current waveform Adaptability to load and network variations	Improvement of voltage waveform is not always obvious
Combined Active Filtering (UPQC)	Improvement of current waveform Improvement of voltage waveform Adaptability to load and network variations	Difficult implementation

I.8 CONCLUSION

In this chapter, we reviewed the main disturbances that degrade the quality of electrical power, such as harmonic distortions, unbalances, reactive power issues, and voltage sags. These phenomena can seriously compromise the performance, efficiency, and lifespan of electrical equipment, making power quality a critical concern in modern power systems.

Traditional passive filtering techniques, although simple and inexpensive, are limited by their fixed tuning, bulky design, and lack of adaptability to varying load conditions. To overcome these drawbacks, active and hybrid filtering solutions have been developed. In particular, parallel active power filters (SAPF) have emerged as a versatile and effective approach for mitigating current harmonics and reactive power in real-time, ensuring stable operation even under dynamic and nonlinear load conditions.

Among the different technologies available, SAPFs based on multilevel inverters especially the Neutral Point Clamped (NPC) structure combine high-quality compensation with improved efficiency and scalability. For this reason, the remainder of this thesis is dedicated to the modeling, control, and

implementation of a parallel active filter using a multilevel inverter, with special attention to achieving reliable, real-time power quality improvement in practical grid-connected environments.

Chapter II

Multilevel Active Power Filter

II.1 Introduction

This chapter is devoted to the study of the parallel active power filter (APF), which represents one of the most effective modern solutions for mitigating current harmonics and improving power quality. The system is composed of two main parts: the power stage and the control stage. The power stage includes a three-level Neutral Point Clamped (NPC) inverter, a coupling filter, and a passive energy storage element such as a DC-link capacitor. The control stage governs the switching of the inverter's semiconductor devices according to a chosen control strategy. By generating suitable compensation currents, the APF attenuates unwanted harmonic components from the source current and contributes to enhancing the overall performance of the electrical network.

II.2 General Structure of The Parallel Active Filter

II.2.1 General Topology

The structure of active filters generally consists of two main sections: the power section and the control section, as illustrated in Figure II.1. The power section typically includes an inverter either voltage-source or current-source, single-phase or multi-phase, and in two-level or multilevel configurations along with a coupling filter and an energy storage element. The nature of the storage element depends on the type of active filter: it is inductive for current-source active filters and capacitive for voltage-source active filters. The control section is responsible for managing the switching of the inverter's semiconductor devices. By applying various control strategies, the inverter can generate harmonic currents that are equal in amplitude but opposite in phase to those present in the electrical network, thereby effectively compensating for harmonic distortions [42].

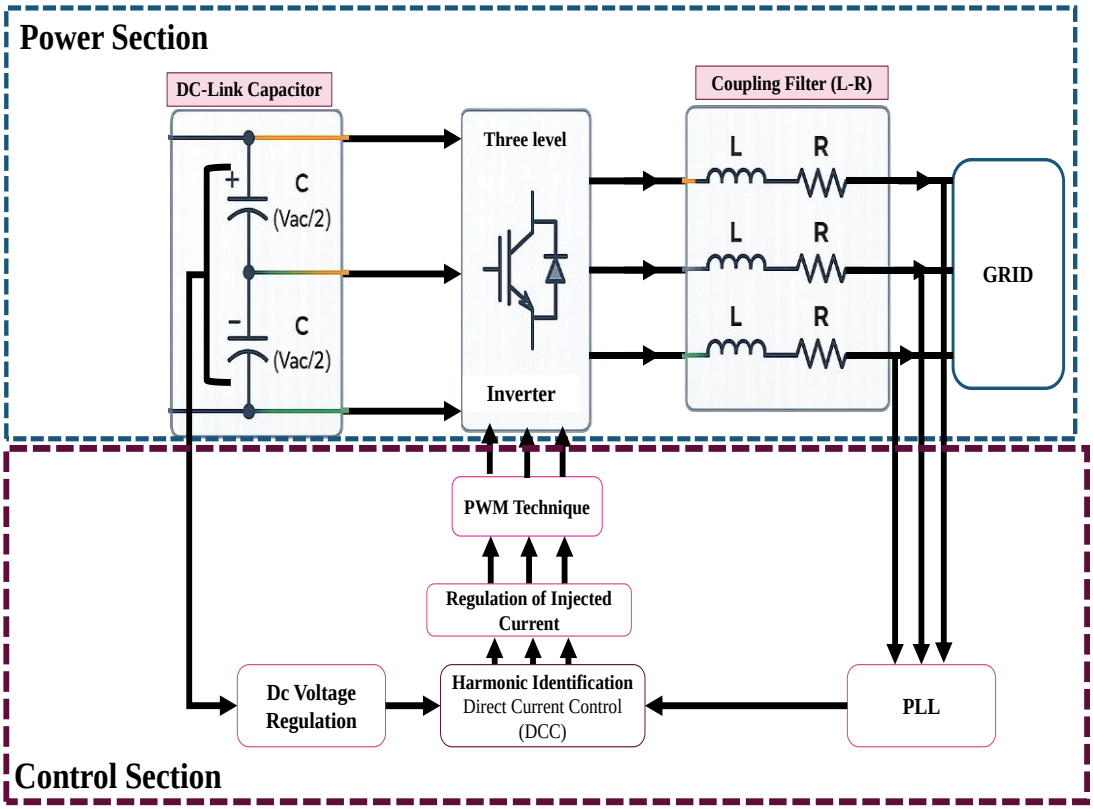

Figure. II.1 General structure of the parallel active filter

II.2.2 Study of the power part

The power stage of the PAF consists of a three-level inverter, a coupling filter, and an energy storage capacitor.

II.2.2.1 Inverter section of a parallel active power filter

An inverter is a static power converter that transforms direct current (DC) into alternating current (AC). In this work, two inverter topologies are considered.

- **Inverter structures**

There are two main configurations: the voltage-source structure and the current-source structure. In the voltage-source configuration, the inverter is connected in parallel with the grid, as illustrated in Figure II.2 for the single-phase case [43]. The DC-link capacitor C_{dc} serves as a source of constant DC voltage.

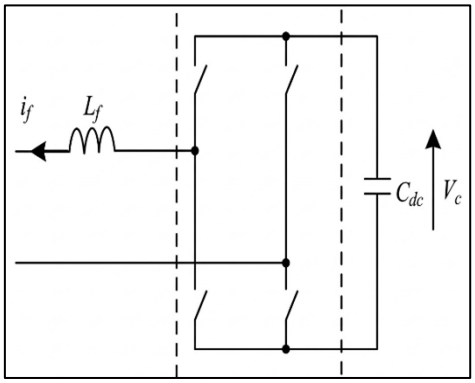

Figure. II.2 Single-phase voltage-source inverter.

In the voltage-source configuration, the inverter is connected to the grid through a first-order filter composed of an inductance $L_{f.\,In}$ contrast, in the current-source configuration, the inductor serves as a DC current source. The current i_f flowing through this inductor is kept nearly constant to preserve the performance of the active filter.

The current-source inverter is interfaced with the grid via a second-order low-pass filter, consisting of an inductance L_f and a capacitance C_f. As a result, the active filter current i_f corresponds to the inverter output current, which is filtered by the LC filter with a natural frequency defined by:

$$f_0 = \frac{1}{2\pi}\sqrt{L_f C_f} \qquad \text{(II.1)}$$

The bandwidth of the active filter is therefore essentially dictated by the selection of L_f and C_f .These components can be appropriately dimensioned to attenuate the high-frequency switching harmonics generated by the inverter's power switches.

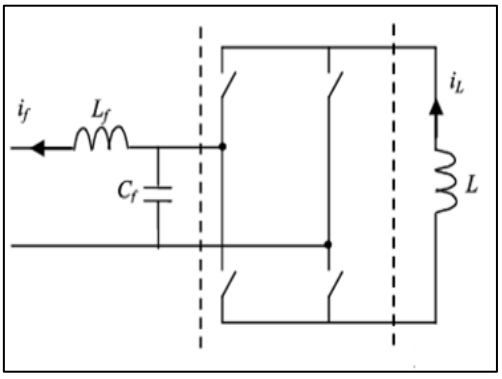

Figure. II.3 Single-phase current-source inverter

The switching devices used in this topology are unidirectional, meaning they conduct current in only one direction. They are composed of transistors that are actively controlled during both their turn-on and turn-off states. However, since these transistors are not capable of

withstanding reverse voltages, a diode must be connected in series with each switch to block any unwanted reverse conduction [44]. The complete structure of the current-source inverter incorporating these unidirectional switches is illustrated in Figure II.3 [45].

- **Comparison of Voltage-Source and Current-Source Inverter Structures**
  - **Sizing of Energy Storage Components**: In low-power applications, energy storage using a capacitor characteristic of the voltage-source configuration is generally more efficient and cost-effective. Conversely, for high-power systems, an inductive energy storage element, as used in the current-source configuration, is often more appropriate due to its ability to handle larger energy flows.
  - **Protection Considerations**: Voltage-source inverters require protection against over currents to safeguard the switching devices. In contrast, current-source inverters demand protection against over voltages, which presents greater technical complexity and implementation challenges.

Given these considerations, the voltage-source structure is better suited for low- and medium-power applications due to its simplicity, lower cost, and ease of implementation [45]. Therefore, this topology will be adopted in the remainder of this work [46].In active filtering, a voltage inverter interfaces an AC current source and a DC voltage source, necessitating that only one switch per arm be engaged to avert short-circuits of the voltage source, while diodes in antiparallel with the switches ensure continuous current flow from the current source; subsequently, we introduce three multilevel inverter topologies suitable for a three-phase filter.

II.2.2.1.1 Two-Level Inverter

This section elucidates the core operating principle of the three-phase two-level inverter, the predominant topology in low-voltage grid-connected applications. As depicted in Figure II.4(a) for a single-phase leg, the inverter topology equates to an ideal switch in series with two symmetric DC sources, each rated at $U_{DC/2}$. This arrangement enables the inverter to impose output voltage levels of $\pm U_{DC/2}$ across the load.

Figure II.4(b) illustrates the output voltage waveform of a single-phase two-level inverter under conventional pulse-width modulation (PWM). The PWM strategy generates switching states that track the sinusoidal reference U_{m1}. The abrupt transitions between DC levels yield a high *di/dt* in the output waveform, a hallmark of PWM-driven inverters.

$$U_{UM} = \begin{cases} +U_{DC}/2 \text{ for S} = +1 \\ -U_{DC}/2 \text{ for S} = -1 \end{cases} \quad \text{(II.2)}$$

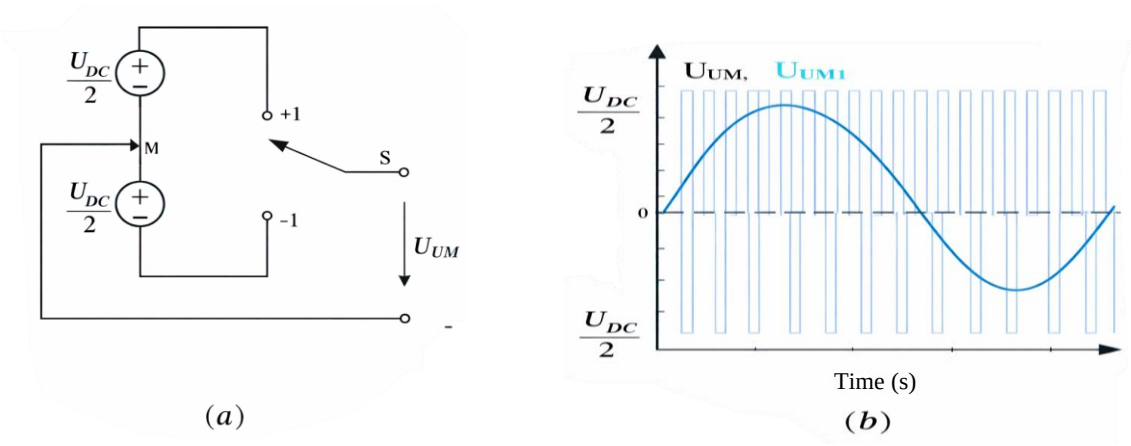

Figure. II.4 simplified model and produced output voltage for a two-level, single-phase inverter

In a three-phase two-level inverter with a shared DC link, the number of possible switching state combinations doubles compared to a single-phase configuration. Figure II.5 depicts the topology of such a three-phase inverter, where each phase comprises two insulated-gate bipolar transistors (IGBTs) connected in series, each equipped with an antiparallel diode.The DC-side configuration replaces the two discrete voltage sources with capacitors that store energy across the DC link, facilitating power transfer between the AC and DC sides.

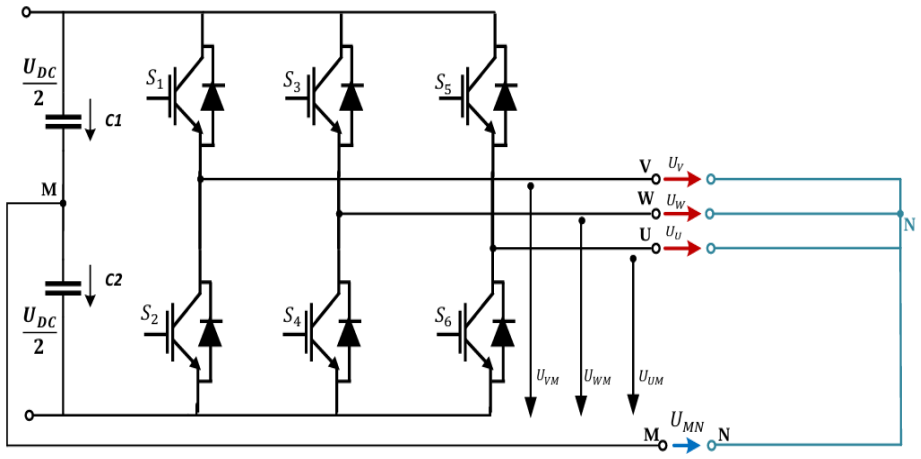

Figure. II.5 Circuit diagram of a three-phase two-level inverter system

The opening and closing of the switches in the inverter depicted in Figure II.5 are governed by the control signals (T1, T2, T3), as defined below:

$$T_1 = \begin{cases} 1, & S_1\ closed\ and\ S_4 open \\ 0, & S_1\ open\ and\ S_4 closed \end{cases}$$

$$T_2 = \begin{cases} 1, & S_2\ closed\ and\ S_5 open \\ 0, & S_2\ open\ and\ S_5 closed \end{cases} \qquad \text{(II.3)}$$

$$T_3 = \begin{cases} 1, & S_3\ closed\ and\ S_6 open \\ 0, & S_3\ open\ and\ S_6 closed \end{cases}$$

The connection between the three phases of a three-wire system can be characterized by expressing

the line voltages U_V, U_W, and U_U with respect to the neutral point *N*. In this context, the auxiliary voltage U_{MN} is obtained from the following relation:

$$U_{MN} = \frac{1}{2}(U_{VM} + U_{WM} + U_{UM}) \quad \text{(II.4)}$$

Table II.1 presents the eight possible switching states, along with the corresponding phase-to-neutral voltages U_V,U_W,*and* U_U, as well as the auxiliary voltage U_{MN}.

Table II. 1 Output voltage states of a three-phase two-level inverter

State	T1	T2	T3	U_V	U_W	U_U
0	0	0	0	0	0	0
1	0	0	1	$2U_{DC}/3$	$-1U_{DC}/3$	$-1U_{DC}/3$
2	0	1	0	$1U_{DC}/3$	$1U_{DC}/3$	$-2U_{DC}/3$
3	0	1	1	$-1U_{DC}/3$	$2U_{DC}/3$	$-1U_{DC}/3$
4	1	0	0	$-2U_{DC}/3$	$1U_{DC}/3$	$1U_{DC}/3$
5	1	0	1	$-1U_{DC}/3$	$-1U_{DC}/3$	$2U_{DC}/3$
6	1	1	0	$1U_{DC}/3$	$-2U_{DC}/3$	$1\ U_{DC}/3$
7	1	1	1	0	0	0

Although the three-phase two-level inverter has eight switching combinations, only seven different voltage levels appear at the output. This is because the switching states [0 0 0]and [1 1 1] both produce a zero output voltage vector. These two switching states are therefore called redundant states and play an important role in modulation and control strategies.

II.2.2.1.2 Topologies of Multi-Level Inverters

By increasing the number of levels in an inverter, the output voltage waveform becomes more refined, offering improved quality compared to that of conventional two-level inverters. Multilevel inverter applications have been extensively studied in the literature from an early stage, particularly involving topologies such as Neutral Point Clamped (NPC), Flying Capacitor, and cascaded H-bridge converters. Among these, the NPC structure remains the most widely adopted topology for active filtering applications, largely due to its relatively simple control especially in the case of three-level inverters, which we have focus in this chapter.

However, when extending beyond three levels, the control of multilevel inverters becomes significantly more complex and sensitive [47]. Below, we briefly present the main multilevel inverter topologies frequently referenced in the literature [48].

II.2.2.1.3 Cascaded H-bridge inverter

One of the earliest implementations of this topology was successfully carried out using polygonal inverters configured within an *N*-level leg, where *N* is an odd number most commonly 3. Each single-phase inverter module, indexed by *n*, is capable of generating three distinct output voltage levels: $-V_{dc}$, 0, and $+V_{dc}$. The output voltages produced by the individual inverter bridges are then combined through transformers to form the total output. Figure II.6 presents a single phase of a three-level cascaded H-bridge inverter.

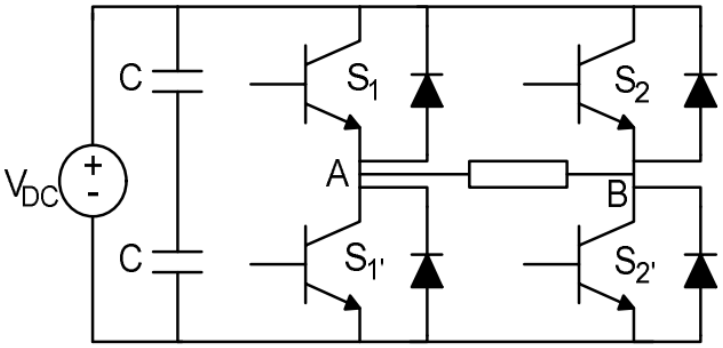

Figure. II.6 Three-level cascaded converter phase.

It is evident that, at any given moment, only one switch from each inverter leg (S1–S1′, S2–S2′) can be turned on to avoid short-circuit conditions. To facilitate the description of all possible switching states, binary indicators H_{xi} are introduced for each fundamental cell in phase *x* as defined below:

$$\boldsymbol{H_{xi}} = \begin{cases} \mathbf{0}\ \boldsymbol{S_{xi} = 0N}\ \ \boldsymbol{and\ S_{xi} = OFF} \\ \mathbf{1}, \boldsymbol{S_{xi} = OFF}\ \ \boldsymbol{and\ S_{xi} = 0N} \end{cases} \tag{II.5}$$

Accordingly, TABLE II.2 displays the three-level basic cell's potential switching configurations using this binary language.

Table II. 2 Switching States for a Single H-Bridge Cell

H_{x1}	H_{x2}	V_{AB}
0	0	**0**
0	1	$\mathbf{-V_{dc}}$
1	0	$\mathbf{V_{dc}}$
1	1	**0**

The fundamental cell used to construct multilevel cascaded converters is this three-level converter. It is simple to construct a multilayer cascaded converter by joining simple three-level cells in series.

II.2.2.1.4 Flying Capacitor Inverter

The Flying Capacitor Inverter (FCI), also known as the imbricated-cell multilevel inverter, is a prominent type of multilevel inverter topology. As the name suggests, it utilizes a series of "flying capacitors" to synthesize multiple voltage levels at its output. A typical structure of a three-phase, three-level Flying Capacitor Inverter (FCI) is shown in Figure II.7. The voltage over each capacitor in Figure II.7 is given by (II.3).

$$V_c=\frac{E}{n-1} \quad \text{(II.6)}$$

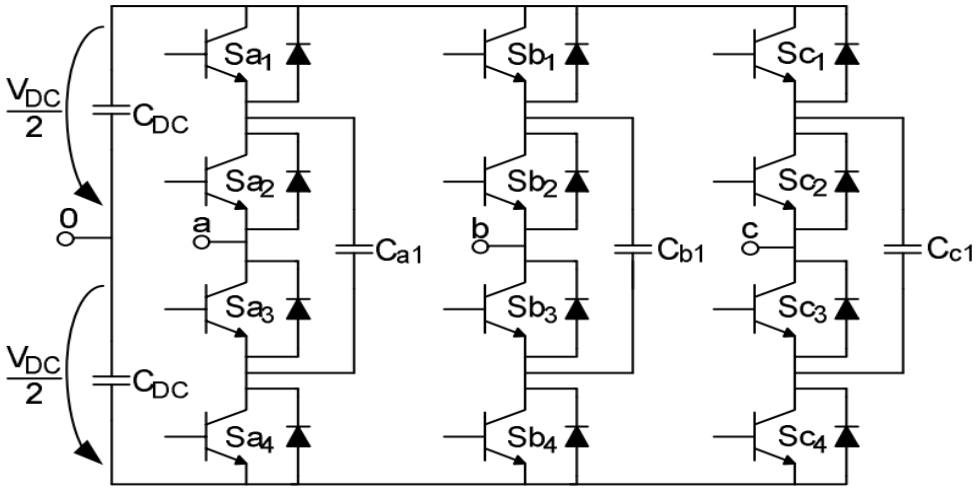

Figure. II.7 Conventional three-phase three-level Flying Capacitor Inverter

The two representations of an onduleur with condensator flottants are shown in the following figure.II.8:

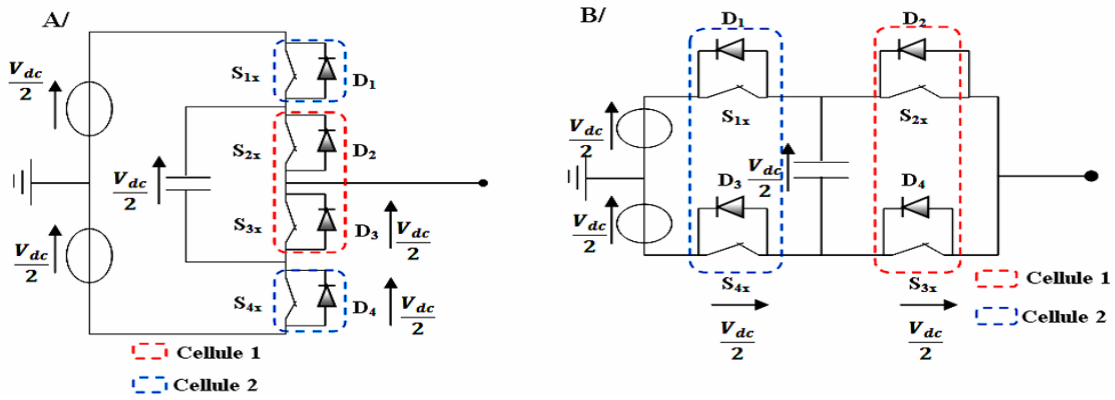

Figure. II.8 Condensator flottant bras d'onduleur (A) representation 1 (B) representation 2

Additionally, these capacitors serve a similar role to the clamping diodes used in the diode-clamped inverter. Their primary function is to maintain a constant voltage difference between the buses to which they are connected. For this reason, they are often referred to as clamping capacitors. The voltage expressed in equation (II.3) also represents the reverse voltage that each switch must withstand when all capacitors are fully charged, as can be confirmed by applying Kirchhoff's Voltage Law (KVL) to the circuit shown in Figure II.8.[49]

As with any inverter, certain switching configurations within the inverter legs are prohibited. For example, in a three-level inverter, switches S_2 and S_2' cannot be turned on simultaneously, as this would result in a short circuit across capacitor C_3. To prevent such conditions whether involving capacitors or DC sources the switches S_x and S_x' (where x refers to a generic switch number) must operate in complementary states [50].

Following this rule, the permissible switching states for an n-level inverter leg are defined as:

$$N_{conf} = 2^{n-1} \tag{II.7}$$

Naturally, the flying-capacitor inverter leg exhibits intra-phase redundancy, as the number of allowed switching configurations exceeds the number of possible output voltage levels. The switching table for the three-level inverter is presented in Table II.3.

Table II. 3 3-level flying-capacitor leg relationships between configurations and output voltages.

S_{x1}	S_{x2}	S_{x3}	S_{x4}	V_{AO}
1	1	0	0	V_{dc}
1	0	0	1	$V_{dc}/2$
0	1	1	0	$V_{dc}/2$
0	0	1	1	**0**

In general, for an *N*-level Flying Capacitor Inverter (FCI), when using the Optimized Flying Capacitor Balancing and Control Strategy (OFBCS) voltage ratio, the number of output voltage levels is limited to $N = M + 1$, where *M* is the number of cells

II.2.2.1.5 Neutral Point Clamped (NPC) inverter

In the 1980s, the power increase (raising voltage or current) of the converter was the main focus of power electronics issues. Actually, the primary focus of the researchers was on current source inverters in order to boost the current. But other authors started working on the notion of raising the voltage rather than the current. To do this, the writers were creating new converter topologies. A new neutral-point-clamped PWM inverter (NPC-PWM) was introduced in 1981 by A. Nabae, I. Takahashi [51]. Based on a modification of the traditional two-level converter topology, this converter was created.

The proposed modification to obtain a three-level converter involves adding two additional transistors per phase (see Figure II.9). In this new topology, each transistor experiences a maximum voltage stress of $V_{DC}/2$. Consequently, if these additional transistors have the same voltage ratings as those used in the two-level configuration, the DC-link voltage can be effectively doubled, reaching a value of $2V_{DC}$.

However, this converter topology introduces a challenge. When switches S_1 and S_2 are turned ON while S_3 and S_4 are OFF, the total DC-link voltage V_{DC} is expected to be evenly distributed across switches S_3 and S_4. However, there is no inherent mechanism in this circuit to ensure this voltage balancing.This issue is resolved through the introduction of clamping diodes. In each phase, two diodes are used to clamp and regulate the voltage across each transistor, ensuring proper voltage sharing.[52]

The final topology, shown in Figure II.9, represents the three-level Diode-Clamped Converter (DCC). In this configuration, the DC-link voltage is equally divided between capacitors C_1 and C_2, allowing stable operation and voltage balancing across the switching devices.

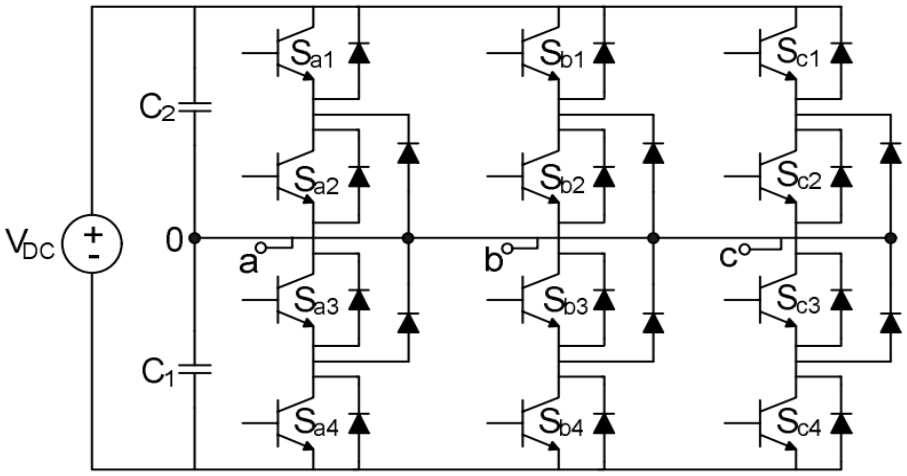

Figure. II.9 Three-level Diode-Clamped Inverter

The reason this topology is called a three-level inverter lies in its possible switching states. To explain this, the allowed switching configurations of the inverter can be examined.

In the three-level neutral-point-clamped inverter (NPC), only three valid switching configurations are permitted. Any other combination would either cause a short circuit across one of the DC-link capacitors or leave the output circuit open. For example, if switches S_1, S_2, and S_3 are turned ON simultaneously, capacitor C_2 would be short-circuited. Moreover, in such a case, the voltage across transistor S_4 would rise to V_{dc}, exceeding its maximum allowable voltage rating of $V_{dc}/2$.[53]

The permitted switching configurations are presented in Table II.4. These configurations allow the inverter to produce only three distinct output voltage levels with respect to the neutral point (the midpoint of the DC-link capacitors). This is the key reason why this topology is referred to as a "three-level inverter."

Table II. 4 Possible switching configurations in a three-level NPC

S_1	S_2	S_3	S_4	Phase-to-Neutral Voltage
1	1	0	0	$+V_{dc}/2$
0	1	1	0	0
0	0	1	1	$-V_{dc}/2$

In general, for an N-level Neutral-Point-diode-Clamped Inverter (NPC) topology, all valid switching configurations involve N−1 adjacent switches being turned ON in each phase. As a result, the possible output phase voltages with respect to the neutral point (0) take N discrete values, equally spaced within the voltage range from $-V_{dc}/2$ to $+V_{dc}/2$.

- **Technological Advantages of Multilevel Inverters**

Multilevel inverters (MLIs) offer significant technological advantages over traditional inverter systems, making them increasingly popular in various applications, particularly in high-power scenarios. Their design allows for improved power quality, efficiency, and reduced electromagnetic interference, which are critical in modern power systems. The following sections outline the key advantages of multilevel inverters.

- **Comparison of Multilevel Inverter Types**

Table II. 5 Comparative Analysis Supporting the Selection of the NPC Inverter

Criterion	Diode-Clamped Inverter (NPC)	Flying Capacitor Inverter	Cascaded H-Bridge Inverter
Structure	Uses clamping diodes to fix voltage levels	Uses capacitors for voltage levels	Series connection of H-bridge cells
DC Source	Single DC source	Single DC source	Multiple isolated DC sources
Voltage Levels	Limited (practically 3–5 levels)	Flexible but complex	Easily scalable (many levels)
Line Voltage Quality	Good (low THD)	Very good	Excellent (very low THD)
Power Capacity	High (suitable for medium/high power)	Medium	High (modular scaling)
Control Complexity	Moderate	High (capacitor balancing)	Moderate
Switching Losses	Low	Medium	Medium
Balancing Issue	Neutral point voltage balancing needed	Capacitor voltage balancing difficult	No balancing issue
Efficiency	High	Medium	High
Industrial Use	Widely used in industry	Limited use	Used in renewable systems

The NPC inverter offers a good compromise between performance, complexity, and cost**,** making it an ideal choice for medium- and high-power applications, compared to Flying Capacitor and Cascaded H-Bridge topologies.

II.2.2.1.6Analytical Model of a Three-Level NPC Inverter

To effectively generate the harmonic components necessary for offsetting those found in the load current or voltage, current-controlled voltage source inverters are frequently utilized. This study focuses on a three-level Neutral Point Clamped (NPC) multilevel inverter (as illustrated in Figure II.10), which presents numerous advantages over traditional two-level inverters, such as enhanced output waveform quality, diminished total harmonic distortion (THD), reduced voltage stress on power switches, and improved electromagnetic compatibility, all while employing a limited number of switching devices and a single DC-link capacitor for

energy storage, rendering it particularly adept for active power filtering applications.

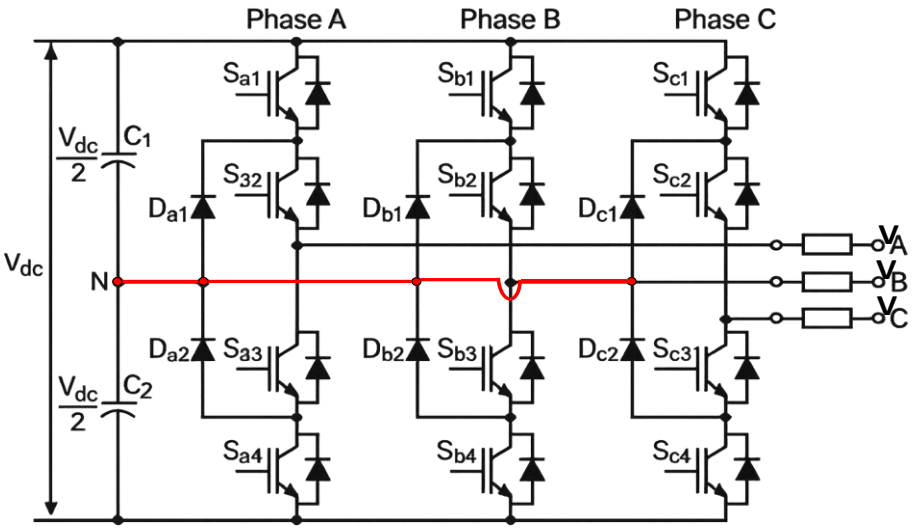

Figure. II.10 Structure of a three-phase, three-level Neutral Point Clamped (NPC) voltage-source inverter (VSI)

In a three-level Neutral Point Clamped (NPC) inverter, each phase leg consists of four power switches and two clamping diodes, resulting in a total of 12 switches and 6 diodes for a three phase system. The switches are unidirectional in voltage and bidirectional in current, allowing the inverter to produce three distinct voltage levels at the output of each phase: +Vdc/2, 0, and -Vdc/2. By controlling the switching sequences appropriately, the inverter delivers balanced alternating phase voltages (Va,Vb,Vc)

The state of each switch is defined by the control signals Sa, Sb, and Sc, as follows:

- In a three-level NPC inverter, each phase leg consists of four switches, typically labeled T_{x1}, T_{x2}, T_{x3}, and T_{x4}, where $x \in \{a,b,c\}$ corresponds to each phase. The control signals determine the output voltage level for each phase relative to the DC bus midpoint (neutral point).

The possible switching states and their corresponding output voltages are:

- 1 means the switch is ON, and 0 means OFF.
- The combination of these switches ensures that the output phase voltage v_x can take on three levels: $+V_{dc}/2$, 0, or $-V_{dc}/2$.
- The middle voltage level (O) is achieved by connecting the output to the neutral point through the clamping diodes.

Table II. 6 3-level inverter switching state

Switching State	**T_{x1}**	**T_{x2}**	**T_{x3}**	**T_{x4}**	**Output Voltage**
P	1	1	0	0	+Vdc/2
O	0	1	1	0	0
N	0	0	1	1	−Vdc/2

- **Functions of switch connections**

A function that characterizes the open or closed state of each T_x switch is known as the connection function:

$$\begin{cases} F_{ks} = 1 \ \ and\ TD_{ks} \ \ is\ closed \\ F_{ks} = 0 \ \ \ and\ TD_{ks} \ \ is\ open \end{cases} \quad \text{(II.8)}$$

By translating the complementary control into the switching functions of leg k (with *k*=1,2, and 3), we obtain:

$$\begin{cases} F_{k1} = 1 - F_{k4} \\ F_{k1} = 1 - F_{k3} \end{cases} \quad \text{(II.9)}$$

The complementary control is expressed for the three legs as follows:

$$\begin{cases} F_{11} = 1 - F_{14} \\ F_{12} = 1 - F_{13} \end{cases} \quad \begin{cases} F_{21} = 1 - F_{24} \\ F_{23} = 1 - F_{23} \end{cases} \quad \begin{cases} F_{31} = 1 - F_{34} \\ F_{32} = 1 - F_{33} \end{cases} \quad \text{(II.10)}$$

- **Connection Functions of the Half-Legs**

For the three-level inverter, the connection function of a half-leg is defined as F_{km} where:

k represents the leg number (k=1, 2, 3)

- m=0 refers to the upper half-leg,
- m=1 refers to the lower half-leg.

The connection functions of the half-legs are expressed in terms of the switching functions of the power switches as follows:

$$\begin{cases} F_{k1}^{b} = F_{k1}.F_{k2} \\ F_{k0}^{b} = F_{k3}.F_{k4} \end{cases} \quad \text{(II.11)}$$

- **Conversion Function**

Notation:

- V_A, V_B, V_C : Phase voltages at the terminals of the load.
- V_{AM}, V_{BM}, V_{CM}: Phase voltages of the inverter with respect to the DC-link midpoint "M".

The potentials at nodes A, B, and C of the inverter with respect to the midpoint M are

expressed using the switching functions of the power devices and the input DC voltages, as follows:

$$\begin{cases} V_{AM} = F_{11}F_{12}U_{c1} - F_{13}F_{14}U_{c2} \\ V_{BM} = F_{21}F_{22}U_{c1} - F_{23}F_{24}U_{c2} \\ V_{CM} = F_{31}F_{32}U_{c1} - F_{33}F_{34}U_{c2} \end{cases} \quad \text{(II.12)}$$

En définissant les fonctions de commutation pour chaque demi-bras, nous obtenons

$$\begin{cases} V_{AM} = {F_{11}}^{b}U_{c1} - {F_{10}}^{b}U_{c2} \\ V_{BM} = {F_{21}}^{b}U_{c1} - {F_{20}}^{b}U_{c2} \\ V_{CM} = {F_{31}}^{b}U_{c1} - {F_{30}}^{b}U_{c2} \end{cases} \quad \text{(II.13)}$$

The line-to-line voltages are expressed as follows:

$$\begin{cases} U_{AB} = V_{AM} - V_{BM} \\ U_{BC} = V_{BM} - V_{CM} \\ U_{CA} = V_{CM} - V_{AM} \end{cases} \quad \text{(II.14)}$$

Hence, the following matrix system expresses the line-to-line voltages in terms of the connection functions of the half-legs:

$$\begin{pmatrix} U_{AB} \\ U_{BC} \\ U_{CA} \end{pmatrix} = \begin{pmatrix} 1 & -1 & 0 \\ 0 & 1 & -1 \\ -1 & 0 & 1 \end{pmatrix} \left\{ \begin{pmatrix} {F_{11}}^{b} \\ {F_{21}}^{b} \\ {F_{31}}^{b} \end{pmatrix} . U_{c1} - \begin{pmatrix} {F_{10}}^{b} \\ {F_{20}}^{b} \\ {F_{30}}^{b} \end{pmatrix} . U_{c2} \right\} \quad \text{(II.15)}$$

The phase (line-to-neutral) voltages are derived as follows:

$$\begin{pmatrix} V_A \\ V_B \\ V_C \end{pmatrix} = \frac{1}{3} . \begin{pmatrix} 2 & -1 & -1 \\ -1 & 2 & -1 \\ -1 & -1 & 2 \end{pmatrix} \left\{ \begin{pmatrix} {F_{11}}^{b} \\ {F_{21}}^{b} \\ {F_{31}}^{b} \end{pmatrix} . U_{c1} - \begin{pmatrix} {F_{10}}^{b} \\ {F_{20}}^{b} \\ {F_{30}}^{b} \end{pmatrix} . U_{c2} \right\} \quad \text{(II.16)}$$

The input currents i_{d1} and i_{d2} are expressed in terms of the load currents i_1,i_2 and i_3 by the following relationships:

$$\begin{cases} i_{d1} = F_{11}F_{12}i_1 + F_{21}F_{22}i_2 + F_{31}F_{32}i_3 \\ i_{d2} = F_{13}F_{14}i_1 + F_{23}F_{24}i_2 + F_{33}F_{34}i_3 \end{cases} \quad \text{(II.17)}$$

From where

$$\begin{cases} i_{d1} = {F_{11}}^{b}i_1 + {F_{21}}^{b}i_2 + {F_{31}}^{b}i_3 \\ i_{d2} = {F_{10}}^{b}i_1 + {F_{20}}^{b}i_2 + {F_{30}}^{b}i_3 \end{cases} \quad \text{(II.18)}$$

Equation (II.13) shows that, for the three-level inverter, the behavior can be interpreted as if the current id1 were the input current of the upper two-level inverter, and i_{d2} the input current of the lower two-level inverter. Moreover, the current i_{d0} is related to the load currents as follows:

$$i_{d0} = F_{11}F_{13}i_1 + F_{21}F_{23}i_2 + F_{31}F_{33}i_3 \quad \text{(II.19)}$$

From equations (I.12) and (I.13), the expression of i_{d0} can be derived as follows:

$$i_{d0} = i_1 + i_2 + i_3 - i_{d1} - i_{d2} \quad \text{(II.20)}$$

Where from

$$i_{d0} = (1 - {F_{11}}^{b} - {F_{10}}^{b})i_1 + (1 - {F_{21}}^{b} - {F_{20}}^{b})i_2 + (1 - {F_{13}}^{b} - {F_{30}}^{b})i_3 \quad \text{(II.21)}$$

II.2.2.1.7 Active Power Filter Model

The inverter output is connected to the grid through a first-order passive filter, consisting of an inductance L_f and a resistance R_f, which serves to attenuate high-frequency switching components and smooth the injected current. As illustrated in Figure II.9, the equivalent circuit of the system comprises a shunt active power filter (SAPF) connected in parallel with both an unbalanced non-linear load (UNLL) and the utility grid, which acts as the energy source [54] . Applying Kirchhoff's voltage law to this circuit results in the following mathematical expressions:

$$\begin{aligned} V_g - V_{PCC} &= R_g i_g + L_g \frac{di_g}{dt} \\ V_f - V_{PCC} &= R_f i_f + L_f \frac{di_f}{dt} \end{aligned} \quad \text{(II.22)}$$

The network (R_g) and filter (R_f) resistances are relatively small, which allows us to neglect their influence. Subtracting equation (II.19) from equation (II.19), we obtain the following expression:

$$V_g - V_f = L_g \frac{di_g}{dt} - L_f \frac{di_f}{dt} \quad \text{(II.23)}$$

The UNLL's current consists of two separate elements: the basic element denoted by i_{lf} and the harmonic element identified as i_{lh}.

$$i_l = i_{l,f} + i_{l,h} \quad \text{(II.24)}$$

while from Figure (II.11) the relationship between filter current, grid current and load current is

$$i_l = i_f + i_g \quad \text{(II.25)}$$

Using equation (II.21) and equation (II.22) we obtain:

$$i_{l,f} + i_{l,h} = i_f + i_g \quad \text{(II.26)}$$

Consequently, it is possible to write that

$$i_{l,h} - i_f = -(i_{l,f} - i_g) \Rightarrow \Delta i_f = -\Delta i_g \quad \text{(II.27)}$$

For small current changes, we can approximate Δi to approximately equal to di. Equation (II.24) can then be written as

$$di_g = -di_f \quad \text{(II.28)}$$

Upon substituting Equation (II.23) into Equation (II.25), the resultant equation can be rewritten as follows:

$$V_f - V_g = L_t \frac{di_f}{dt} \;\; where\,, L_t = (L_f + L_g) \quad \text{(II.29)}$$

To predict the filter current $i^p_{f,abc}$ (k+1) using actual measurements i_f(k), V_g(k), and V_f(k), it is important to employ a discrete-time model. By applying the same derivative approximation

strategy as outlined in Equation (II.25), the resulting relationship can be expressed as follows:

$$\frac{di_f}{dt} \approx \frac{\Delta i_f}{\Delta t} = \frac{i_f(k+1)-i_f(k)}{T_s} \quad \text{(II.30)}$$

By substituting Equation (II.26) into Equation (II.27), the prediction law is derived, resulting in the following expression for the APF compensating current:

$$\begin{aligned} i_{fa}^{p}(k+1) &= i_{fa}(k) + \frac{T_s}{L_t}(V_{fa}(k) - V_{ga}(k)) \\ i_{fb}^{p}(k+1) &= i_{fb}(k) + \frac{T_s}{L_t}(V_{fb}(k) - V_{gb}(k)) \\ i_{fc}^{p}(k+1) &= i_{fc}(k) + \frac{T_s}{L_t}(V_{fc}(k) - V_{gc}(k)) \end{aligned} \quad \text{(II.31)}$$

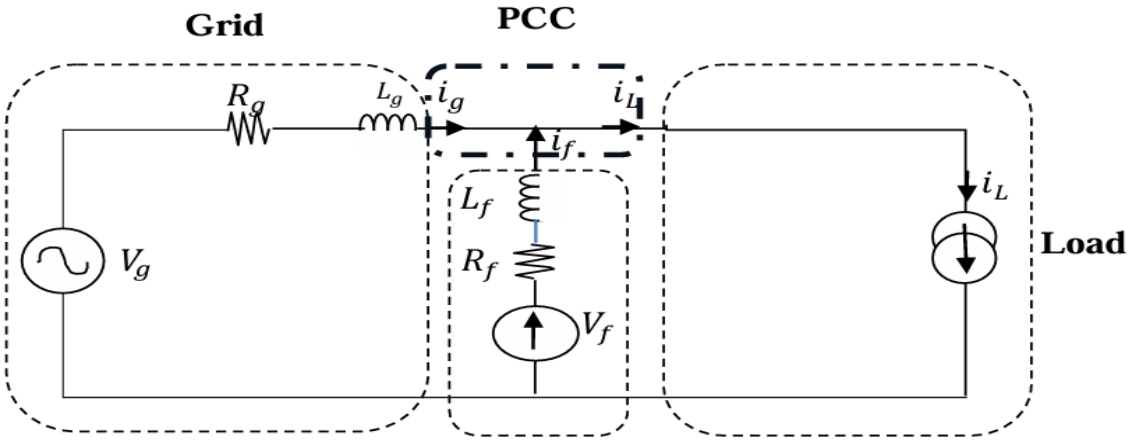

Figure. II.10 An equivalent circuit featuring an Active Power Filter (APF) connected in parallel.

II.2.2.2 Energy Storage System

The capacitor C_{dc} functions as a DC voltage source, with the voltage across its terminals, V_{dc}, maintained nearly constant through a regulation mechanism. The selected DC voltage level and the capacitance value critically influence the dynamics and compensation effectiveness of the parallel active filter. Higher V_{dc} values enhance the filter's dynamic response. However, voltage ripples in V_{dc}, caused by currents generated by the active filter and limited by C_{dc}, can deteriorate the compensation quality. Such fluctuations become more pronounced with larger filter current amplitudes and lower frequencies. It is imperative to keep these ripples minimal to prevent exceeding semiconductor voltage ratings and to preserve filter performance. Consequently, when designing the energy storage parameters, typically only the first harmonic components are considered. [55]Various methods have been proposed in the literature to determine the appropriate DC bus capacitance. One notable approach calculates the energy balance between that supplied by the active filter and that consumed by the nonlinear load, providing a basis for capacitor sizing and ensuring stable DC voltage regulation. This careful design is essential for optimizing both the dynamic behavior and the harmonic compensation capabilities of the parallel active power filter.[56]

The magnitudes of the AC load currents in the three phases are given by:

$$\sqrt{\frac{1}{2\pi}\int_0^{2\pi} I_d^2 \, d\omega t} = I_d \quad \text{(II.32)}$$

Here, I_d denotes the DC-side load current. The fundamental component of the load current is expressed as:

$$I_{s1} = \frac{2\sqrt{2}}{\pi} I_s = 0.9 I_d \quad \text{(II.33)}$$

The harmonic currents generated by the load correspond to the difference between the fundamental component and the total RMS value of the load's alternating current. These harmonic currents are defined as follows:

$$\sum_{i=2}^{\infty} I_{si} = (I_s^2 - I_{s1}^2) = 0.43 I_s \quad \text{(II.34)}$$

The active filter is required to supply power that compensates for the harmonics generated by the load. By selecting the capacitor voltage ripple period to be one-sixth of the mains voltage period, the following relationship can be established:

$$C_{dc} \geq \frac{0.43 I_s}{6f(V_{dc\,max}^2 - V_{dc\,\min}^2)} \quad \text{(II.35)}$$

f_s represents the fundamental frequency of the electrical network. A permissible ripple rate for V_{dc} is typically selected, commonly around 2% of V_{dc}. An alternative, simpler approach involves measuring the lowest harmonic current I_h. Using this measurement, the C_{dc} capacitance can be calculated as follows [57][58]:

$$C_{dc} = \frac{I_h}{V_{dc}\Delta V_{dc}\omega_h} \quad \text{(II.36)}$$

ω_h: the angular frequency of the lowest harmonic to be compensated.

The following Table II.7 summarizes the influence of the parameters L_f, C_{dc}, and V_{dc} on the behavior of the parallel active power filter (FAP) [59]:

Table II. 7 summarizes the influence of the parameters

Parameter	**Influence on FAP Behavior**
L_f	Determines the filtering of high-frequency switching harmonics; smaller values improve dynamic response and allow higher surge and harmonic currents but may increase ripple currents. Larger inductance reduces ripple but can slow response time.
C_{dc}	Affects the DC bus voltage ripple and energy storage capability. Larger capacitance reduces voltage ripple, improving compensation quality and stability, especially under large or low-frequency filter currents. However, excessively large capacitance can increase size and cost.

V_{dc}	Sets the DC link voltage level, influencing the active filter's dynamic performance. Higher V_{dc} improves dynamic response but can increase the voltage stress on semiconductor devices and the magnitude of voltage ripples.

This table reflects the trade-offs in selecting these key parameters to optimize the active filter's performance, including compensation quality, dynamic behavior, and device stress[60].

II.2.2.3 Coupling Filter

The coupling filter is the passive filter placed between the inverter and the grid, typically consisting of a first-order inductor with internal resistance, often enhanced by ferrite cores to improve magnetic characteristics. It serves two primary functions: first, it produces harmonic currents due to the voltage difference between the inverter output and the grid, with the inductor L_f playing a crucial role in regulating the filter current; second, it reduces the amplitude of the voltage pulses injected at the grid connection point (GCP), thereby smoothing the voltage waveform.[61] The sizing of this passive coupling filter is guided by two key criteria related to controlling harmonic emissions and limiting voltage ripple to meet grid standards.

Ensure the dynamics of the filter current by:

$$\frac{di_f}{dt} = \frac{di_h}{dt} \quad \text{(II.37)}$$

with

i_f: Filter current

i_h: Load harmonic current

Prevent switching-related components from propagating into the electrical grid.

A small inductance value in the passive filter enhances current dynamics, while a relatively large inductance helps prevent switching harmonics from propagating into the network. A comparative analysis of five different methods for determining the value of L_f is presented in [62].

Below, two approaches for determining L_f are presented. By neglecting the resistance of the coupling filter, we derive:

$$\left(\frac{di_f}{dt}\right)_{max} = \frac{V_{fmax} - V_{smax}}{L_f} \quad \text{(II.38)}$$

V_{fmax}: the maximum voltage at the inverter input

V_{smax}: the maximum phase-to-neutral voltage at the filter connection point

For small variations in the filter current, we have:

$$\frac{\Delta i_f}{\Delta T} = \frac{V_{fmax} - V_{smax}}{L_f} \quad \text{(II.39)}$$

$\Delta T = \frac{1}{fond}$:The period of variation of the filter current. Assuming that the maximum change in the filter current is 25% of the maximum network current, the coupling inductance is calculated as follows [63]:

$$L_f = \frac{V_{fmax} - V_{smax}}{0.25 i_{smax} f_{ond}} \quad \text{(II.40)}$$

The sizing of L_f can be performed under the constraint that, for a given switching frequency, the slope of the filter current i_f remains lower than the slope of the triangular carrier waveform that defines this switching frequency. The slope of the triangular carrier is expressed as:

$$\alpha = 4.\epsilon.f_c \quad \text{(II.41)}$$

Where:

- ε is the amplitude of the triangular wave,
- f_c is the switching frequency of the active filter switches.

The maximum slope of i_f for a mid-point reactive filter is expressed as:

$$\frac{di_f}{dt} = \frac{0.5V_{dc} + V_{sm}}{L_f} \quad \text{(II.42)}$$

With an estimated value of L_f as provided in [64] and [65]:

$$L_f = \frac{0.5V_{dc} + V_{sm}}{4.\epsilon.f_c} \quad \text{(II.43)}$$

II.2.3 Study of the control-command part

The control system plays a crucial role in the performance of a parallel active filter. Its primary objective is to compensate for the harmonic currents generated by nonlinear loads by producing and injecting harmonic currents that accurately track their reference signals in real time. The first step, therefore, involves accurately determining these reference harmonic currents. To achieve this, the control system can be structured into the following functional components:

1. Harmonic Current Identification Circuit.
2. Phase-Locked Loop (PLL) Synchronization.
3. DC-Link Voltage Regulation.
4. Inverter Switching Control.

This systematic control approach ensures optimal filtering performance, reliable operation, and effective harmonic mitigation in the electrical network.

II.2.3.1 Methods for identifying disturbed currents

The fundamental role of an active power filter (APF) lies in its ability to accurately and rapidly determine the reference currents required for injection into the grid, thereby compensating for power quality issues. These reference currents precisely represent the harmonic and reactive components that need to be eliminated from the system [66].

Numerous algorithms and techniques have been developed for extracting these reference currents, broadly categorized into time-domain and frequency-domain methods. Figure II.12 illustrates these harmonic current identification methods, grouping them into these two main families.

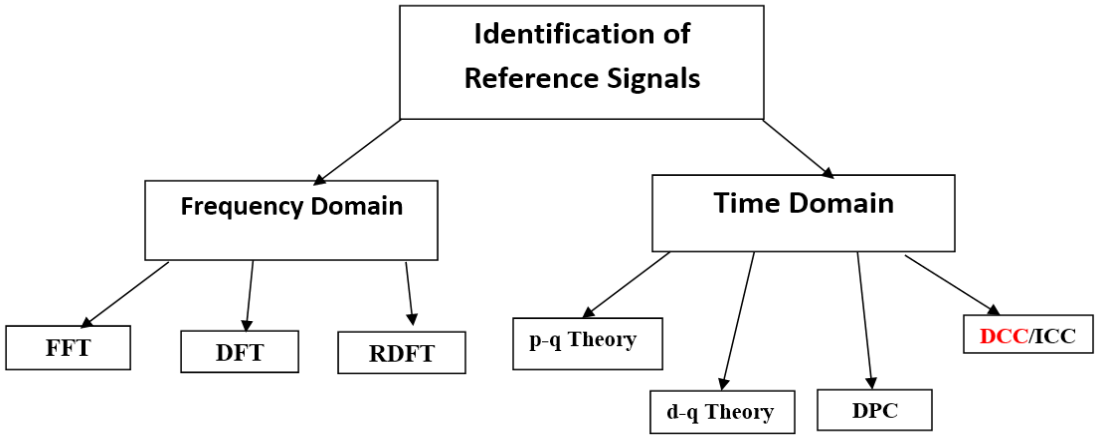

Figure. II.11 Different Harmonic Current Identification Methods

A comparative analysis of these methods is summarized in Table II.8, highlighting their main characteristics in terms of complexity, dynamic response, and suitability for real-time implementation.

Table II. 8 Comparison of Harmonic Current Identification Methods

Method	Domain	Principle	Advantages	Limitations	Suitability for Real-Time Control
FFT / DFT / RDFT	Frequency Domain	Signal decomposition into harmonics	✓Accurate harmonic analysis	High computation time, delay	Not suitable
p–q Theory	Time Domain	Instantaneous power calculation (α-β frame)	✓Good for balanced systems	Sensitive to distortions and unbalance	Moderate
d–q Theory	Time Domain	Transformation to rotating reference frame	✓Good steady-state performance	Requires PLL, slower dynamic response	Moderate
DPC (Direct Power Control)	Time Domain	Direct control of active/reactive power	✓Fast response	Variable switching frequency, ripple	Moderate
DCC (Direct Current Control)	Time Domain	Direct control of grid/inverter current	✓Fast dynamic ✓response Simple implementation ✓ High accuracy ✓ Fixed switching frequency	Requires current measurement	Highly suitable

This study focuses on a key harmonic current identification algorithm applied to a three-phase, three-level NPC inverter controlled by PWM: the Direct Current Control (DCC) method. This algorithm relies on specific formulations, derived either from power theory or direct current measurements, to accurately generate the reference harmonic currents required for effective compensation

II.2.3.1.1 Direct Current Method (DCC)

The Direct Current Control (DCC) method is a straightforward and effective approach for generating reference currents in parallel active power filters. It employs a Phase-Locked Loop (PLL) to synchronize with the grid voltage, ensuring accurate phase tracking. A DC voltage regulator is then used to establish the peak value of the source current. This peak current is multiplied by sinusoidal signals derived from the PLL to produce the sinusoidal reference source currents required for compensation. This method enables simple implementation and reliable generation of reference currents for active filtering applications.[67]

The simplified mathematical framework facilitates straightforward real-time application,

with the three source voltages provided by a PLL articulated as follows:

$$v_{sa}^{*}(t) = \sin(\omega t)$$
$$v_{sb}^{*}(t) = \sin(\omega t - 120) \quad \text{(II.44)}$$
$$v_{sc}^{*}(t) = \sin(\omega t - 240)$$

The source current at the Point of Common Coupling (PCC) can be expressed as:

$$i_{s_{(t)}} = i_{L_{(t)}} - i_{f_{(t)}} \quad \text{(II.45)}$$

Here, $i_s(t)$ the source current, $i_L(t)$, load current, and $i_f(t)$ filter current.

Using Fourier series expansion, the load current can be expressed in the following form:

$$i_{L_{(t)}} = \sum_{n=1}^{\infty} I_n \, sin(n\omega t + \varphi_n) = I_1 \, sin(\omega t + \varphi_1) + \sum_{n=2}^{\infty} I_n \, sin(n\omega t + \varphi_n) \quad \text{(II.46)}$$

Here, In and φ_n represent the amplitude and phase angle of the nth harmonic current, while I_1 and φ_1 denote the amplitude and phase angle of the fundamental current.

The instantaneous load power can thus be defined as

$$p_{L_{(t)}} = v_{s_{(t)}} * i_{L_{(t)}} = V_m I_1 \, sin^2(\omega t) \times cos(\varphi_1) + V_m I_1 \, sin(\omega t) \times cos(\omega t) \times sin(\varphi_1)$$
$$+ V_m \, sin(\omega t) \times \sum_{n=2}^{\infty} I_m \, sin(n\omega t + \varphi_n) \quad \text{(II.47)}$$

The instantaneous load power can therefore be decomposed as follows:

$$p_{L_{(t)}} = p_{fun_{(t)}} + p_{r_{(t)}} + p_{h_{(t)}} \quad \text{(II.48)}$$

where:

- $p_{fun}(t)$is the fundamental active power,
- $p_r(t)$ is the reactive power,
- $p_h(t)$ is the harmonic power.

Based on the previous equations, the fundamental power of the nonlinear load can be determined as follows:

$$p_f(t) = V_m I_1 \, sin^2(\omega t) * cos(\varphi_1) = v_s(t) * i_s(t) \quad \text{(II.49)}$$

Therefore, after compensation, the source current can be expressed as:

$$i_{s_{(t)}} = \frac{p_{fun_{(t)}}}{v_{s_{(t)}}} = I_1 \, cos(\varphi_1) * sin(\omega t) = I_{sm} \, sin(\omega t) \quad \text{(II.50)}$$

Where:

$$i_s(t) = I_{sm} \sin(\omega t) \quad \text{(II.51)}$$

There is also switching losses in the inverter

$$I_{sp} = I_{sm} + I_{sl} \quad \text{(II.52)}$$

Where: I_{sp} The total peak current supplied by the source.

The source current is(t) should be sinusoidal and in phase with the source voltage.

The filter current supplied by the SAPF is given by:

$$i_{f_{(t)}} = i_{L_{(t)}} - i_{s_{(t)}} \quad \text{(II.53)}$$

Finally, the three source currents after compensation are expressed as follows:

$$\begin{aligned} i_{sa}^{*}(t) &= I_{sp}\sin(\omega t) \\ i_{sb=}^{*} I_{sp}\sin(\omega t - 120^{\circ}) \\ i_{sc=}^{*} I_{sp}\sin(\omega t + 120^{\circ}) \end{aligned} \quad \text{(II.54)}$$

The aforementioned identification algorithm is encapsulated in the block diagram presented in Figure II.13.

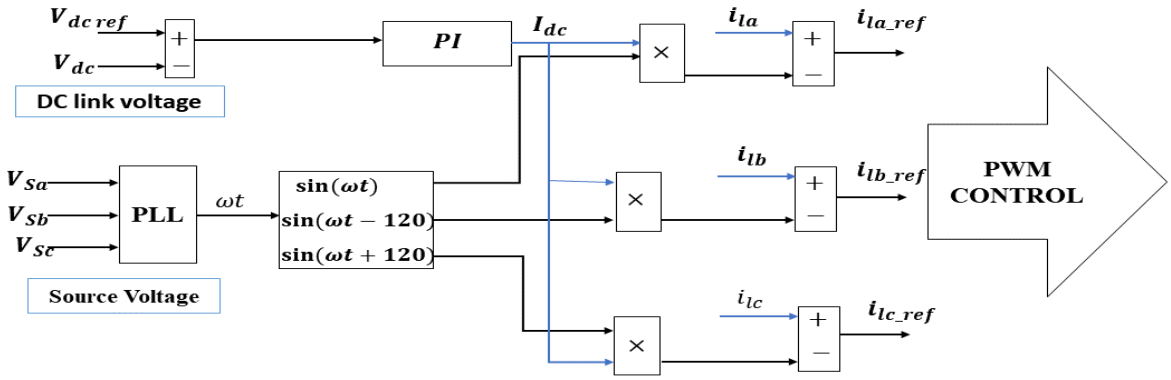

Figure. II.12 Design of the Direct Current Control (DCC) system.

II.2.3.2 The PLL-Based System

A Phase-Locked Loop (PLL) is employed to detect the phase angle of the power grid voltage. Its schematic diagram is illustrated in the figure.II.14 below. The loop achieves lock when the estimated angle matches the actual voltage phase.[68]

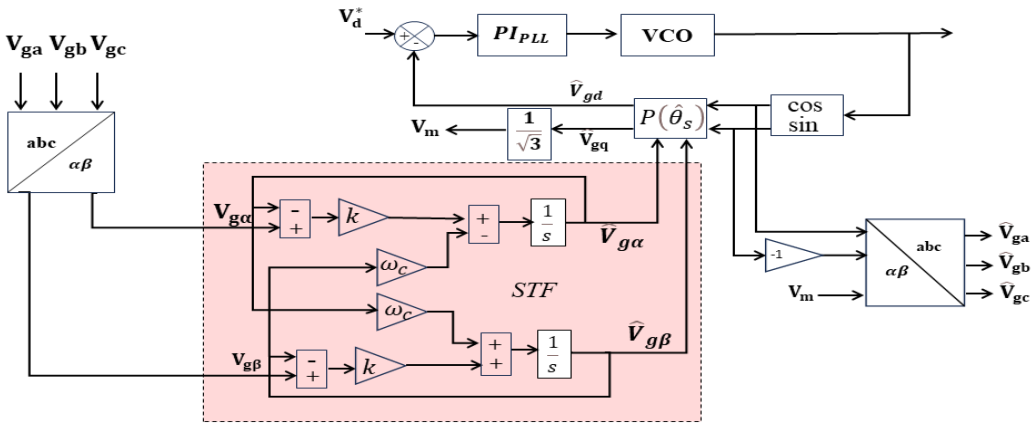

Figure. II.13 Schéma fonctionnel de PLL

II.2.3.3 The Regulation of the DC-Bus

Assuming that the losses in the inverter and the coupling filter are negligible, the relationship between the power absorbed by the capacitor and the voltage across its terminals can be expressed as:

$$P_{dc} = \frac{dE_{dc}}{dt} = \frac{d}{dt}(\frac{1}{2}C_{dc}v_{dc}^2) \quad \text{(II.55)}$$

Applying the Laplace transform to this relationship yields:

$$P_{dc}(s) = \frac{1}{2}C_{dc}v_{dc}^2 \quad \text{(II.56)}$$

The square of the voltage across the capacitor is expressed as:

$$v_{dc}^2 = \frac{2P_{dc}(s)}{C_{dc}} \quad \text{(II.57)}$$

The DC link control scheme is shown in Figure (II.15), where the PI controller coefficients are tuned to achieve a minimal response time, ensuring that the dynamics of the active filter remain unaffected.[69]

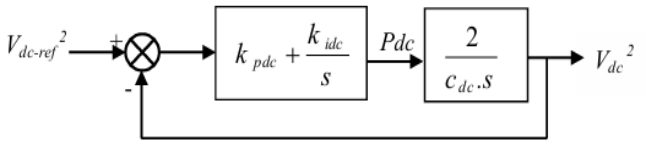

Figure. II.14 DC Voltage Control Loop

According to Figure (II.15), the transfer function of the DC voltage control loop is expressed as:

$$G_{vdc} = \frac{1+s.\frac{K_{pdc}}{K_{idc}}}{2s+2\frac{K_{pdc}}{C_{dc}}+2\frac{K_{idc}}{C_{dc}}} \quad \text{(II.58)}$$

Using the second-order transfer function presented in equation (II.66), we obtain:

$$K_{pdc} = \xi\sqrt{2C_{dc}K_{idc}} \quad \text{(II.59)}$$

$$K_{idc} = \frac{1}{2}C_{dc}w_c^2 \quad \text{(II.60)}$$

II.2.3.4 Active Filter Inverter Control Techniques

The selection and performance of the inverter control strategy are directly related to the efficacy of an active filter, especially in lowering the total harmonic distortion (THD) of the source current. Multilevel inverters are significantly impacted by the modulation or control technique, which uses reference and carrier signals to regulate the switching of semiconductor devices. Although there are numerous control techniques,[70] the two primary control families are:

- hysteresis control.
- pulse width modulation control.

II.2.3.4.1 Pulse Width Modulation (PWM) Control

The PWM control principle is explained in Figure II.16. The difference between the

reference current, i_f^* and the actual current, i_f, is produced by this control. A regulator's input will subsequently be subjected to this error. The switching commands for the switches will be determined by comparing the modulator, the regulator's output signal, with the carrier, a triangular signal with a fixed frequency. Since the carrier signal has a set frequency, the power semiconductors' switching frequency is likewise set.[73] Natural sampling PWM, sometimes referred to as intersecting PWM, is without a doubt the most straightforward and well-known type of pulse width modulation.

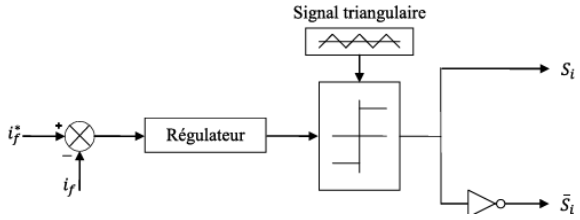

Figure. II.15 Principle of current control by PWM.

Finally, for the rest of our study, we selected the natural sampling PWM control technique. This method corresponds to analog PWM and is well-suited for the simulation phase due to its straightforward modeling and implementation.

- **Principle of PWM Inverters**

The semiconductor devices used in PWM inverters are fully controllable for switching on and off and are equipped with antiparallel diodes. Typically, either analog or digital control techniques are employed to determine the precise switching instants in real time. As a result, the inverter output voltage consists of a series of pulses generated by the controlled opening and closing of the power switches.[74]

Key parameters in PWM control include:

- The modulation frequency f_p.
- f: is the fundamental frequency of the inverter output quantities
- The modulation index m: which is defined as the ratio of the carrier frequency to the modulating frequency.

$$m=f_p/f \quad \text{(II.61)}$$

A higher modulation index generally indicates more effective harmonic cancellation.

The adjustment coefficient r: is defined as the ratio of the modulating amplitude to the unmodulated carrier amplitude.

$$r=A_r/A_p \quad \text{(II.62)}$$

This ratio should never be equal to 1; adequate time must be maintained for the on and off

intervals of the switches within the same arm.

II.3 Simulation results

In this study, simulations of a three-level Neutral Point Clamped (NPC) shunt active power filter (SAPF), controlled using the Direct Current Control Pulse Width Modulation (DCC-PWM) technique, were carried out in MATLAB/Simulink.

As shown in Figure II.17, before the application of compensation, the three-phase supply voltage remains almost sinusoidal and balanced; however, the load current is highly distorted due to the presence of a nonlinear load. This distortion is clearly reflected in the harmonic spectrum, where several low-order harmonics are observed. The corresponding Total Harmonic Distortion (THD) of the load current reaches approximately 27.80%, which represents a very high distortion level and largely exceeds the limits recommended by power quality standards such as IEEE 519. These results clearly confirm the necessity of an effective compensation strategy to reduce harmonic pollution and improve the overall quality of the electrical system.

Figure 18 illustrates the voltage and current waveforms after compensation using a two-level inverter. The load current waveform is nearly sinusoidal, demonstrating that the active power filter effectively mitigates harmonics. The total harmonic distortion (THD) of the current is reduced to 1.33%, showing excellent harmonic compensation performance. The voltage waveform remains stable, confirming that the active filter primarily targets current harmonics without distorting the supply voltage. These results indicate that even with a two-level inverter, the proposed compensation strategy can achieve significant harmonic reduction in grid-connected systems.

Figure II.19 illustrates the simulation results after compensation using the three-level NPC inverter. The source voltage remains purely sinusoidal, while the load current is highly distorted due to the nonlinear nature of the load. Once the shunt active power filter is activated, the injected compensation current effectively cancels the harmonic components, leading to a nearly sinusoidal source current that is well synchronized with the grid voltage. The harmonic spectrum confirms the effectiveness of the proposed approach, showing a dominant fundamental component at 50 Hz with an amplitude of 5.057 A and a reduced Total Harmonic Distortion (THD) of 1.14%, which satisfies IEEE 519 requirements and demonstrates the superior harmonic mitigation capability of the three-level inverter topology. This demonstrates that the multilevel inverter provides superior switching resolution and significantly reduced ripple compared to conventional two-level architectures. In comparison, the two-level inverter achieves a THD of 1.33%, indicating that the three-level NPC inverter delivers smoother

currents, lower ripple, and better overall performance for high-quality grid-connected applications.

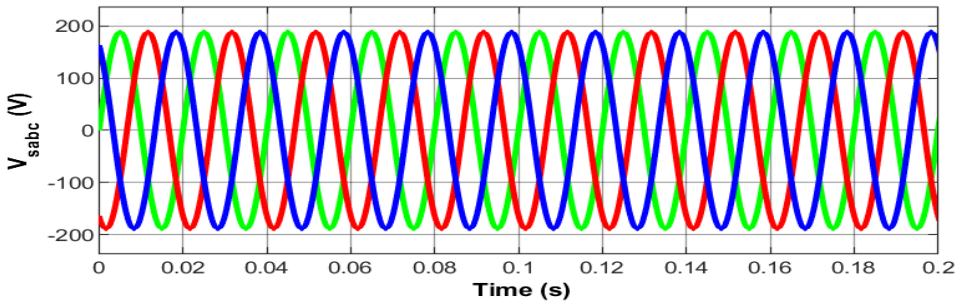

(a)

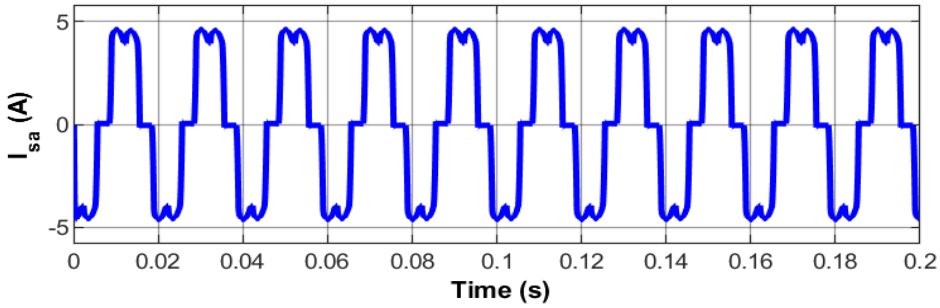

(b)

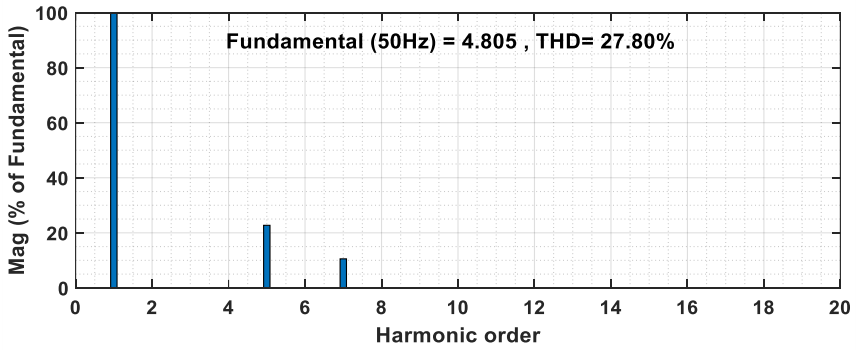

(c)

Figure. II.16 (a) Voltage, (b) current, and (c) THD waveforms before compensation

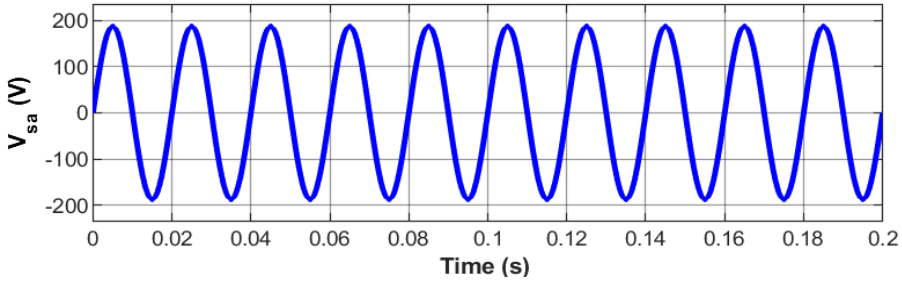

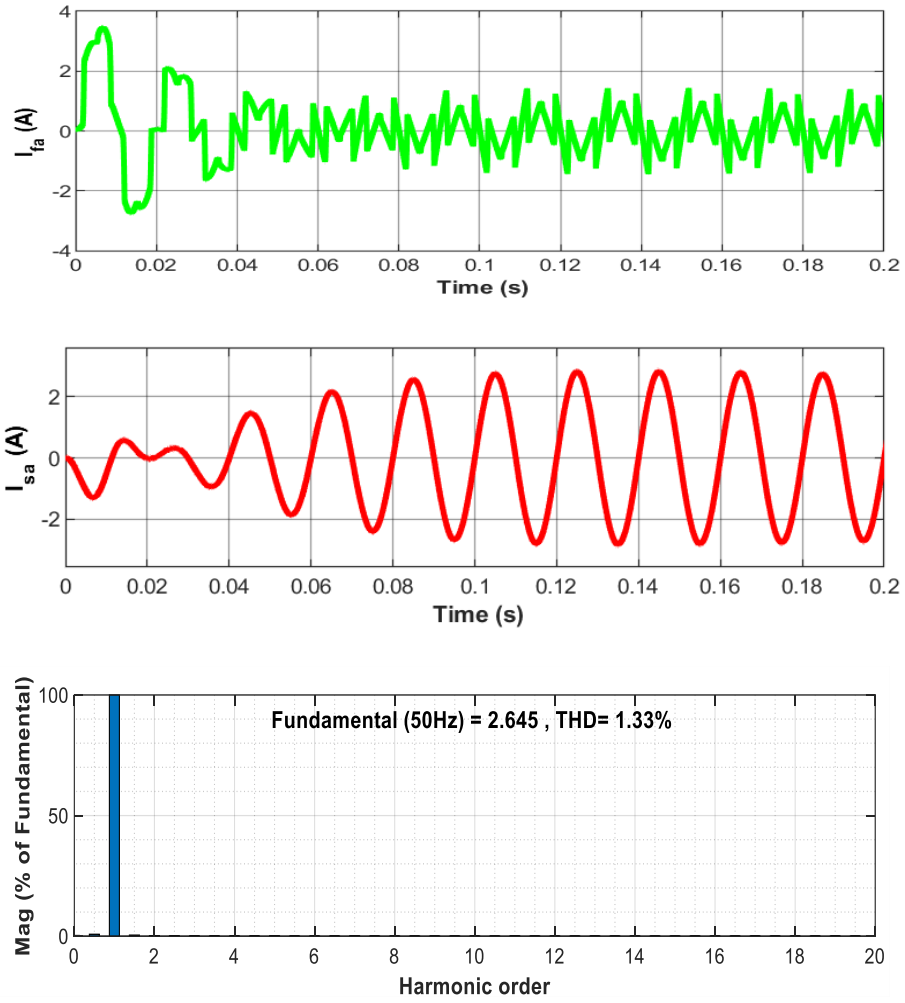

Figure. II.17 Results after compensation using 2-level inverter

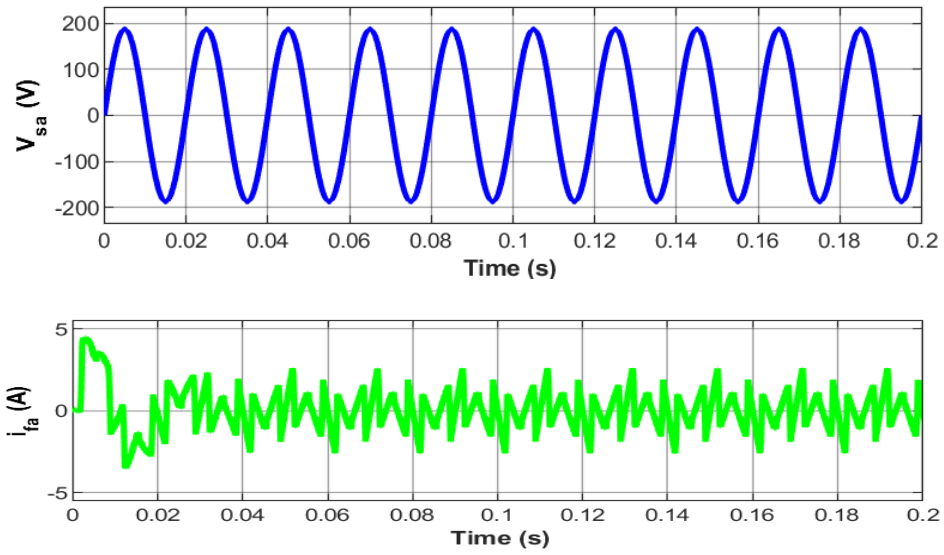

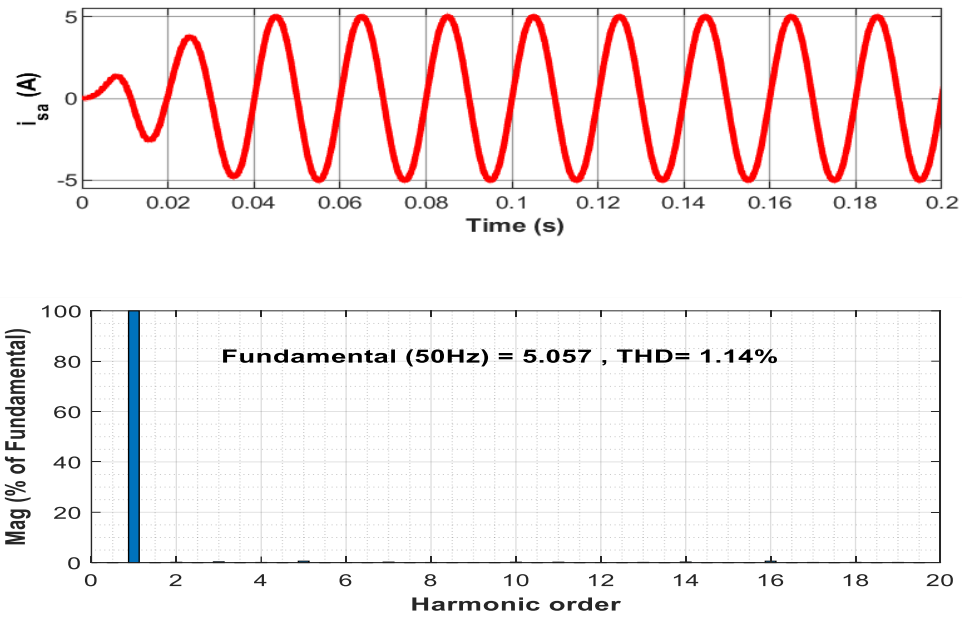

Figure. II.18 Results after compensation using 3-level inverter

II.4. Conclusion

This chapter has presented the modeling of a multilevel shunt active power filter based on a three-level Neutral Point Clamped (NPC) inverter. The system was described through its main elements: the power stage, including the inverter, coupling filter, and DC-link capacitor, and the control stage, which governs the generation of compensation currents. The Direct Current Control (DCC) PWM technique was applied to track the reference currents, enabling both harmonic mitigation and reactive power compensation.

These results highlight the potential of multilevel Shunt Active Power Filters for improving power quality in modern electrical systems. The enhanced performance of the three-level NPC inverter is particularly beneficial in applications involving renewable energy sources, where maintaining low harmonic distortion, stable voltage, and efficient power flow is essential. Incorporating such advanced filtering techniques ensures that grid-connected renewable systems can operate reliably and contribute effectively to sustainable and high-quality energy networks.

Chapter III

Photovoltaic-Supported Three-Level Active Power Filter

III.1 Introduction

In recent years, solar energy has gained significant attention and has become one of the most important and promising sources of electrical power across various sectors, thanks to the abundance of sunlight and its environmentally friendly nature. Photovoltaic (PV) systems are particularly utilized in rural or isolated areas where public electricity access is limited or unavailable. Advances in semiconductor technologies and photovoltaic cell materials have played a major role in accelerating the adoption of this renewable energy source. One of the main challenges in PV systems is extracting the maximum available solar energy, given that the system's efficiency is highly dependent on solar irradiance and ambient temperature. This has led to the development of real-time maximum power point tracking (MPPT) techniques to optimize energy conversion. However, due to the widespread presence of nonlinear loads in modern power networks, grid-connected PV systems are increasingly being designed not only to inject clean energy but also to enhance power quality. A promising solution is to equip photovoltaic inverters with active filtering capabilities. The objective of this work is to develop and simulate a three-level active power filter (APF) supported by a photovoltaic generator, capable of achieving both maximum solar energy extraction and harmonic current compensation. The proposed system aims to ensure compliance with international power quality standards while promoting the integration of renewable energy into smart and efficient electrical networks.[75]

III.2. Overview of Photovoltaic Energy Systems

Photovoltaic (PV) energy systems are designed to convert solar radiation directly into electrical energy using the photovoltaic effect. A typical PV system consists of solar panels composed of multiple photovoltaic cells, usually made from semiconductor materials such as silicon. When exposed to sunlight, these cells generate direct current (DC) electricity, which can be harnessed for various applications, including grid integration, standalone systems, and hybrid configurations [76].

III.2.1 Principle of Photovoltaic Conversion

Photovoltaic (PV) conversion is the process of transforming sunlight directly into electricity using solar cells. It relies on a p-n junction within semiconductor materials like silicon. When sunlight hits the cell, photons free electrons, which are then separated by the electric field at the junction, creating a voltage. Once connected to an external circuit, this separation generates a direct current (DC) as electrons flow through the circuit [77], as illustrated in Figure III.1.

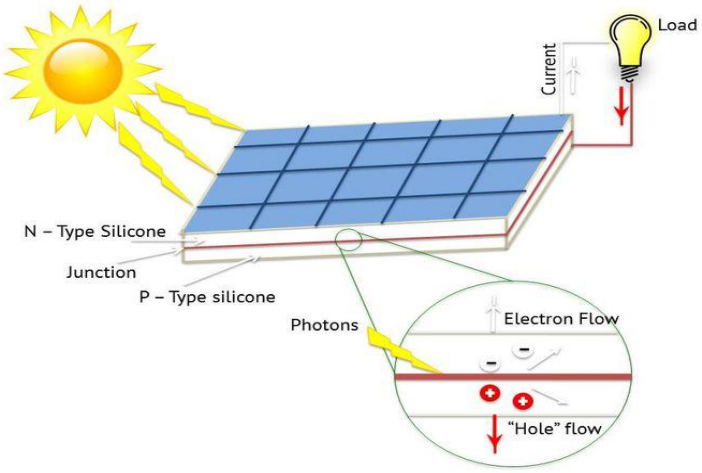

Figure. III.1 Principle of photovoltaic cell operation

III.3. Modeling of a Photovoltaic System

The modeling of a photovoltaic (PV) system involves representing the electrical behavior of a solar panel or array under varying environmental conditions. Accurate modeling is essential for simulation, control, and performance analysis, especially when the PV system is integrated with power electronics like inverters or active filters. A typical PV generator comprises several PV modules connected in series and/or parallel to meet specific voltage and current requirements. The model helps to predict the output power, evaluate the effect of temperature and irradiance, and optimize the power extraction through techniques like MPPT (Maximum Power Point Tracking).[78]

III.3.1 Photovoltaic Panel Modeling

The modeling of a photovoltaic (PV) panel aims to represent its electrical behavior under various environmental conditions. A PV panel consists of several solar cells connected in series and/or parallel to produce the desired voltage and current levels. Each solar cell converts sunlight into electricity through the photovoltaic effect and can be represented by an equivalent electrical circuit.[79]The most widely used model for a PV cell is the single-diode model, which captures the essential characteristics of the cell. This model includes a current source representing the photocurrent, a diode that simulates the p-n junction, and two resistors: a series resistance R_s representing internal losses and a shunt resistance R_{sh} accounting for leakage currents. [80]

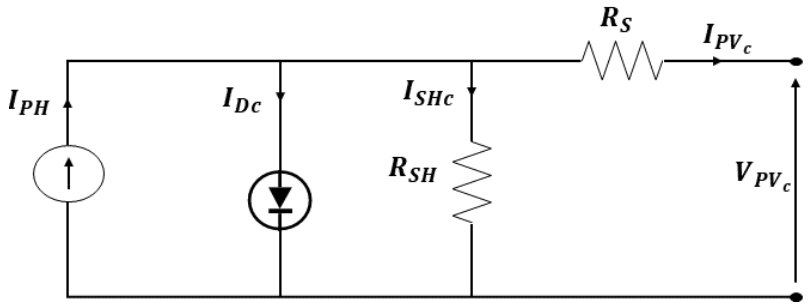

Figure. III. 2 The PV cell circuit equivalent electrically.

Accordingly, the output current I_{pv} and voltage V_{pv} of a solar cell can be expressed as follows:

$$I_{pv} = I_{ph} - I_{Dc}\left[esp\left(\frac{q}{nkT}V_{Dc}\right) - 1\right] - \left(\frac{V_{pv}+R_S\,I_{pv}}{R_{sh}}\right) \quad \text{(III.1)}$$

$$V_{pv} = V_{Dc} - R_s I_{pvc} \quad \text{(III.2)}$$

Where I_{ph} is the photocurrent, I_{Dc} is the reverse saturation current, n is the diode ideality factor, T is temperature, q is the electron charge, and k is Boltzmann's constant.

III.3.2 Modeling of a Photovoltaic Module

A single photovoltaic (PV) cell, typically covering only a few square centimeters, can produce just a few watts of power, with an output voltage below one volt this being the characteristic voltage of a p-n junction.[81] To achieve greater power output, multiple cells are interconnected to form a solar module or panel. Series connections increase the total voltage, whereas parallel connections raise the output current. This series-parallel configuration allows the PV generator to meet specific electrical requirements.[82] Since the model discussed earlier refers to an individual PV cell, modeling a complete module requires incorporating the number of series- and parallel-connected cells. Accordingly, the output current of the PV module is expressed by equation (III.3). The current-voltage (I-V) characteristic for a PV array composed of N_s cells in series and N_p in parallel is illustrated in Figure III.3 [83].

$$I_{PV} = N_{PV}I_{ph} - N_p I_O\left[\exp\left(\frac{q}{N_S K_\gamma T}\left(V_{PV} + \left(\frac{N_S}{N_P}R_S\right)\right) - 1\right) - N_p\left(\frac{V_{PV}+\left(\frac{N_S}{N_P}R_S\right)I_{PV}}{\left(\frac{N_S}{N_P}R_S\right)}\right)\right] \quad \text{(III.3)}$$

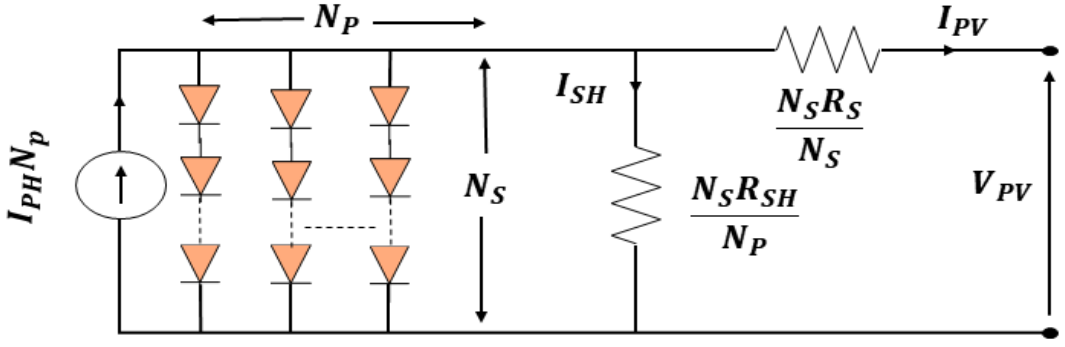

Figure. III.3 Equivalent circuit model of a solar PV array

III.3.2.1 Electrical Characteristics of a Photovoltaic Module

The electrical characteristics of a photovoltaic module are essentially scaled versions of those of individual solar cells, determined by the number of cells connected in series and parallel. The current-voltage (I-V) relationship of the PV module is nonlinear. To understand the module's behavior, its I-V curve (shown in Fig. III.4) is obtained by exposing the cell to constant illumination at a fixed temperature, varying the load resistance, and measuring the resulting current.[85]

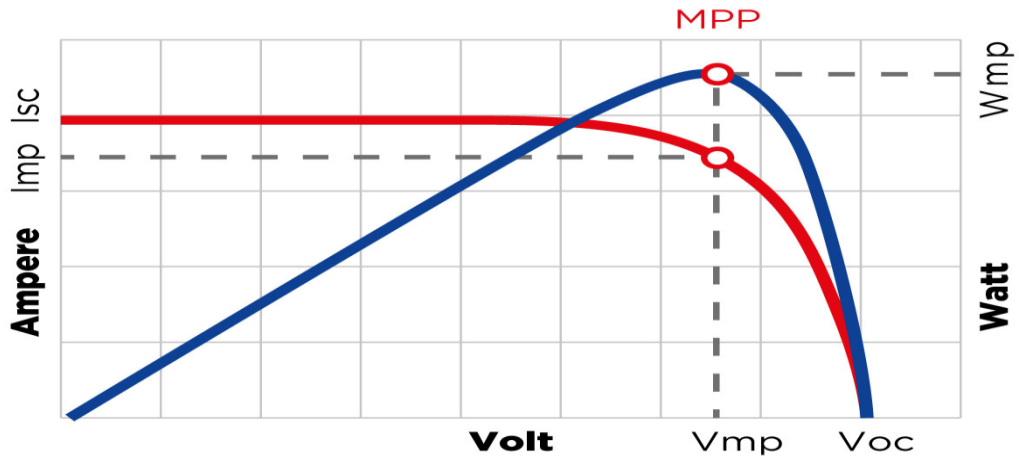

Figure. III.4 Solar cell I–V and P–V characteristic.

- **Short-Circuit Current (I_{sc})**

The short-circuit current (I_{sc}) is the maximum current that a photovoltaic cell or module can produce when its output terminals are directly connected (short-circuited), resulting in zero voltage across the terminals. It occurs under standard test conditions (STC), which typically include a solar irradiance of 1000 W/m², a cell temperature of 25 °C, and an air mass of 1.5. The ISC value is primarily determined by the intensity of incident sunlight and the surface area of the PV cell. It represents one of the key parameters on the I–V characteristic curve and is used to assess the current-generating capacity of the PV device.

The expression for the short-circuit current can be given as follows [86]:

$$I_{SC} = N_p \left(\frac{I_{SC_{STC}}}{1000} G + K_i (T - T_{STC}) \right) \quad \text{(III.4)}$$

Where:

I_{sc}: Short-circuit current of the PV module (A).

N_p: Number of parallel-connected PV cells.

I_{sc_stc}: Short-circuit current at standard test conditions (A).

G: Solar irradiance (W/m²).

K_i: Temperature coefficient of short-circuit current (A/°C).

T: Actual cell temperature (°C).

T_{stc} : Cell temperature under standard test conditions.

- **Open-Circuit Voltage (VOC)**

The open-circuit voltage (V_{oc}) represents the maximum voltage of a photovoltaic system under open-circuit conditions, i.e., when no load is connected and there is no current flow through the external circuit. This voltage level is higher than the maximum power point voltage (V_{mppt}), which governs the normal operating condition of a PV generator.[87]

The value of V_{oc} is strongly influenced by temperature, as reflected by the voltage temperature coefficient. In contrast, its dependence on solar irradiance E is relatively weak and follows a logarithmic relationship. Furthermore, V_{oc} is directly proportional to the number of PV cells connected in series, as each cell contributes additively to the total voltage.[88]The expression for V_{oc} can be derived :

$$V_{oc} = nV_{th}\ln\left(\frac{I_{ph}}{I_0}\right) \quad \text{(III.5)}$$

- **Maximum Power Point (MPP)**

The Maximum Power Point (MPP) represents the unique operating point on a photovoltaic (PV) module's current-voltage (I-V) curve where the product of the output current and voltage is maximized, thereby yielding the highest possible power output.[89] Ensuring the PV module operates precisely at this point is crucial for optimal energy extraction from the solar resource. Given the inherent non-linear characteristics of the I-V curve, continuously tracking and maintaining operation at this peak power point necessitates the use of a Maximum Power Point Tracking (MPPT) algorithm, which typically operates in real-time.[90]

- **Efficiency (η)**

The efficiency of a photovoltaic cell or module η is defined as the maximum fraction of incident solar energy that can be converted into useful electrical power. It quantifies the overall performance of the cell under standard test conditions.

Mathematically, efficiency is given by the ratio of the maximum output power P_{max} to the product of the incident irradiance E and the cell area S, as follows:

$$\eta = \frac{\text{Output Power}}{\text{Input Power}} = \frac{P_{max}}{P_i} = \frac{V_{\text{mppt}} \times I_{\text{mppt}}}{E \times S} \quad \text{(III.6)}$$

Efficiency depends on several factors, including the cell material, temperature, and optical losses. It is one of the most critical parameters for evaluating and comparing different photovoltaic technologies [91].

- **Fill Factor (FF)**

The fill factor (FF) is a critical parameter in evaluating the performance of a photovoltaic (PV) module. It indicates how closely the actual maximum power output of the module approaches the theoretical maximum power, defined by the product of the open-circuit voltage V_{oc} and the short-circuit current I_{sc}. A higher fill factor reflects lower losses and better solar cell quality.[92]

To maximize the overall efficiency of a PV module, the fill factor must be optimized to approach unity on the I–V characteristic curve. Mathematically, the fill factor is given by:

$$FF = \frac{P_{max}}{I_{sc} \times V_{oc}} = \frac{V_{mppt} \times I_{mppt}}{I_{sc} \times V_{oc}} \quad \text{(III.7)}$$

III.3.3 Influencing Factors

III.3.3.1 Influence of Irradiation

Accurate modeling of solar irradiance, especially the global irradiance on a PV module's tilted surface, is crucial for reliably simulating and predicting photovoltaic system performance. Since both current and voltage outputs of a PV module are highly sensitive to irradiance levels, the annual energy yield closely follows the cumulative irradiance received over time, often showing a nearly linear relationship at moderate to high irradiance. Precise irradiance models incorporate not only direct and diffuse components but also account for solar position and environmental factors, making them vital inputs for performance and yield calculations.[94] This relationship is illustrated by the module's current-voltage (I-V) and power-voltage (P-V) curves, which vary significantly with irradiance levels, as depicted between 200 W/m² and 1000 W/m² in incremental steps. which are given by Fig III.5. Consequently, advanced irradiance modeling underpins the accurate assessment, design, and optimization of PV systems for dependable energy production.

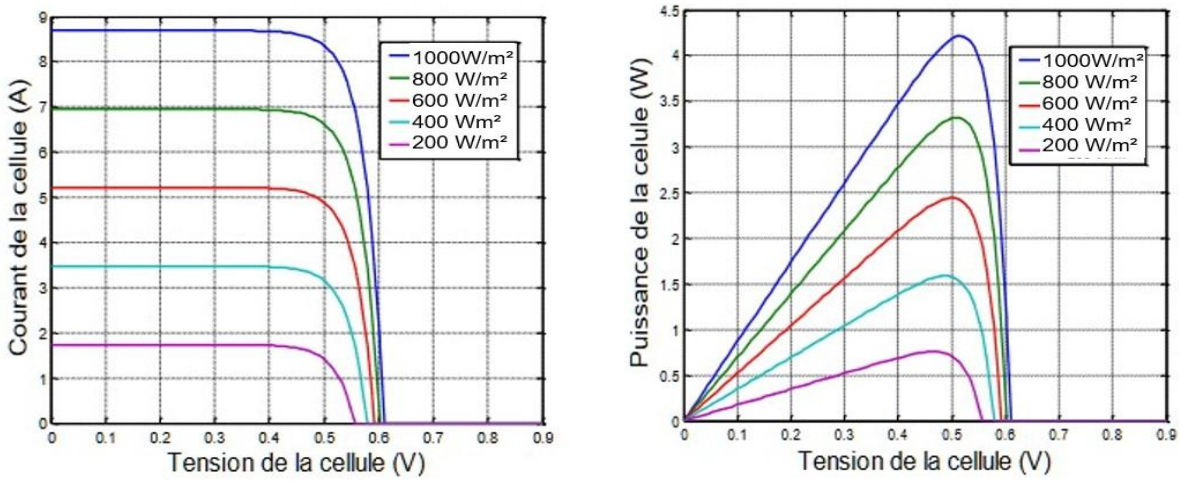

Figure. III. 5 Current-Voltage (I-V) and Power-Voltage (P-V) Characteristics under Variable Irradiance

III.3.3.2 Influence of temperature

Temperature significantly influences the electrical performance of photovoltaic (PV) modules. As PV modules absorb solar radiation, their surface temperature rises, which primarily affects the output voltage by causing it to decrease, while the output current experiences only a slight increase.[95]

This decline in voltage with increasing temperature results in a reduction of the overall power output, leading to lower conversion efficiency and decreased energy yield of the PV system.

Therefore, accurate temperature modeling is vital for reliably predicting system performance under actual operating conditions. This effect is illustrated in Figure II.6, which shows the I–V and P–V characteristic curves across a temperature range from 0°C to 75°C, clearly demonstrating the performance degradation as temperature rises.[96]

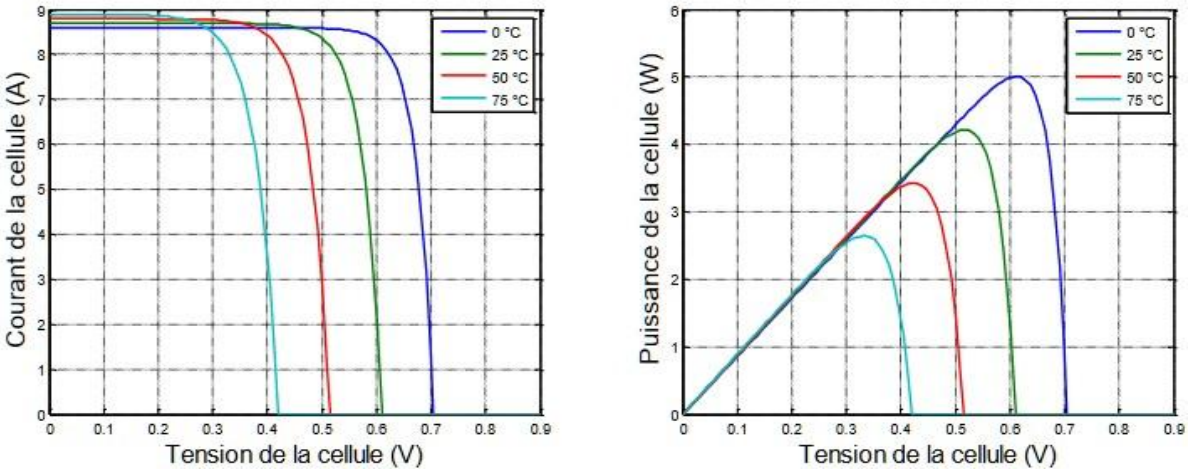

Figure. III.6 P/V and I/V characteristics under varying temperature

III.4 DC-DC Boost Converter

A DC-DC boost converter, also known as a step-up converter, is a power electronic device used to increase the input voltage to a higher output voltage level. In photovoltaic (PV) systems, the boost converter plays a crucial role by adapting the relatively low voltage generated by the PV panels to the required DC bus level or to the input level of an inverter.

The boost converter operates using a high-frequency switching mechanism involving an inductor, a power switch (typically a MOSFET), a diode, and an output capacitor. When the switch is turned on, energy is stored in the inductor.[97] When the switch turns off, this stored energy is released to the load through the diode, resulting in an output voltage greater than the input. This type of converter is particularly suitable for Maximum Power Point Tracking (MPPT) algorithms, which dynamically adjust the duty cycle of the switch to ensure the PV array operates at its maximum power point under varying irradiance and temperature conditions. [98]

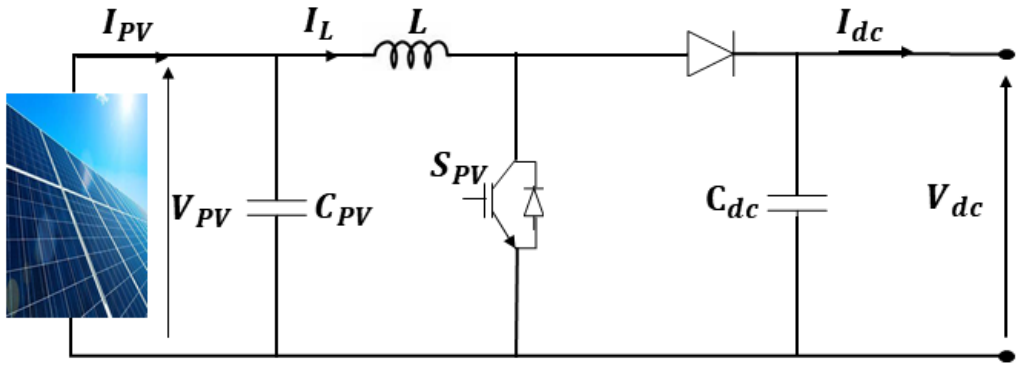

Figure. III.7 DC/DC boost converter in a PV system

III.4.1 DC-DC Converter Modeling

The modeling of a DC-DC boost converter involves analyzing its different operating modes, typically assuming a fixed switching period. The converter operates in two main sequences based on the state of the switch (transistor S): ON-state (switch closed) and OFF-state (switch open). Each sequence can be described by distinct sets of differential equations, which define the converter's behavior during each phase of operation.[99]

When the switch S is closed (ON-state):The input voltage is applied directly across the inductor, causing energy to accumulate in its magnetic field. During this interval, the diode is reverse-biased, and the load is powered by the output capacitor.

The state equations are:

$$\begin{cases} L\frac{di_{L_{pv}}}{dt} = v_{pv} \\ C_{pv}\frac{dv_{pv}}{dt} = \frac{1}{R_{ipv}}v_{pv} - i_{L_{pv}} \end{cases} \quad \text{(III.8)}$$

When the switch S is open (OFF-state):

The stored energy in the inductor is released to the load through the diode, increasing the output voltage beyond the input voltage. The inductor current flows into both the load and the capacitor.The state equations are:

$$\begin{cases} L\frac{di_{L_{pv}}}{dt} = V_{pv} - V_{dc} \\ C_{pv}\frac{dV_{pv}}{dt} = \frac{1}{R_{ipv}}V_{pv} - i_{L_{pv}} \end{cases} \quad \text{(III.9)}$$

By setting u=0 when the transistor is open and u=1 when it is closed, and defining u=1−(V_{pv}/V_{dc}), equations (III.8) and (III.9) can be combined into a single system of equations expressed as follows:

$$\begin{cases} \frac{di_{L_{pv}}}{dt} = \frac{1}{L}V_{pv} - \frac{V_{dc}}{L}(1-u) \\ \frac{dV_{pv}}{dt} = -\frac{1}{C_{pv}}i_{L_{pv}} + \frac{V_{dc}}{C_{pv}R_{ipv}}(1-u) \end{cases} \quad \text{(III.10)}$$

The instantaneous model demonstrates the converter's nonlinear characteristics, particularly due to the products of the control variable u and the state variables V_{dc} and i_{pv}. By substituting the control variable u with its averaged value over a switching period $T_c=1/f_c$, equivalent to the duty cycle D, the averaged model of the boost converter can be subsequently derived:"

$$\begin{cases} \frac{di_{L_{pv}}}{dt} = \frac{1}{L}V_{pv} - \frac{V_{dc}}{L}(1-D) \\ \frac{dV_{pv}}{dt} = -\frac{1}{C_{pv}}i_{L_{pv}} + \frac{V_{dc}}{C_{pv}R_{ipv}}(1-D) \end{cases} \quad \text{(III.11)}$$

These equations form the basis for simulation and control of the boost converter in photovoltaic applications, particularly when integrated with MPPT algorithms for optimal power extraction.

III.5 MPPT Techniques for Enhancing PV Panel Efficiency

A wide variety of Maximum Power Point Tracking (MPPT) techniques have been developed to improve the efficiency of photovoltaic (PV) systems, ranging from simple to advanced algorithms. Among the most commonly used are the Perturb and Observe (P&O) method [100], known for its ease of implementation, and the more precise Incremental Conductance (INC) technique[101], which is effective under rapidly changing conditions. Simpler methods such as the Fractional Open Circuit Voltage (FOCV) and Fractional Short Circuit Current (FSCC) [102]

rely on empirical relationships to estimate the MPP with minimal computational effort. Each method presents its own trade-offs in terms of complexity, tracking speed, accuracy, and cost. These MPPT strategies are essential to modern PV system design, enabling solar installations to operate at their maximum power output under varying environmental conditions.

III.5.1 Open-Circuit Voltage Method (FOCV)

The Fractional Open Circuit Voltage (FOCV) method is predicated on the empirical observation that the voltage at the Maximum Power Point (V_{MPP}) of a photovoltaic (PV) module maintains an approximate proportionality to its open-circuit voltage (V_{OC}). This relationship is mathematically articulated by Equation (III.1):

$$V_{MPP} = K_{OC} \times V_{OC} (K_{OC} < 1) \quad \text{(III.12)}$$

While the FOCV method offers simplicity, its accuracy is influenced by the inherent variability of the proportional constant KOC. This constant is not a fixed universal value; instead, it is affected by key factors including the PV module's fill factor, its underlying cell technology, and prevalent environmental conditions such as solar irradiance and ambient temperature [103]. The

practical implementation of this attribute is detailed in the flowchart presented in Figure III.8:

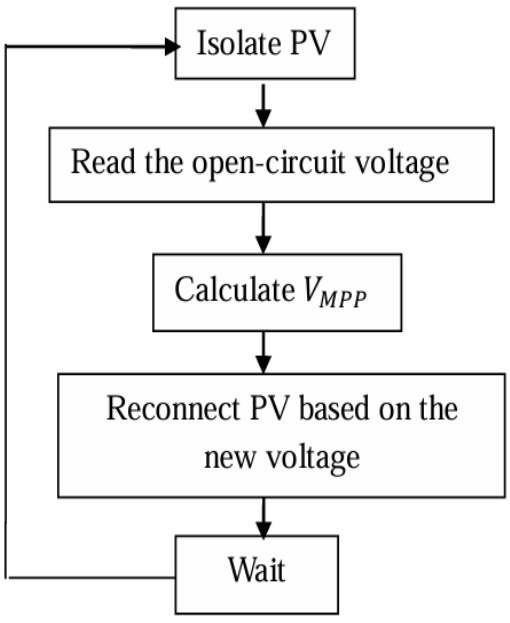

Figure. III.8 Flowchart of the FOCV method [103]

III.5.2 Fractional Short-Circuit Current (FSCC)

The Fractional Short-Circuit Current (FSCC) method is a Maximum Power Point Tracking (MPPT) technique for photovoltaic (PV) systems, recognized for its simplicity and low implementation cost. Like the Fractional Open Circuit Voltage (FOCV) method, it falls under the category of "indirect" or "offline" MPPT algorithms.

The fundamental premise of the FSCC method is an observed empirical relationship: the current at the maximum power point (I_{MPP}) of a PV module is approximately a constant fraction of its short-circuit current (I_{sc}). This proportionality is particularly strong because I_{sc} is highly correlated with the amount of solar irradiance striking the panel. The relationship is mathematically expressed as:

$$I_{MPP} = K_{SC} \times I_{SC} \quad (K_{SC} < 1) \tag{III.13}$$

The proportional constant K_{SC} in this method is influenced by the PV cell technology and environmental conditions. The core of this technique involves periodically measuring the short-circuit current and then calculating the optimal operating current using this K_{SC} constant. Despite its simplicity and cost-effectiveness, the necessity for frequent current interruptions during I_{SC} measurements can be detrimental to the system's overall efficiency. As depicted in Figure III.9, the control flowchart for this method bears a strong resemblance to the open-circuit voltage approach.[104]

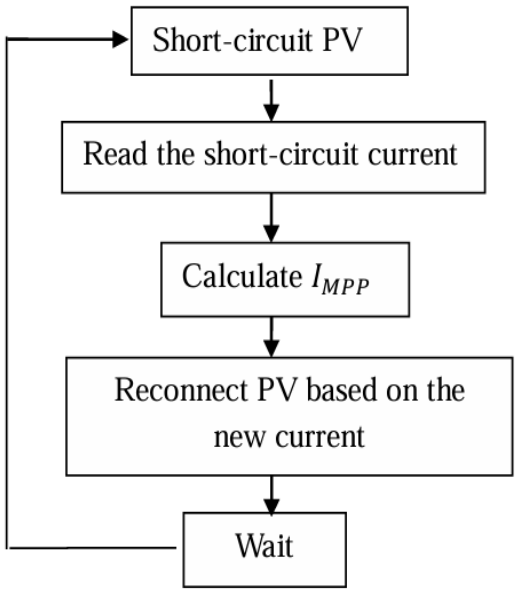

Figure. III.9 The FSCC Method Flowchart [104].

III.5.3 Perturb and Observe (P&O) Algorithm

The Perturb and Observe (P&O) algorithm is one of the most widely used MPPT techniques, valued for its simplicity and ease of implementation. It operates by periodically perturbing (i.e., increasing or decreasing) the PV panel's operating voltage or duty cycle. The algorithm then observes the resulting change in output power: if the power increases, the perturbation continues in the same direction; otherwise, it is reversed. The operational flow of the P&O technique is presented in Figure III.10

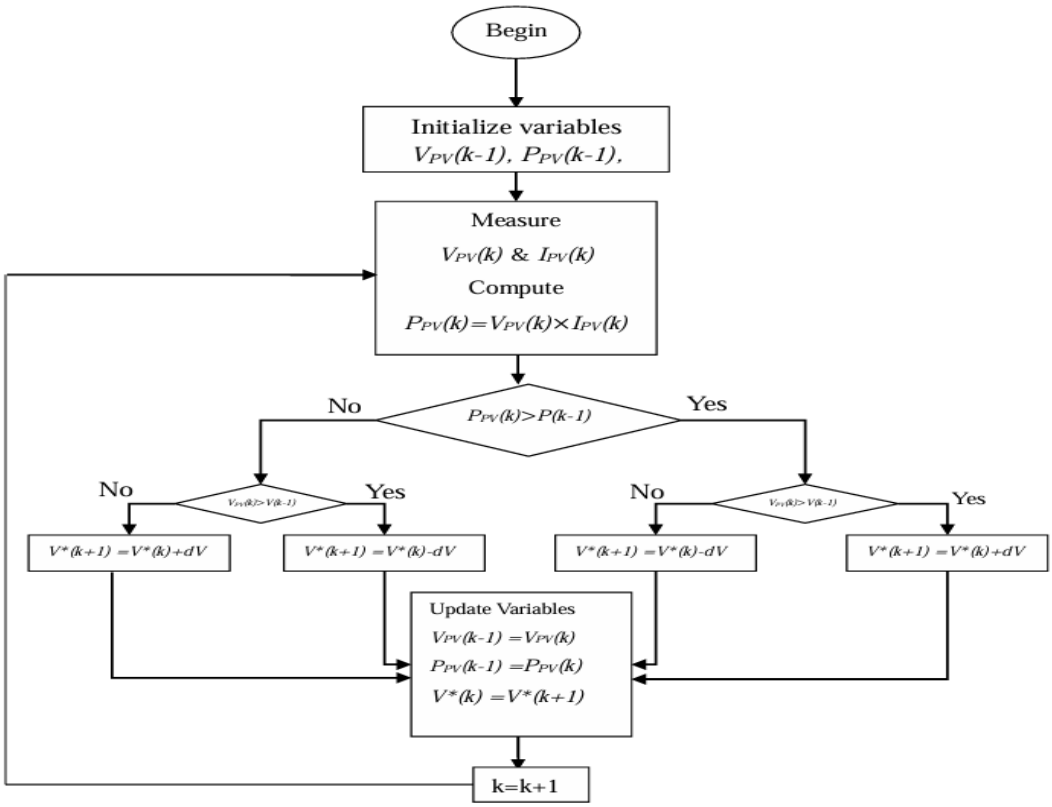

Figure. III.10 P&O Technique Flowchart.

The tracker controller operates by taking real-time readings of the photovoltaic voltage and current along the I-V curve during each cycle. It then precisely calculates the instantaneous photovoltaic power and dynamically adjusts the operating point by scanning the operating voltage while observing the associated power variation. This iterative process continues until optimal performance is achieved. Specifically, if an increase in power is detected, the subsequent voltage perturbation is applied in the same direction. Conversely, if power decreases, the operational voltage's direction is reversed. Each iteration of this scenario persists until the Maximum Power Point (MPP) is attained, which is theoretically the point where $\frac{d_{P_{PV}}}{d_{V_{PV}}} = 0$ [105]. A significant limitation of this method, related to its monitoring speed and perturbation step, is its tendency to generate oscillations in the vicinity of the MPP, preventing it from accurately capturing the true maximum power point [106].

III.5.4 The Incremental Conductance algorithm

The Incremental Conductance (Inc-Cond) algorithm achieves Maximum Power Point (MPP) tracking by leveraging specific characteristics of the PV curve [107], addressing key limitations of the Perturb and Observe (P&O) technique. Unlike P&O, which suffers from oscillations near the MPP and slow adaptation to rapidly changing atmospheric conditions, Inc-Cond was designed to mitigate these drawbacks [108]. Its core objective is to adjust the electrical converter's duty cycle to reach the MPP by comparing instantaneous conductance (I/V) with incremental conductance (ΔI/ΔV) [109]. Figure III.11 illustrates the Inc-Cond flowchart. The MPP is achieved when the ratio of voltage variation is zero, as expressed by the formulas below [110]:

$$\frac{dP_{PV}}{dV_{PV}} = \frac{d(V_{PV} \times I_{PV})}{dV_{PV}} = I_{PV} + V_{PV}\frac{dI_{PV}}{dV_{PV}} = 0$$
$$\frac{I_{PV}}{V_{PV}} = -\frac{dV_{PV}}{dI_{PV}} \cong -\frac{\Delta V_{PV}}{\Delta I_{PV}} \quad \text{(III.14)}$$

At the Maximum Power Point (MPP), the power-voltage (P-V) curve exhibits a slope of zero. This indicates that power increases when operating to the left of the MPP, and decreases when operating to the right [111]:

$$\frac{dP_{PV}}{dV_{PV}} = 0 \text{ if } \frac{dI_{PV}}{dV_{PV}} = -\frac{I_{PV}}{V_{PV}} \text{ at MPP} \quad \text{(III.15)}$$

$$\frac{dP_{PV}}{dV_{PV}} > 0 \text{ if } \frac{dI_{PV}}{dV_{PV}} > -\frac{I_{PV}}{V_{PV}} \text{ left of MPP} \quad \text{(III.16)}$$

$$\frac{dP_{PV}}{dV_{PV}} < 0 \text{ if } \frac{dI_{PV}}{dV_{PV}} < -\frac{I_{PV}}{V_{PV}} \text{ right of MPP} \quad \text{(III.17)}$$

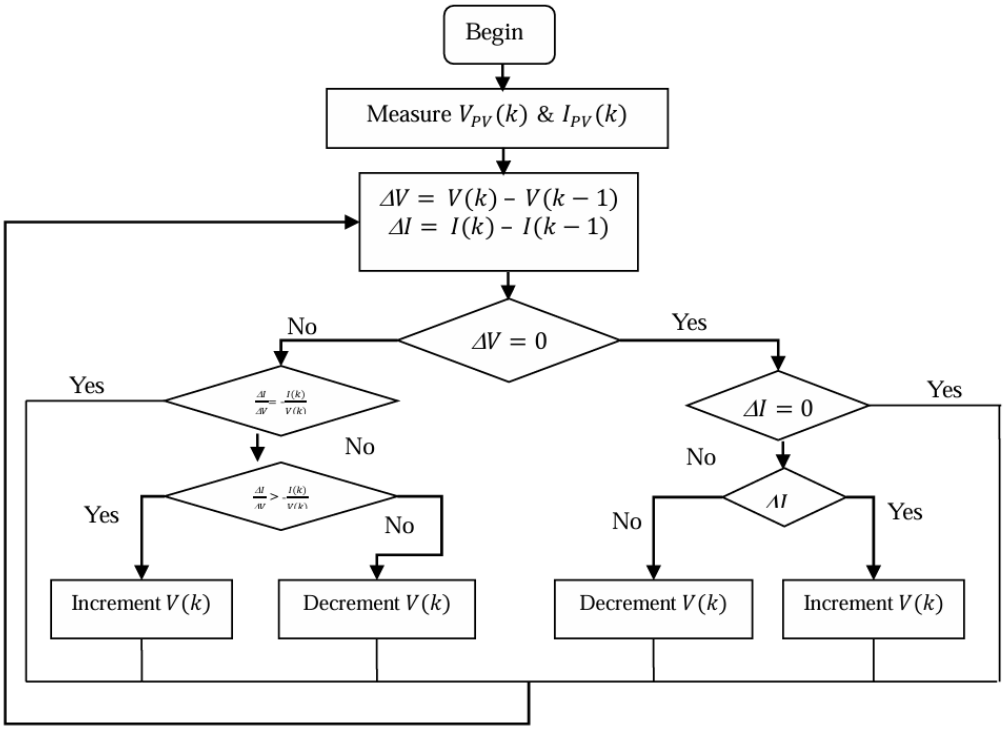

Figure. III.11 Flowchart of the INC Technique

The MPPT technique, as modeled in Figure III.12, incorporates two algorithms: P&O and INC. The INC method leverages the derivative of the PV conductance, specifically the ΔG=ΔI/ΔV ratio, to track the MPP. Meanwhile, the P&O technique determines the MPP's position and applies control by comparing the power variation (ΔP) caused by a perturbed operating voltage in each cycle

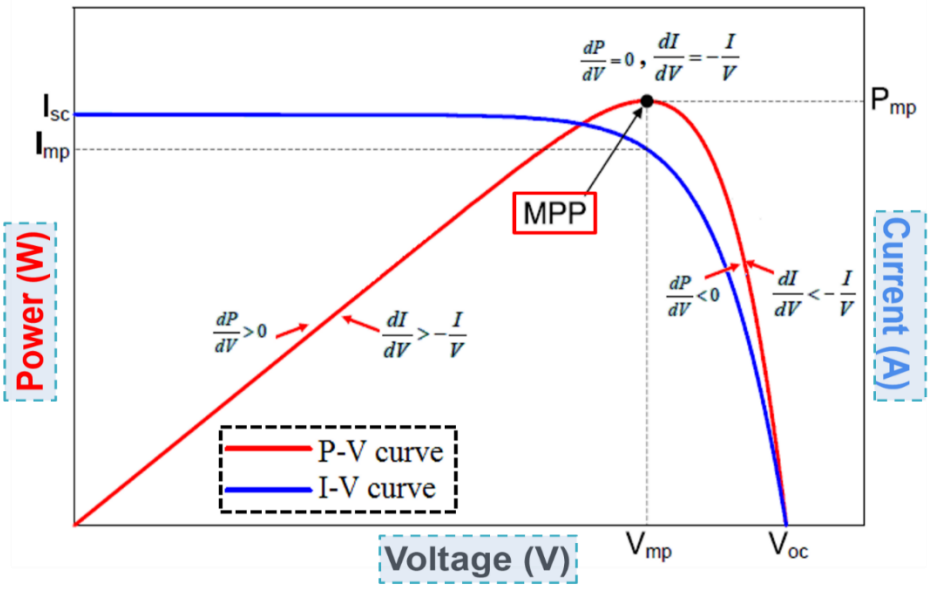

Figure. III.12 Principle of MPPT Using (INC) Method

III.5.5 Intelligent MPPT algorithms

The P-V characteristic curve of a photovoltaic (PV) module is nonlinear, which means that it changes with both temperature and irradiation. This can cause multiple power peaks. Because of this complexity, traditional MPPT control methods often don't work. To solve this problem, many intelligent MPPT control techniques based on advanced algorithms have been created and put into use successfully. The Fuzzy Logic Controller (FLC) and the Sliding Mode Controller (SMC) are two of the most common techniques used. Below is a list of some of the most popular intelligent MPPT control methods [113]:

III.5.5.1 Sliding Mode Control

Sliding Mode Control (SMC) is recognized as a robust control technique well-suited for managing switched systems. It maintains high resistance to various uncertainties, including external disturbances and measurement errors [116]. In a conventional SMC design, the sliding variable is chosen so that it has a relative degree of one with respect to the control input.

In the case of photovoltaic (PV) systems, the design procedure generally involves two main steps:

- **Sliding Surface Design:** Define a switching function that ensures the internal dynamics are stable once the system enters the sliding mode.
- **Control Law Design:** Develop a control strategy that drives the system state toward the sliding surface and ensures it remains there.

For MPPT purposes, the sliding surface is typically defined by setting the maximum power point identification condition to zero, as expressed in Equation (III.18).

$$\frac{\partial P}{\partial I} = I\left(\frac{\partial V}{\partial I} + \frac{V}{I}\right) = 0 \tag{III.18}$$

The solution to (III.18) that is not trivial is

$$\left(\frac{\partial V}{\partial I} + \frac{V}{I}\right) = 0 \tag{III.19}$$

Consequently, the following is a definition of a correct sliding manifold in the state space:

$$\sum = \left\{x \setminus S(t,x) = \frac{\partial V}{\partial I} + \frac{V}{I} = 0\right\} \tag{III.20}$$

It is referred to as a switching surface. Controlling the plant state to be driven to the switching surface and kept there is the most crucial task. The following is how the SMC's switching control is displayed:

$$u_d = \begin{vmatrix} u^+ & \text{if} & S(z) > 0 \\ u^- & \text{if} & S(z) < 0 \end{vmatrix} \tag{III.21}$$

One way to express a basic sliding mode control design is as

$$u = u_{eq} + u_d \tag{III.22}$$

The equivalent control (u_{eq}) is the specific control input that ensures the system's state remains precisely on the sliding surface (S(z)=0). When this control is active, any trajectory that begins on the manifold S(z)=0 will stay there, because the time derivative of the sliding surface, $\dot{\boldsymbol{S}}$(z), will be zero.

We determine the equivalent control (u_{eq}) by solving the condition $\dot{\boldsymbol{S}}$ (z)=0 for the control input, which gives us:

$$S(t,z) = \dot{S}(t,z) = 0 \tag{III.23}$$

This guarantees the invariance of the sliding surface. The proposed discontinuous control, u_d, ensures convergence to the surface in finite time and is defined as:

$$u_d = M\text{sign(S)} \tag{III.24}$$

The formulation for our photovoltaic (PV) system's equivalent control is given by equation (III.23). The formulation is as follows:

$$\dot{S} = \left[\frac{\partial S}{\partial Z}\right]^{\top} \dot{Z} = \left[\frac{\partial S}{\partial Z}\right]^{\top} \left(\phi(Z) + \psi(Z)u_{eq}\right) = 0 \tag{III.25}$$

It will now be evident that the corresponding control is defined as

$$u_{eq} = -\frac{\left[\frac{\partial S}{\partial Z}\right]^{\top} \phi(Z)}{\left[\frac{\partial S}{\partial Z}\right]^{\top} \psi(Z)} = 1 - \frac{V_{pv}}{V_{\text{out}}} \tag{III.26}$$

The following is the suggested genuine control signal:

$$u = \begin{cases} 1 & \text{if} \quad u_{eq} + M\text{sign}(S) > 1 \\ u_{eq} + M\text{sign}(S) & \text{if} \quad 0 < u_{eq} + M\text{sign}(S) < 1 \\ 0 & \text{if} \quad u_{eq} + M\text{sign}(S) < 0 \end{cases} \tag{III.27}$$

To analyze the stability of the system under Sliding Mode Control, we define the following Lyapunov candidate function:

$$V(x) = \frac{1}{2}S^2(x) \tag{III.28}$$

This function is positive definite and continuously differentiable. Taking its time derivative along system trajectories gives:

$$\dot{V}(x) = S(x) \cdot \dot{S}(x) \tag{III.29}$$

To ensure stability in the sense of Lyapunov, the control law is designed such that:

$$\dot{V}(x) < 0 \Rightarrow S(x) \cdot \dot{S}(x) < 0 \tag{III.30}$$

This condition guarantees that the system states are attracted to and remain on the sliding surface *S*(x)=0, ensuring both stability and convergence. Thus, the system's dynamics are governed by the reduced-order motion on the sliding manifold.

III.5.5.2 Super Twisting Sliding Mode Controller

The Super-Twisting Sliding Mode Controller (STSMC) is a modern control strategy that has been successfully applied in a wide range of fields, including power electronics [117] and renewable energy systems such as photovoltaic (PV) generation [118]. It belongs to the family of higher-order sliding mode controllers, starting from the second-order case, which ensures the finite-time convergence of both the sliding variable and its derivative. As an enhancement of conventional sliding mode control, it is designed to improve system robustness, transient performance, and dynamic response, while significantly mitigating the chattering effect. In addition, STSMC provides higher accuracy and superior tracking capability under time-varying operating conditions. In the following section, the design procedure of the STSMC for the FLIBC-based PV system is presented, and the corresponding control law is given as:

$$u_{ST-SMC} = u_{eq} + u_{ST} \tag{III.31}$$

The term ueq represents the equivalent control law, which is similar to the one derived for a Sliding Mode Control (SMC) system in equation (III.26). In contrast, u_{st} is the super-twisting control law, as defined in reference [119]:

$$u_{ST} = \left(U_1(t) + U_2(t)\right) \tag{III.32}$$

With

$$\begin{cases} U_1(t) = \lambda_1 \sqrt{|S|}.sign(S) \\ U_2(t) = \lambda_2 \int sign(S).dt \end{cases} \tag{III.33}$$

The positive design parameters λ_1 and $\lambda_2$determine the Super-Twisting Sliding Mode Control (STSMC) system's convergence rate and its ability to reduce chattering.

III.6 PV-Integrated NPC Active Filter

The integration of solar energy into electrical grids relies on photovoltaic (PV) inverters. These inverters improve power quality and power factor by employing a three-level Neutral Point Clamped (NPC) Voltage-Source Inverter (VSI) to introduce compensating harmonic currents into the grid. A crucial enhancement involves connecting a PV source to the inverter's DC bus, which allows the system to utilize the active power generated by the solar panels. With this configuration, the inverter transforms into a multipurpose converter. It functions as an active power filter, mitigating harmonic distortion and compensating for reactive power.

Furthermore, when powered by the PV source, it acts as a flexible and effective energy interface by supplying active power to the grid, as depicted in Figure III.13: Topology of a PV Generator Connected to an Active Filter.

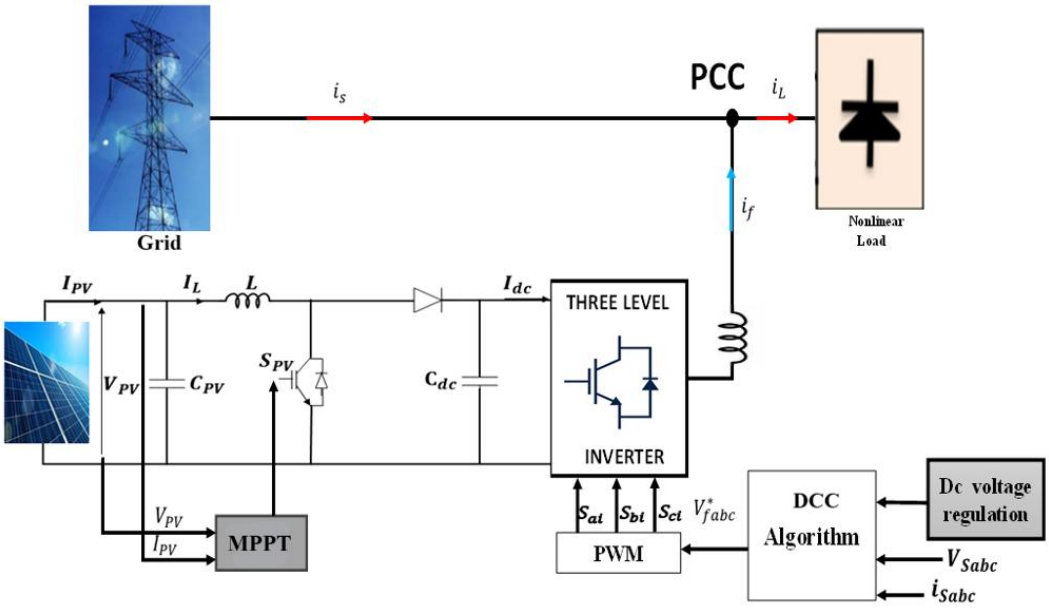

Figure. III.13 Photovoltaic Generator Connected to Active Filter Topology

III.7 Conclusion

In this chapter, the integration of a photovoltaic source with a three-level active power filter was studied to improve both energy efficiency and power quality. The modeling of the PV system was presented along with various MPPT techniques, starting from classical methods like Perturb and Observe, to more advanced intelligent strategies such as fuzzy logic and Sliding Mode Control (SMC). While traditional methods are simple and easy to implement, they often suffer from slow dynamic response and steady-state oscillations. Intelligent approaches, particularly SMC, are expected to offer faster convergence to the maximum power point and improved tracking accuracy, as suggested in the literature.

Combined with the advantages of the three-level NPC inverter, this configuration has the potential to provide effective harmonic compensation, reactive power support, and optimal renewable energy integration into the grid.

Chapter IV

Third Order Sliding Mode Control Strategy for a Multilevel Active Power Filter in Grid-Connected PV Systems

IV.1 Introduction

Maintaining high power quality while integrating renewable energy sources presents a fundamental challenge in contemporary electrical networks. Grid-connected photovoltaic (PV) systems must not only maximize energy harvesting but also mitigate disturbances induced by nonlinear loads. In this context, integrating active power filtering capabilities into multilevel inverter architectures offers a compelling approach to concurrently deliver solar energy and suppress harmonic currents.

This chapter introduces a control strategy based on Third Order Sliding Mode Control (TOSMC), applied to a three-level Neutral Point Clamped (NPC) inverter functioning as a Shunt Active Power Filter (SAPF) within a grid-connected PV framework. The proposed TOSMC ensures robust current tracking and effective harmonic compensation, even under dynamically varying load conditions. On the DC side, TOSMC is leveraged for Maximum Power Point Tracking (MPPT), enabling precise and efficient energy extraction from the PV array. On the AC side, it is integrated with a Direct Current Control Pulse Width Modulation (DCC-PWM) method to regulate inverter output currents and suppress total harmonic distortion (THD) across the grid interface.By employing third order sliding mode control for both MPPT and current regulation, the system achieves a unified, high-performance solution that enhances overall efficiency, grid stability, and power quality. This chapter elaborates on the modeling process, control architecture, and performance validation of this advanced strategy within smart grid applications.

IV.2 Third Order Sliding Mode Control Principle (TOSMC)

The Third-Order Sliding Mode Control (TOSMC) represents a significant evolution of classical sliding mode control techniques, designed to enhance performance in systems requiring high precision and robustness. Unlike first-order and second-order sliding mode approaches, TOSMC enables finite-time convergence not only of the sliding variable but also of its first and second derivatives. This deeper level of control offers improved disturbance rejection, better tracking capability, and smoother control signals features particularly advantageous in fast-switching systems such as power converters and grid-connected renewable energy systems.

In TOSMC, the control objective is achieved by enforcing a third-order sliding condition on the system trajectories. This is done by designing a control law that consists of three nonlinear terms, each associated with a derivative of the sliding variable. The resulting controller provides

a continuous and robust control signal capable of handling modeling uncertainties, system nonlinearities, and rapid dynamic changes.[120]

The general expression of the TOSMC control law is given by:

$$U_{TOSMC} = \left(U_1(t) + U_2(t) + U_3(t)\right) \tag{IV.1}$$

With

$$\begin{cases} U_1(t) = \lambda_1\sqrt{|S|}.sign(S) \\ U_2(t) = \lambda_2\int sign(S).dt \\ U_3(t) = \lambda_3.sign(S) \end{cases} \tag{IV.2}$$

The sliding surface of the controller is denoted as S , while $U_1(t)$ and $U_2(t)$ represent the second-order and first-order components of the sliding mode control law, respectively.

$$S = x^* - x \tag{IV.3}$$

Utilizing The tuning constants (λ_1, λ_2, and λ_3), the TOSMC performance controller was enhanced. Figure IV.1 displays the TOSMC approach's control law structure.

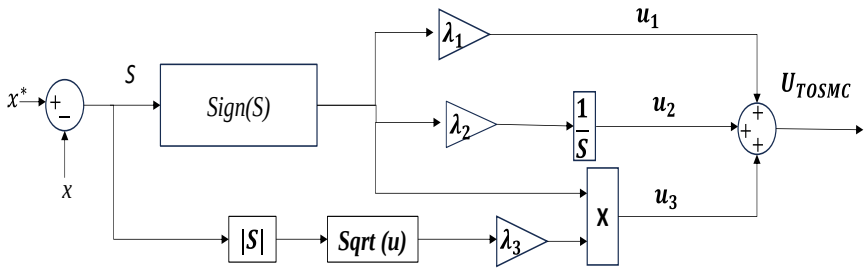

Figure. IV.1 The structure of TOSMC

IV.2.1 TOSMC for Maximum Power Point Tracking (MPPT)

The MPPT technique based on Third-Order Sliding Mode Control (TOSMC) is a novel strategy proposed in this study to maximize the output power of the photovoltaic (PV) system while simultaneously mitigating harmonic currents in the grid. This control approach is an enhancement of the super-twisting sliding mode algorithm, in which the conventional PI controller is replaced with a TOSMC-based controller. The primary advantage of adopting this method lies in its improved system robustness and energy efficiency, as evidenced by reduced power ripples and enhanced current quality when compared to traditional control techniques [121].

The sliding surface used in the proposed TOSMC algorithm is constructed based on the power slope derived from the principle of the Incremental Conductance (INC) method, and is expressed as follows [121]:

$$\frac{\boldsymbol{dP_{pv}}}{\boldsymbol{dV_{pv}}} = \boldsymbol{I_{pv}} + \boldsymbol{V_{pv}}\frac{\boldsymbol{dI_{pv}}}{\boldsymbol{dV_{pv}}} = \boldsymbol{V_{pv}}\left(\frac{\boldsymbol{I_{pv}}}{\boldsymbol{V_{pv}}} + \frac{\boldsymbol{dI_{pv}}}{\boldsymbol{dV_{pv}}}\right) \quad \text{(IV.3)}$$

If this is how the sliding surface is selected:

$$S = \left(\frac{I_{pv}}{V_{pv}} + \frac{dI_{pv}}{dV_{pv}}\right) \quad \text{(IV.4)}$$

Subsequently, the power slope drops to zero when the sliding surface is zero. The PV system generates MPPT electricity in this instance.

$$S = 0 => \frac{dP_{pv}}{dV_{pv}} = V_{pv}S = 0 \quad \text{(IV.5)}$$

- **MPPT - TOSMC algorithm**

The controller is composed of the following terms: the corresponding control word U_{eq} and the TOSMC algorithm term U_{TOSMC}:

$$U = U_{eq} + U_{TOSMC} \quad \text{(IV.6)}$$

The following equation must be solved in order to find the equivalent control term:

$$\dot{S} = \left[\frac{dS}{dX}\right]^T \dot{X} = 0 \quad \text{(IV.7)}$$

The boost converter's state-space equation can be represented as follows using equation (IV.7):

$$\dot{X} = \begin{bmatrix}\frac{dI_{pv}}{dt}\\ \frac{dV_0}{dt}\end{bmatrix} = \begin{bmatrix}\frac{V_{pv}-V_0}{L}\\ \frac{I_{pv}}{C_{out}} - \frac{V_0}{C_{out}R}\end{bmatrix} + \begin{bmatrix}\frac{V_0}{L}\\ -\frac{I_{pv}}{C_{out}}\end{bmatrix} U_{eq} = f(X) + \mathrm{g}(X)U_{eq} \quad \text{(IV.8)}$$

where:

$$X = \begin{bmatrix}I_{pv}\\ V_0\end{bmatrix}; f(X) = \begin{bmatrix}\frac{V_{pv}-V_0}{L}\\ \frac{I_{pv}}{C_{out}} - \frac{V_0}{C_{out}R}\end{bmatrix} \; and \; \mathrm{g}(X) = \begin{bmatrix}\frac{V_0}{L}\\ -\frac{I_{pv}}{C_{out}}\end{bmatrix} \quad \text{(IV.9)}$$

Finally, by adding Eqs. (IV.8) and (IV.9) to Eq. (IV.7) and simplifying, The following is how we could obtain the comparable word Ueq [122]:

$$\dot{X} = \begin{bmatrix}\frac{dI_{pv}}{dt}\\ \frac{dV_0}{dt}\end{bmatrix} = \begin{bmatrix}0 & -\frac{(1-U)}{L}\\ \frac{(1-U)}{C_{out}} & -\frac{1}{RC_{out}}\end{bmatrix}\begin{bmatrix}I_{pv}\\ V_0\end{bmatrix} + \begin{bmatrix}\frac{1}{L}\\ 0\end{bmatrix} V_{pv} = f(x) + \mathrm{g}(X)U_{eq} \quad \text{(IV.10)}$$

Last but not least, the analogous term Ueq is determined by:

$$U_{eq} = -\frac{\left[\frac{dS}{dX}\right]^T f(X)}{\left[\frac{dS}{dX}\right]^T \mathrm{g}(X)} = \left(1 - \frac{V_{pv}}{V_0}\right) \quad \text{(IV.11)}$$

The TOSMC terms expression is developed [121], it contains three terms:

$$U_{TOSMC} = \left(U_1(t) + U_2(t) + U_3(t)\right) \quad \text{(IV.12)}$$

Where

$$\begin{cases} U_1(t) = \lambda_{1pv}\sqrt{|S|}.sign(S) \\ U_2(t) = \lambda_{2pv}\int sign(S).dt \\ U_3(t) = \lambda_{3pv}.sign(S) \end{cases} \quad \text{(IV.13)}$$

The three tuning constants (λpv1, λpv2, and λpv3) of the TOSMC controller offer more versatility than the typical SMC controller's single tuning parameter. Better performance of the MPPT approach will be ensured by the selection and identification of these elements. The control signal suggested The following is the final expression for this study:

$$U(t) = \left[\left(1 - \frac{V_{pv}}{V_0}\right) + \left(\lambda_1\sqrt{|S|}.sign(S) + \lambda_2\int sign(S).dt + \lambda_3.sign(S)\right)\right] \quad \text{(IV.14)}$$

- **The stability analysis:**

This is how the Lyapunov function is provided

$$V(t) = \frac{1}{2}S^2(t) \quad \text{(IV.15)}$$

sach as

$$\begin{cases} V(0) = 0 \\ V(t) > 0 \quad for \ S(t) \neq 0 \\ \dot{S}(t) \neq 0 \end{cases} \quad \text{(IV.16)}$$

When a system's Lyapunov function derivative is negative, it is said to be stable. Please verify the following criteria:

$$\begin{cases} V(t) < 0 \\ S(t) \neq 0 \\ \dot{S(t)} \neq 0 \end{cases} \quad \text{(IV.17)}$$

The following form can be used to rewrite the stability condition (17).

$$S.\dot{S} < 0 \quad \text{(IV.18)}$$

Equation (IV.9) is utilized to rewrite the sliding surface derivative as follows:

$$\dot{S} = \left[\frac{\partial S}{\partial I_{pv}}\right]\left(-\frac{V_0}{L}(1-6) + \frac{V_{pv}}{L}\right) \quad \text{(IV.19)}$$

It is simple to demonstrate the first term (∂S/∂Ipv) positively [56]:

$$\left[\frac{\partial S}{\partial I_{pv}}\right] = \frac{\partial}{\partial I_{pv}}\left(\frac{I_{pv}}{V_{pv}}\right) + \frac{\partial}{\partial I_{pv}}\left(\frac{\partial I_{pv}}{\partial V_{pv}}\right) \quad \text{(IV.20)}$$

By using the characteristics of derivatives and the chain rule of differentiation, The following form can be used to decrease the first term:

$$\frac{\partial}{\partial I_{pv}}\left(\frac{I_{pv}}{V_{pv}}\right) = \frac{1}{V_{pv}} - \frac{I_{pv}}{V_{pv}^2}\frac{\partial V_{pv}}{\partial I_{pv}} \quad \text{(IV.21)}$$

The PV current Ipv equation given by Eq. (IV.5) may be used to simplify the second half of

Eq. (IV.22) as follows, assuming that Rs is small and Rp is extremely large:

$$\frac{\partial}{\partial I_{pv}}\left(\frac{\partial I_{pv}}{\partial I_{pv}}\right)=\frac{\partial}{\partial I_{pv}}\left(-\frac{1}{aV_{th}}I_0\exp\left(\frac{V_{pv}}{aV_{th}}\right)\right) \quad \text{(IV.22)}$$

Where:

$$I_{pv}\approx I_{pv}-I_0\left[exp\left(\frac{V_{pv}}{aV_{th}}\right)-1\right] \quad \text{(IV.23)}$$

The voltage of The PV panel can be calculated by utilizing the previously Equation (IV.23).

$$V_{pv}=aV_{th}\ln\left[\frac{I_{ph}+I_0+I_{pv}}{I_0}\right] \quad \text{(IV.24)}$$

The final formulation for the second term in Equation (IV.22) is as follows:

$$\frac{\partial}{\partial I_{pv}}\left(\frac{I_{pv}}{V_{pv}}\right)=\frac{1}{aV_{th}}\frac{\partial I_{pv}}{\partial V_{pv}}\frac{\partial V_{pv}}{\partial I_{pv}} \quad \text{(IV.25)}$$

When (IV.23) and (IV.25) are substituted into (IV.22) the following equation is produced:

$$\left[\frac{\partial S}{\partial I_{pv}}\right]=\frac{1}{V_{pv}}-\frac{I_{pv}}{V_{pv}^2}\frac{\partial V_{pv}}{\partial I_{pv}}+\frac{1}{aV_{th}}\frac{\partial I_{pv}}{\partial V_{pv}}\frac{\partial V_{pv}}{\partial I_{pv}} \quad \text{(IV.26)}$$

This derivative, which is always negative, can be found by taking the derivative of the current Ipv with respect to the voltage.

$$\frac{\partial I_{pv}}{\partial V_{pv}}=-\frac{1}{aV_{th}}I_0 exp\left(\frac{V_{pv}}{aV_{th}}\right)<0 \quad \text{(IV.27)}$$

Additionally, the voltage V_{pv} derivative of the current is always negative:

$$\frac{\partial I_{pv}}{\partial V_{pv}}=-aV_{th}\left(\frac{I_0}{I_{ph}+I_0+I_{pv}}\right)<0 \quad \text{(IV.28)}$$

One may infer from Eqs. (IV.27) and (IV.28) that Eq. (IV.21)'s first term is always positive.

$$\left[\frac{\partial S}{\partial I_{pv}}\right]>0 \quad \text{(IV.29)}$$

The following is a simplified version of the second term in Eq. (IV.21):

$$\dot{X}=\left(-\frac{V_0}{L}(1-U)+\frac{V_{pv}}{L}\right) \quad \text{(IV.30)}$$

$$\dot{X}=\left(-\frac{V_0}{L}\left(1-\left(U_{eq}+U_{TOSMC}\right)\right)+\frac{V_{pv}}{L}\right) \quad \text{(IV.31)}$$

$$\dot{X}=\left(-\frac{V_0}{L}\left(1-\left(\left(1-\frac{V_{pv}}{V_0}\right)+U_{TOSMC}\right)\right)+\frac{V_{pv}}{L}\right) \quad \text{(IV.32)}$$

$$\dot{X}=\left(\frac{V_0}{L}(U_{TOSMC})\right) \quad \text{(IV.33)}$$

$$\dot{X}=\left(\frac{V_0}{L}\left(\lambda_{pv1}\sqrt{|S|}.sign(S)+\lambda_{pv2}\int sign(S).dt+\lambda_{pv3}.sign(S)\right)\right) \quad \text{(IV.34)}$$

The sign of the second term in Eq. (IV.21) depends on the sign of the control term UTOSMC, as we can see from Eqs. (IV.33) and (IV.34).

In conclusion, the following is an expression for the stability criterion (IV.35):$S.\dot{S}=$

$$S\left[\frac{dS}{dI_{pv}}\right]\frac{V_0}{L}\left(\lambda_{pv1}\sqrt{|S|}.sign(S)+\lambda_{pv2}\int sign(S).dt+\lambda_{pv3}.sign(S)\right)<0 \quad \text{(IV.35)}$$

The following is an expression for the stability criterion, provided that (∂S/∂Ipv) is always positive:

$$S.\dot{S}<0 \Rightarrow \left(\lambda_{pv1}\sqrt{|S|}.sign(|S|)+\lambda_{pv2}\int sign(S).dt+\lambda_{pv3}.sign(|S|)\right)<0 \quad \text{(IV.36)}$$

The λ_{pv1}, λ_{pv2}, and λ_{pv3} numbers must all be negative. Moreover, $|\lambda_{pv1}|$ and $|\lambda_{pv3}|$ must be greater than $|\lambda_{pv2}|$ to guarantee system stability. The following formula still holds true in this case.

$$\left(\lambda_{pv1}\sqrt{|S|}.|S|+\lambda_{pv3}|S|\right)<-S.\lambda_{pv2}\int sign(S).dt \quad \text{(IV.37)}$$

Figure.IV.2 illustrates the recommended MPPT technique for a solar system based on the TOSMC approach.

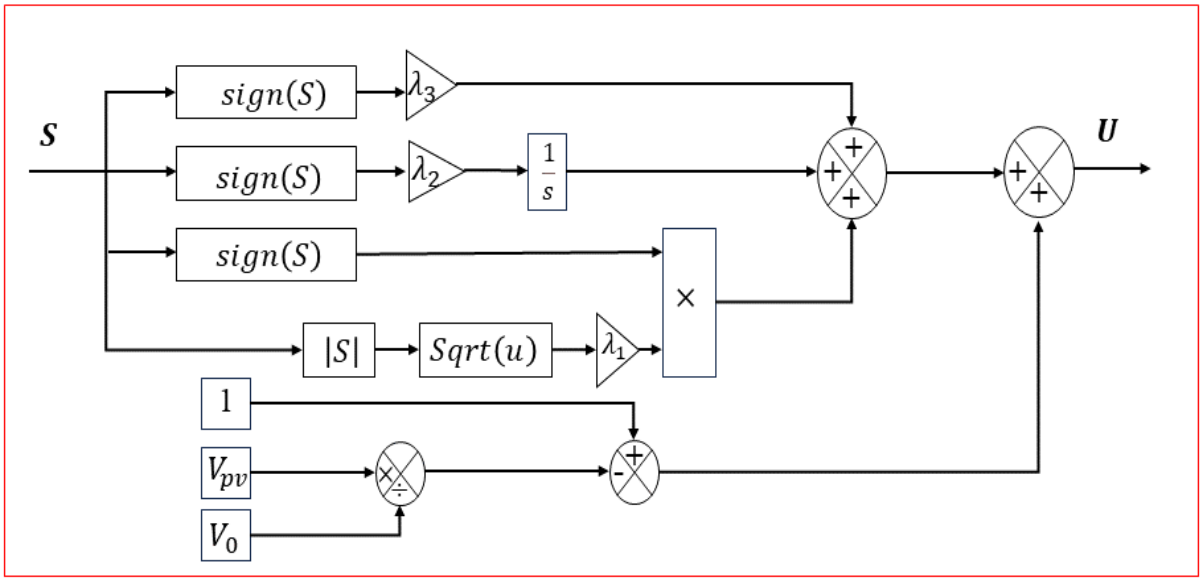

Figure. IV.2 Structure of the suggested MPPT-based PV system TOSMC algorithm

IV.2.2 TOSMC for Inverter Current Control Using DCC-PWM

The purpose of this control strategy is to ensure that the inverter injects the appropriate compensation current into the grid in order to eliminate harmonic distortions caused by nonlinear loads. To achieve this objective, a Third Order Sliding Mode Control (TOSMC) technique is proposed and combined with Direct Current Control using Pulse Width Modulation (DCC-PWM) to generate precise and robust switching signals for the inverter.

Using Kirchhoff's Voltage Law (KVL), the dynamic equation for one phase of the shunt active power filter (SAPF) can be expressed as:

$$L_f\frac{di_f}{dt}+R_f i_f=V_{inv}-V_g \quad \text{(IV.38)}$$

Rewriting this equation, the plant model is:

$$\frac{di_f}{dt} = \frac{1}{L_f}\left(V_{inv} - V_g - R_f i_f\right) \quad \text{(IV.39)}$$

This represents the dynamic behavior of the system that will be regulated using TOSMC. The control objective is to make the inverter current i_f accurately track a reference current i_f^*, which is obtained from a harmonic detection algorithm.

The sliding surface used in this work is defined as the difference between the reference and the measured current:

$$S(t) = i_f^*(t) - i_f(t) \quad \text{(IV.40)}$$

The TOSMC control action for each phase is implemented as a sum of three components:

$$u_{i_b}(t) = u_{i_{b1}} + u_{i_{b2}} + u_{i_{b3}} \quad \text{(IV.41)}$$

Where:

$$\begin{aligned} u_{i_{b1}} &= k_{i_{b1}}\sqrt{|S_{i_b}|}\,\text{sign}(S_{i_b}) \\ u_{i_{b2}} &= k_{i_{b2}}\int \text{sign}(S_{i_b})\,dt \\ u_{i_{b3}} &= k_{i_{b3}}\,\text{sign}(S_{i_b}) \end{aligned} \quad \text{(IV.42)}$$

where $k_{i_{b1}}$, $k_{i_{b2}}$, $k_{i_{b3}}$ are the control gains,

IV.2.2.1 Application to DCC-PWM

The control output *u(t)* generated by the TOSMC block is applied to the DCC-PWM scheme, where it is compared to a high-frequency triangular carrier signal. The points where *u(t)* intersects this carrier define the switching instants for generating PWM pulses. These pulses control the switches of the three-level neutral point clamped (NPC) inverter. This method allows precise modulation of the inverter's output voltage and current, resulting in accurate current tracking and robust performance even with dynamic load changes and grid disturbances.[123]

Specifically, the process involves:

- Using *u(t)* from the TOSMC (Third-Order Sliding Mode Control) as the reference control input.
- Comparing *u(t)* against a high-frequency triangular carrier waveform in the DCC-PWM (Direct Current Control Pulse Width Modulation) scheme.
- Switching instants are determined at intersections of *u(t)* and the carrier, which generates PWM signals.
- These PWM signals drive the three-level NPC inverter switches, enabling multi-level voltage output.

- The multi-level output reduces voltage stress on switches, improves harmonic characteristics, and enhances inverter efficiency and control accuracy.
- Consequently, this setup enhances current tracking accuracy, ensuring stable and robust inverter operation under varying loads and grid conditions.

This combination of TOSMC and DCC-PWM modulation enables high-performance control of the three-level NPC inverter with precise voltage regulation and improved dynamic response. Figure.IV.3 illustrates the TOSMC controller structure based on the DCC-PWM technique.

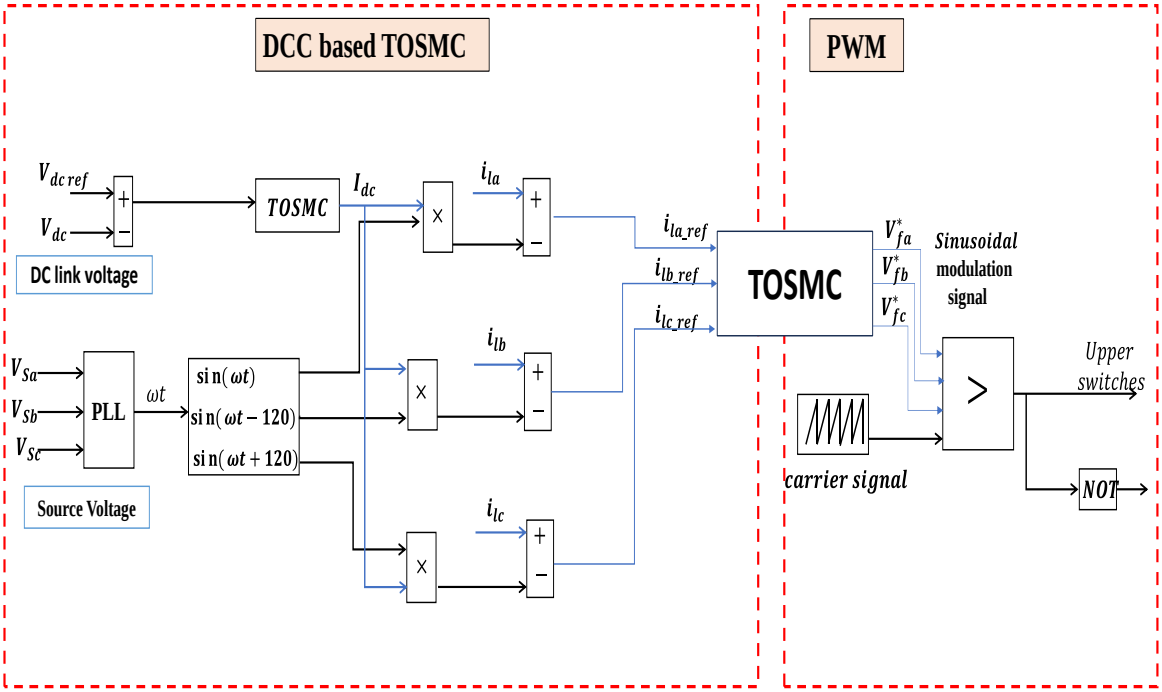

Figure. IV.3 TOSMC controller based on DCC-PWM

IV.2.3 Dc link voltage management

The goal of the DC voltage control loop is to maintain the DC voltage at a specified reference value without generating errors [124]. As shown in Figure.IV.4, vdc is the intermediate circuit voltage and vdc* is the reference voltage. The TOSMC rule is:

$$U_{TOSMC_{vdc}} = \left(U_{vd1}(t) + U_{vdc2}(t) + U_{vdc3}(t)\right) \quad \text{(IV.43)}$$

With

$$\begin{cases} U_{vdc1}(t) = \lambda_{1vdc}\sqrt{|S|}.sign(S) \\ U_{vdc2}(t) = \lambda_{2vdc}\int sign(S).dt \\ U_{vdc3}(t) = \lambda_{3vdc}.sign(S) \end{cases} \quad \text{(IV.44)}$$

where λ_{1vdc} , λ_{2vdc} and λ_{3vdc} are the control gains of TOSMC.

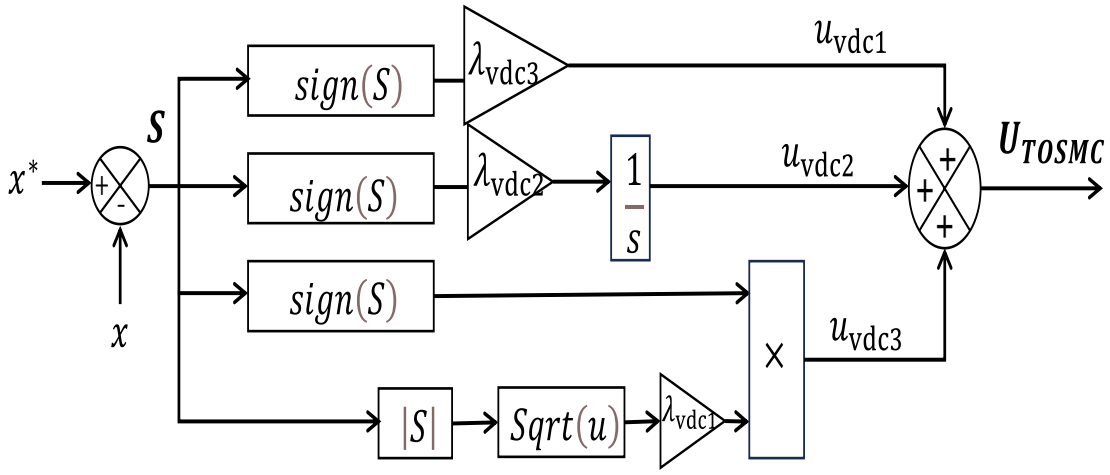

Figure. IV.4 Schematic for DC bus voltage regulation

IV.3 Simulation Results and Discussion

In order to evaluate the performance of the proposed control strategies, a series of simulations have been carried out in MATLAB/Simulink using the parameters defined in the previous sections. The study is divided into three parts:

Part 0: (System Performance Before Filtering) The nonlinear load is connected directly to the grid without the presence of the shunt active power filter (APF). This baseline case illustrates the level of harmonic distortion, voltage quality, and DC-link voltage fluctuations in the absence of compensation.

Part 1: (TOSMC for PV with PI for SAPF) The PV system's maximum power point tracking (MPPT) is implemented using the Third-Order Sliding Mode Control (TOSMC) algorithm, while the APF is regulated by a classical Proportional-Integral (PI) controller for harmonic mitigation.

Part 2: (TOSMC for PV with TOSMC for SAPF) Both the PV system and the APF are controlled by the TOSMC algorithm, allowing for a fully sliding-mode-based regulation strategy.

For each part, the control scheme design is briefly described, followed by the corresponding simulation results and performance evaluation.

Part 0 : System Performance Before Filtering

Before implementing any active filtering strategy, the system was simulated under the same load and grid conditions to establish a baseline reference for harmonic distortion and power quality. In this configuration, the nonlinear load is connected directly to the grid without the APF, while the PV generator remains connected to the DC-link but operates without harmonic compensation on the AC side. The system configuration of the studied baseline case, without APF, is illustrated in Figure IV.5.

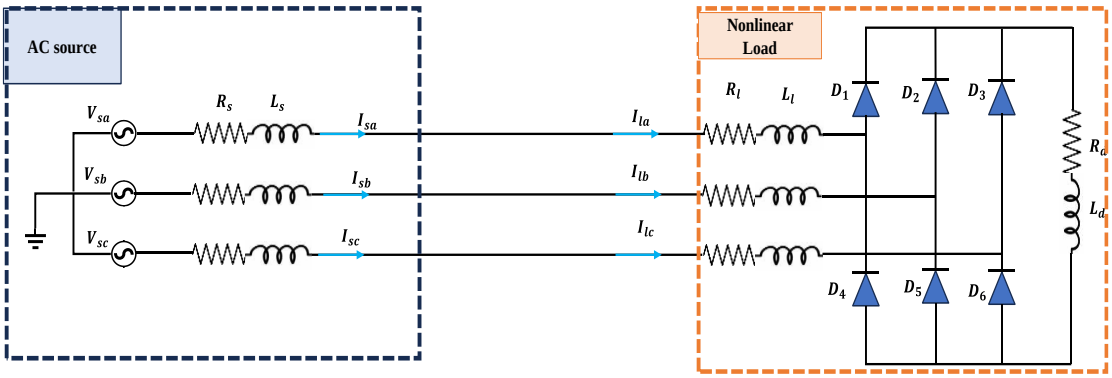

Figure. IV. 5 System Configuration Without Active Power Filter

Figures.IV.6 present the source current and voltage waveforms.The nonlinear load strongly impacts the harmonic spectrum of the grid source current. As shown in Figure.IV.7, the Total Harmonic Distortion (THD) reaches 27.53%, indicating a high level of distortion in the absence of filtering. The amplitude of the fundamental current component at 50 Hz is measured at 4.805 A. This relatively low value, combined with the significant harmonic content, highlights the inadequate power quality prior to the filtering stage.

These results clearly demonstrate the need for an active power filter to improve current waveform quality, reduce harmonic distortion.

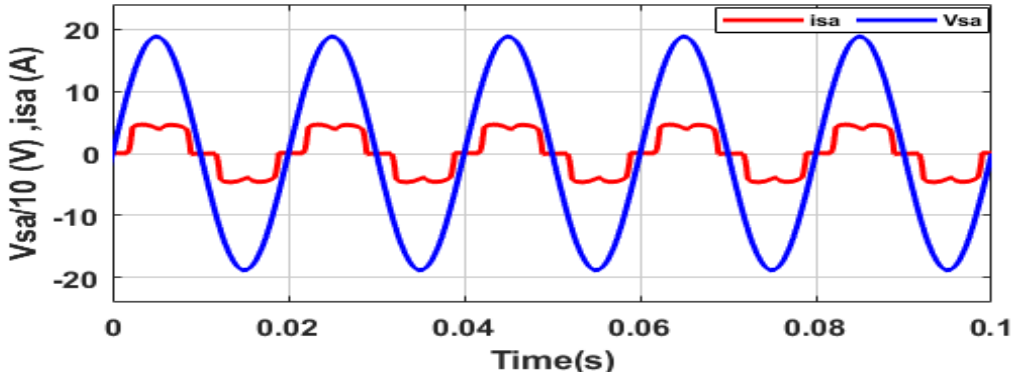

Figure. IV. 6 voltage, current source before filtering

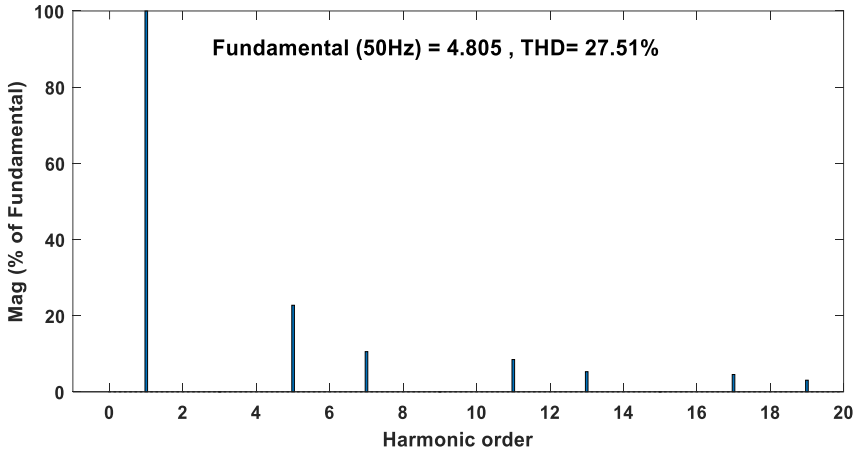

Figure. IV.7 harmonic spectra of the grid source before filtering.

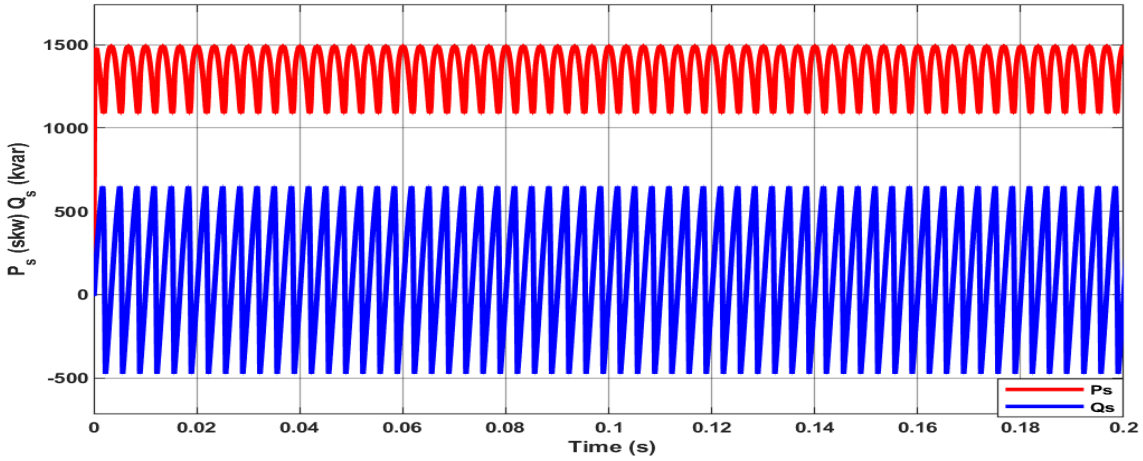

Figure. IV.8 active and reactive power of grid

Figure.IV.8 shows the active power (Ps) and reactive power (Qs) at the grid side *before* any filtering is applied. The presence of a nonlinear load causes significant oscillations in both powers due to harmonic components. The active power (Ps) oscillates around an average of 1400 kW with a pronounced high-frequency ripple. Meanwhile, the reactive power (Qs) fluctuates between approximately (+600 KVAR) and (–500 KVAR). These variations indicate

a poor power quality and considerable reactive power exchange with the grid. The high ripple in both signals is a direct result of harmonic distortion, which leads to unstable instantaneous power and inefficient energy transfer.

Part 1: **TOSMC for PV System with PI Control for Active Power Filter**

The first configuration connects the PV generator to the NPC inverter's DC-link via a boost converter controlled by a TOSMC-based MPPT for fast and accurate power tracking. A PI-controlled APF regulates the DC-link voltage and compensates harmonics using a selected detection method and PWM strategy. The design (Figure.IV.9) demonstrates the TOSMC's effectiveness in maintaining maximum PV power and the PI regulator's role in improving power quality.

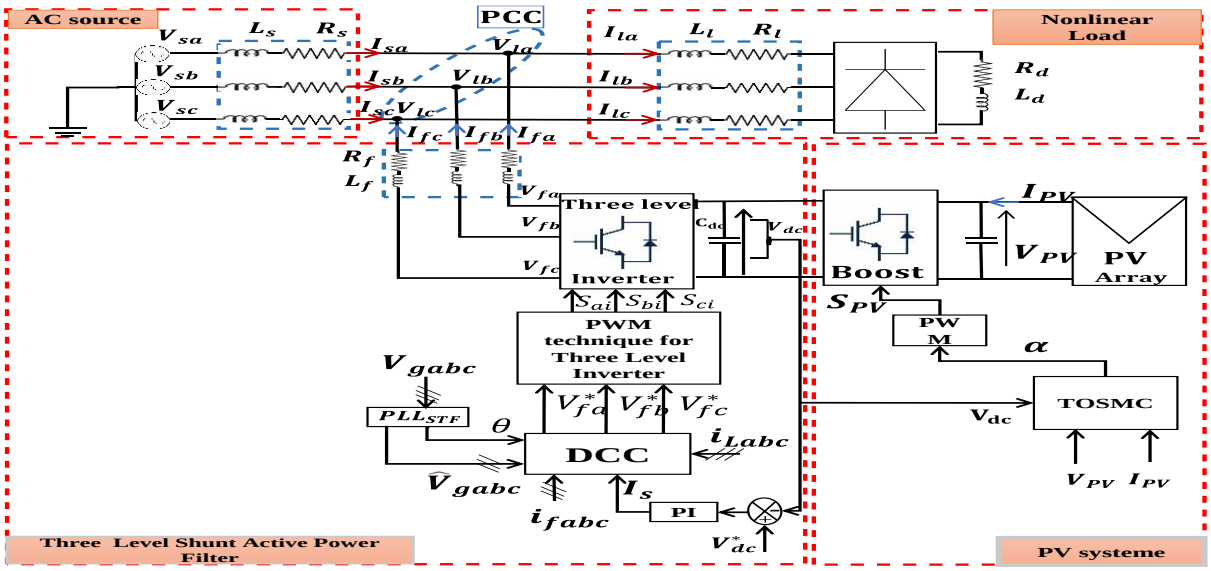

Figure. IV.9 General circuit diagram for the grid-connected solar system.

The aim of this configuration is to demonstrate the capability of the TOSMC to maintain maximum power extraction from the PV system under dynamic environmental conditions, while evaluating the performance of the PI-controlled APF in reducing source current harmonics and stabilizing the DC-link voltage. To assess the robustness of both control methods, four test cases were simulated for different combinations of nonlinear load values and solar irradiation levels:

Case 1 (0–0.4 s) Rd3 = 300 Ω, G = 1000 W/m²;

Case 2 (0.4–0.7 s) Rd2 = 150 Ω, G = 1000 W/m²;

Case 3 (0–0.4 s) Rd1 = 100 Ω with a decrease in irradiation from G = 1000 W/m² to 0 W/m².

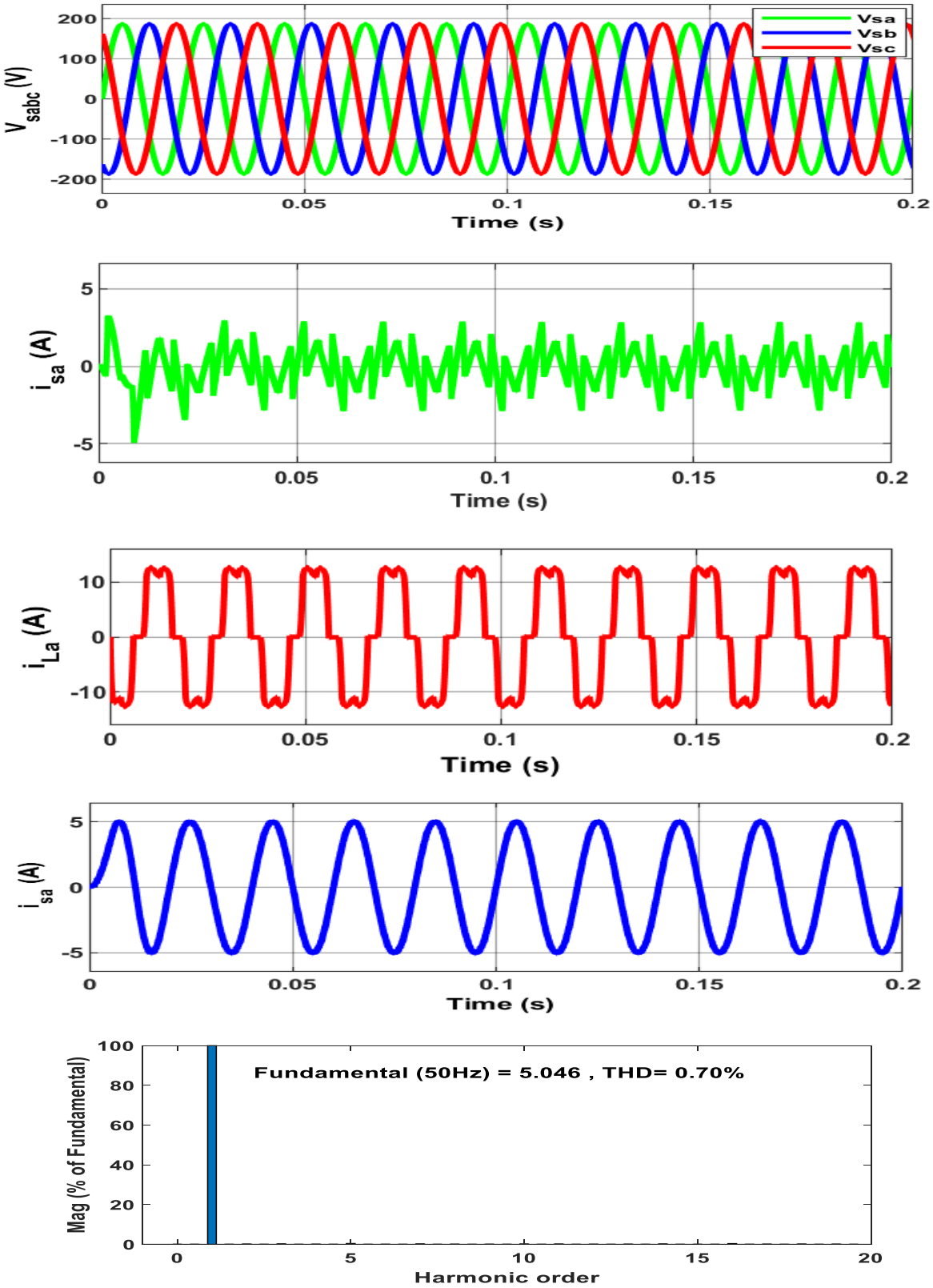

Figure. IV.10 presents the results obtained when the system operates under TOSMC for PV System with PI Control for Active Power Filter

Figure.IV.10 illustrates the performance of the system when the photovoltaic (PV) generation is controlled using the Third-Order Sliding Mode Control (TOSMC) strategy for MPPT, while the shunt

active power filter is managed by a conventional Proportional–Integral (PI) controller. The presented results include the grid current waveforms before and after filtering, as well as the corresponding harmonic spectrum. In this operating mode, the load current contains pronounced harmonic distortion; however, the PI-controlled active filter significantly improves the quality of the grid-side current, producing a waveform that is smoother and much closer to a pure sinusoid. This enhancement is confirmed by the harmonic spectrum, which shows a Total Harmonic Distortion (THD) of approximately 0.70%, indicating effective harmonic mitigation.

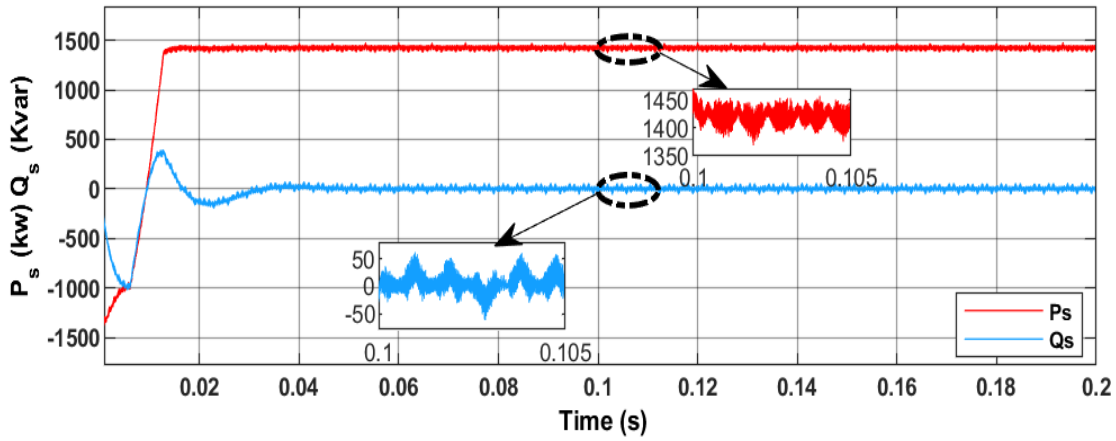

Figure. IV.11 active and reactive power of grid

Figure.IV.11 presents the dynamic response of the system when the PV generation is controlled using the Third-Order Sliding Mode Control (TOSMC) for MPPT, and the shunt active power filter is governed by a conventional PI regulator. After an initial transient phase, the active power rapidly stabilizes at around 1400 kW, with the oscillations considerably reduced compared to the pre-filtering case. Simultaneously, the reactive power converges toward zero, indicating effective compensation of reactive components. However, the zoomed views reveal small residual fluctuations in both Ps and Qs , which suggests that while the PI controller improves the steady-state performance and mitigates harmonics, it does not completely eliminate the high-frequency components. Overall, the use of the PI-based filter control achieves satisfactory results but still leaves a margin for further enhancement in power quality.

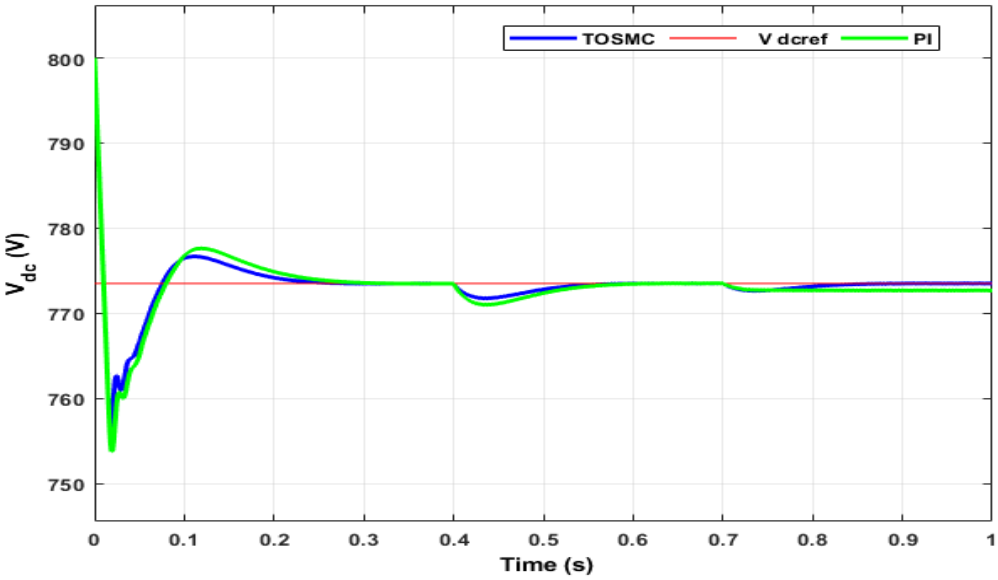

Figure. IV.12 Response of DC-link voltage.

Figure.IV.12 shows the DC-link voltage Vdc response for the PV system controlled by TOSMC (blue) and PI (green), with a reference voltage $V_{dc,ref}$ of 773 V (red). At start-up, both controllers overshoot, but TOSMC settles faster and with fewer oscillations. Following a disturbance at t=0.4 s, TOSMC restores the voltage more quickly than PI, confirming its superior transient and steady-state performance.

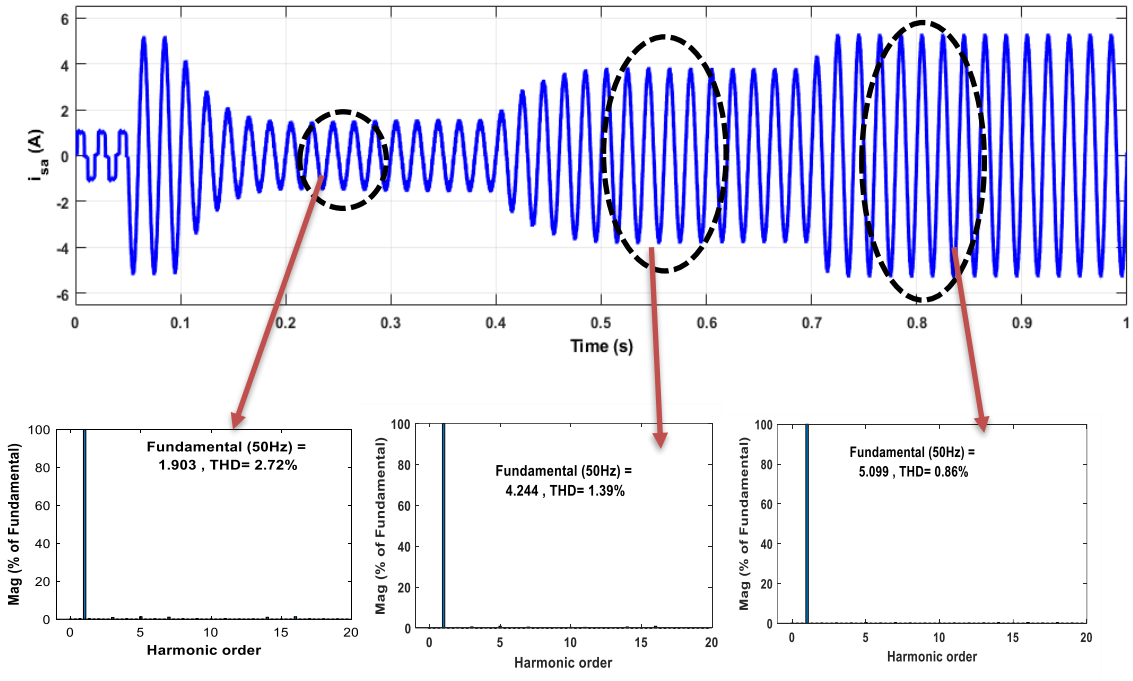

Figure. IV.13 Grid source current with a spectral harmonic based on PI after filtering.

Figure.IV.13 presents the grid source current waveform after filtering using the conventional Proportional Integral (PI) controller during a robustness test involving a sudden load change. At around 0.2 s, shortly after the disturbance, the current shows transient oscillations with a

THD of 2.72%. By 0.5 s, the controller partially compensates for the new load conditions, lowering the THD to 1.39%. In the steady state, at approximately 0.85 s, the current waveform approaches a sinusoidal shape, and the THD is reduced to 0.86%. Although the PI controller improves current quality compared to the unfiltered case, the harmonic suppression and transient recovery are less effective than those achieved with the TOSMC, as reflected by the higher residual THD values and slower settling time

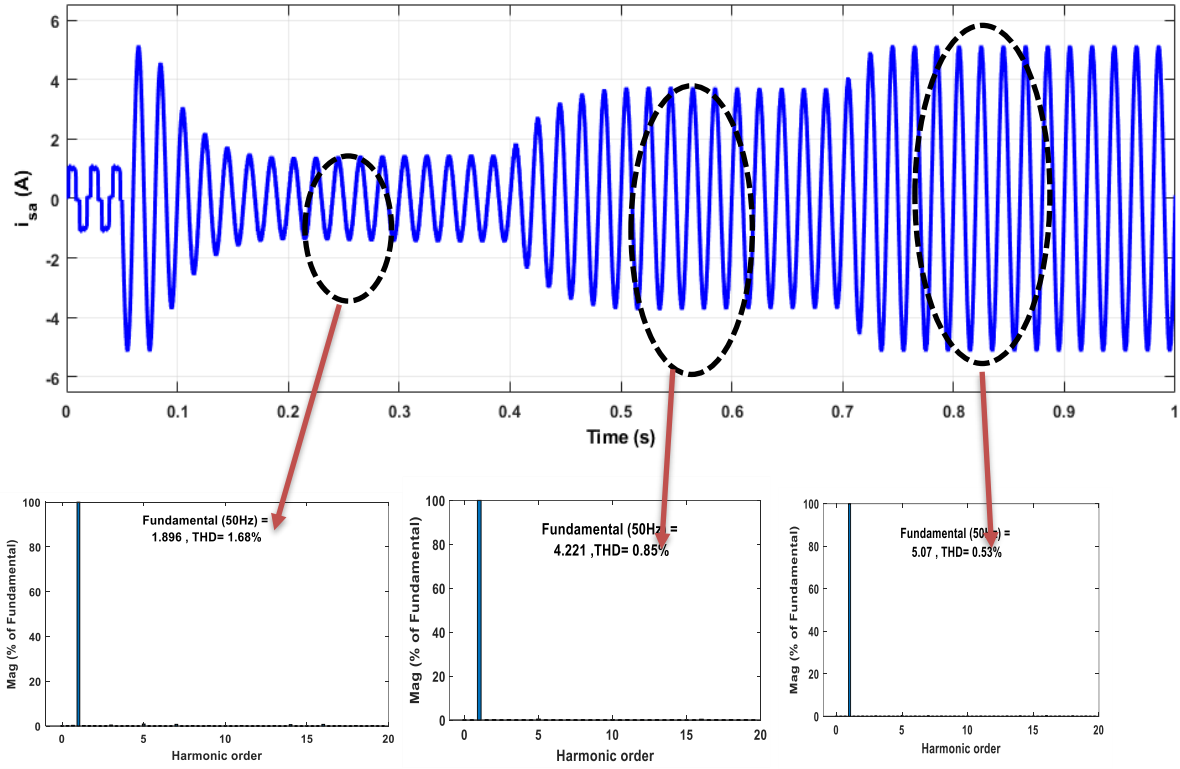

Figure. IV.14 Grid source current after filtering using spectral harmonic determined by TOSMC.

Figure.IV.14 shows the grid source current waveform after filtering using the Third-Order Sliding Mode Control (TOSMC) strategy during a robustness test, in which the load was intentionally changed to evaluate the controller's adaptability. At approximately 0.2 s, shortly after the load change, the current exhibits transient oscillations with a THD of 1.58%. By around 0.5 s, the controller compensates for the new load conditions, improving the current quality and reducing THD to 0.85%. In the steady state, at about 0.85 s, the current becomes nearly perfectly sinusoidal, with the THD minimized to 0.35%. These results confirm that the TOSMC not only achieves excellent harmonic suppression but also maintains robust performance and fast dynamic response under sudden load variations.

In all scenarios, THD values are well below the IEEE-519 recommended limit of 5%, and consistently better than those achieved by PI control. This validates the superior harmonic mitigation and dynamic performance of the TOSMC–PV system in grid-connected applications

with nonlinear loads.

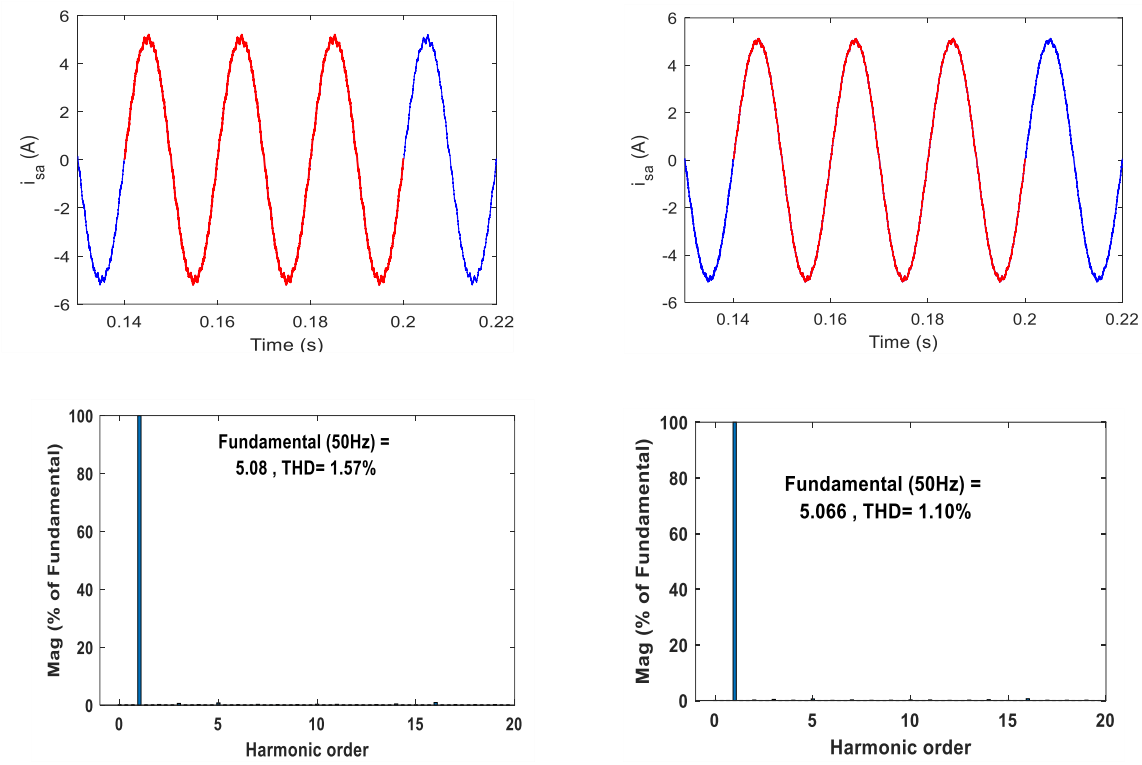

(a) **(b)**

Figure. IV.15 THD of source current after filtering and without PV system at G=0 W/m2: (a) PI, (b) TOSMC.

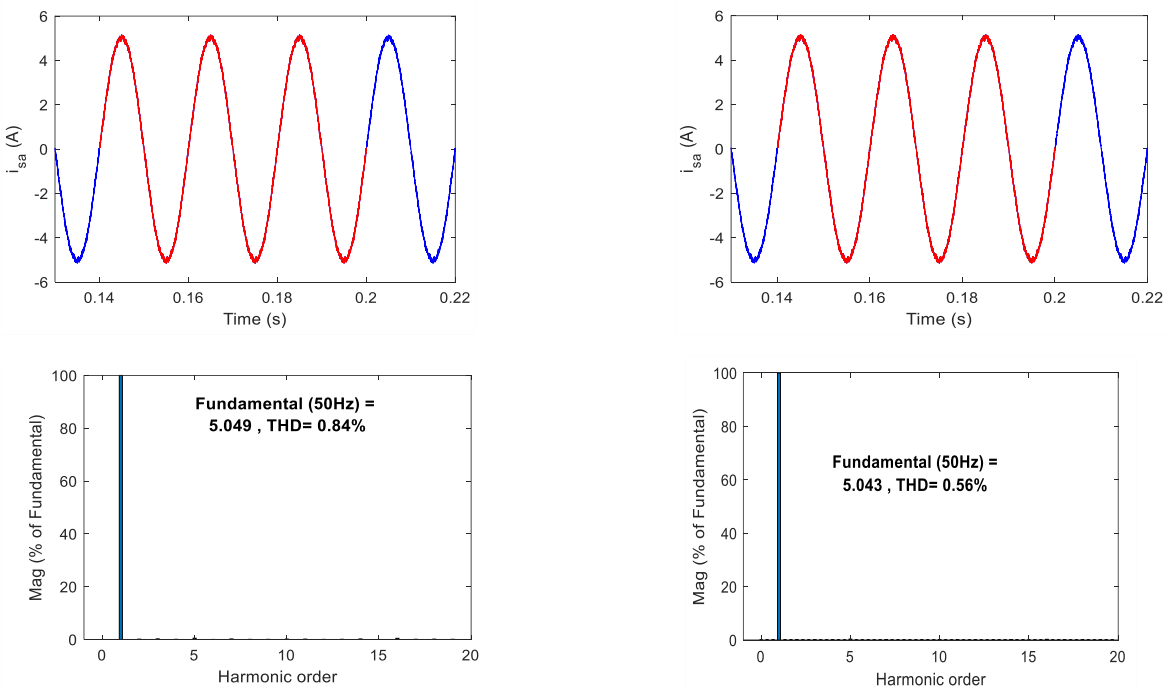

(a) (b)

Figure. IV.16 Source current THD values: (a) PI, (b) TOSMC, following PV system filtration at G = 1000 W/m2.

The provided figures (IV.15, IV.16) collectively demonstrate the effectiveness of different control strategies and the role of a photovoltaic (PV) system in enhancing power quality. Figure.IV.15, which shows the system without the PV system, indicates that the TOSMC controller is more effective than the PI controller, achieving a lower Total Harmonic Distortion (THD) of 1.10% compared to the PI's 1.57%. This trend is reinforced in Figure.IV.16, where the PV system is active. In this scenario, both controllers show improved performance, with the PI's THD dropping to 0.84% and the TOSMC's THD further decreasing to an impressive 0.56%. This consistent data across both figures confirms that the TOSMC controller consistently outperforms the PI controller, and the integration of the PV system provides a significant additional benefit in reducing harmonic distortions and improving overall power quality.

Part 2 : TOSMC for Both PV System and Active Power Filter

As shown in Figure.IV.17, the system applies Third Order Sliding Mode Control (TOSMC) to both the PV generator and the shunt active power filter. On the PV side, TOSMC-based MPPT optimizes energy capture under changing conditions. On the grid side, TOSMC with DCC-PWM regulates inverter current for harmonic elimination and reactive power compensation. This configuration improves robustness, accelerates response, stabilizes the DC link, and reduces THD compared to the PI-based control in Part 1.

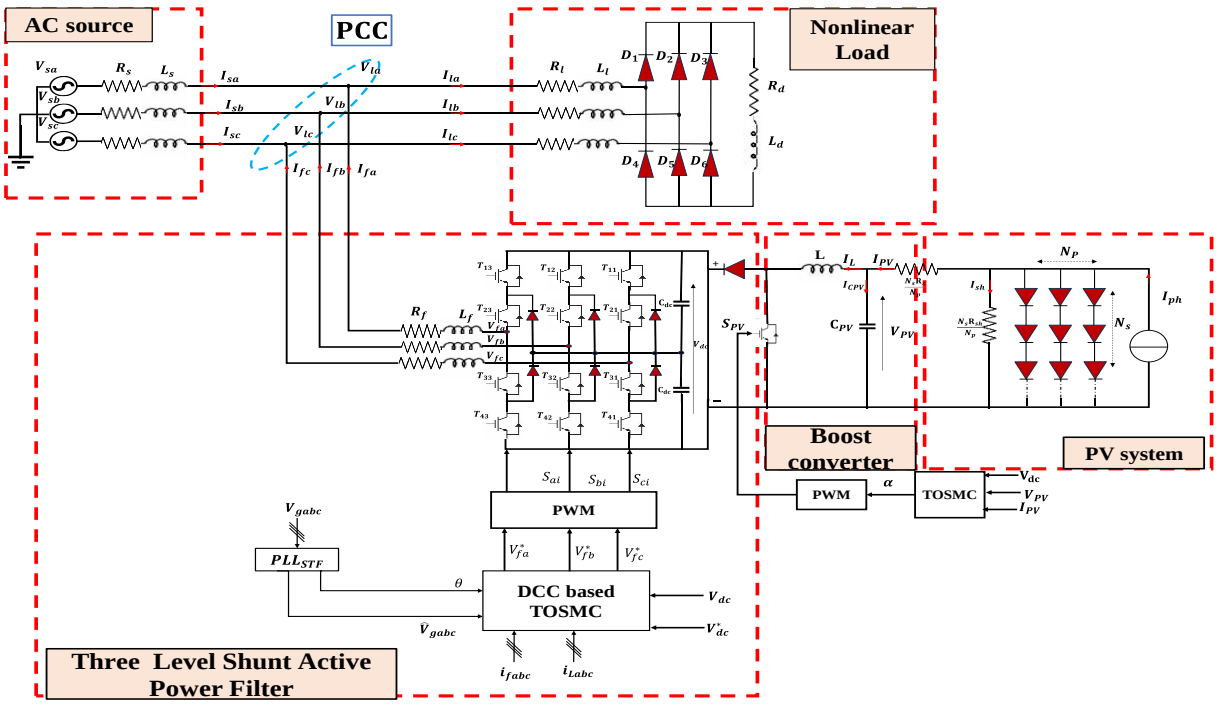

Figure. IV.17 shows the overall architecture of the proposed grid system.

The aim of this second configuration is to evaluate the combined performance of the Third-Order Sliding Mode Control (TOSMC) applied to both the MPPT of the PV generator and the current control of the multilevel Shunt Active Power Filter (SAPF) using the DCC-PWM strategy. This test scenario focuses on verifying the ability of the integrated control system to simultaneously ensure maximum power extraction from the PV array and effective mitigation of load-induced current harmonics under varying operating conditions. To challenge the robustness of the proposed control approach, three test cases were conducted with step changes in nonlinear load and solar irradiation:

Case 1 (0–0.3 s) – Rd3 = 300 Ω, G = 1000 W/m²;

Case 2 (0.3–0.6 s) – Rd2 = 150 Ω with a reduction of solar irradiation to G = 1000 W/m²;

Case 3 (0–0.4 s) Rd1 = 100 Ω with a decrease in irradiation from G = 1000 W/m² to 0 W/m².

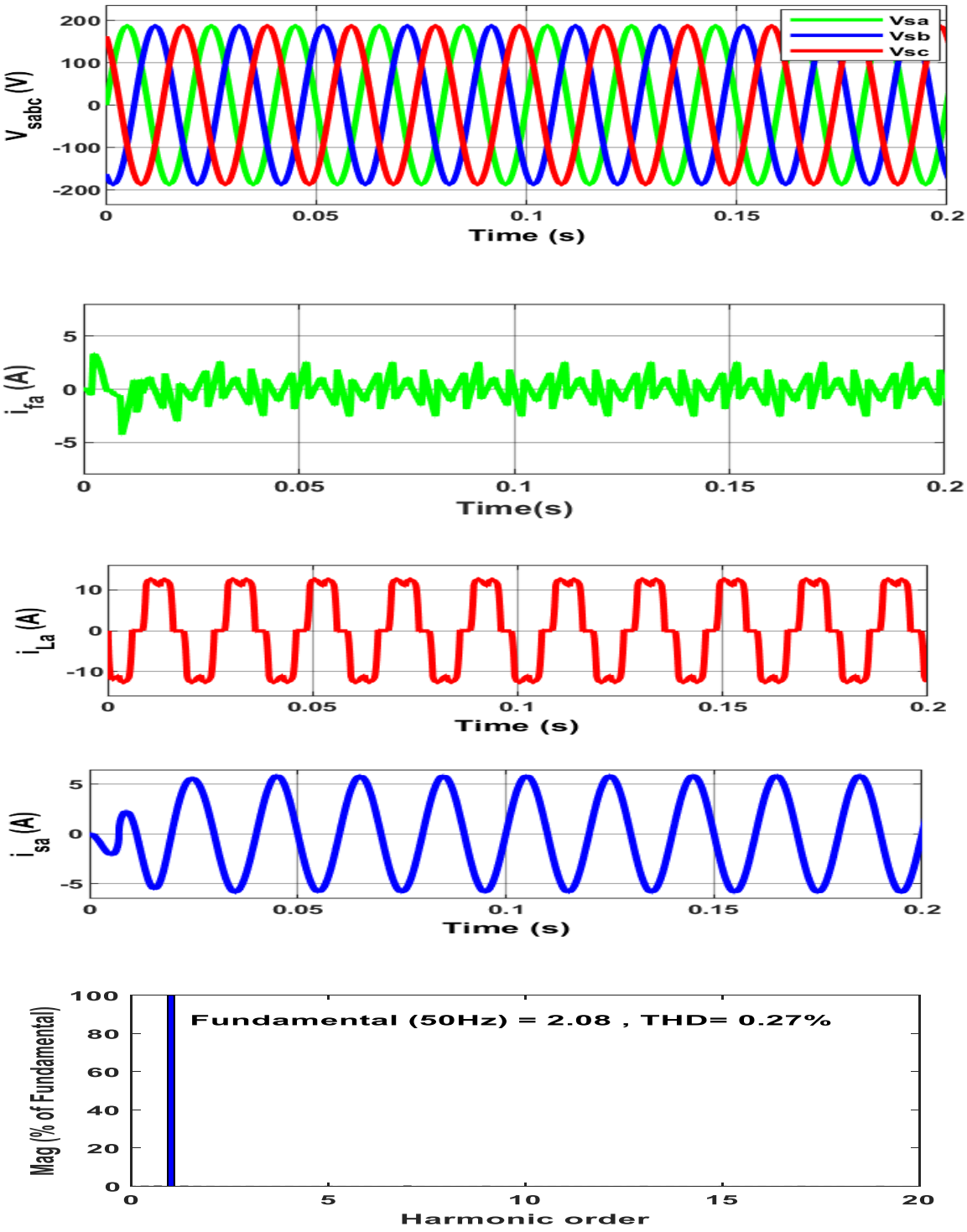

Figure. IV.18 presents the results obtained when the system operates under Third Order Sliding Mode Control (TOSMC)

Figure.IV.18 presents the system's performance when controlled by a Third-Order Sliding Mode Control (TOSMC) strategy. The top plots show the clean sinusoidal grid voltages and currents, while a separate plot reveals the non-sinusoidal, harmonically-rich current of the nonlinear load. The core result is shown in the fourth plot, where the grid-side current (i_{sa}) is a

clean sinusoid, indicating successful harmonic elimination. The effectiveness of the TOSMC is confirmed by the final plot, a harmonic spectrum showing a dominant fundamental frequency and an exceptionally low Total Harmonic Distortion (THD) of 0.27%, which signifies excellent power quality and robust harmonic compensation.

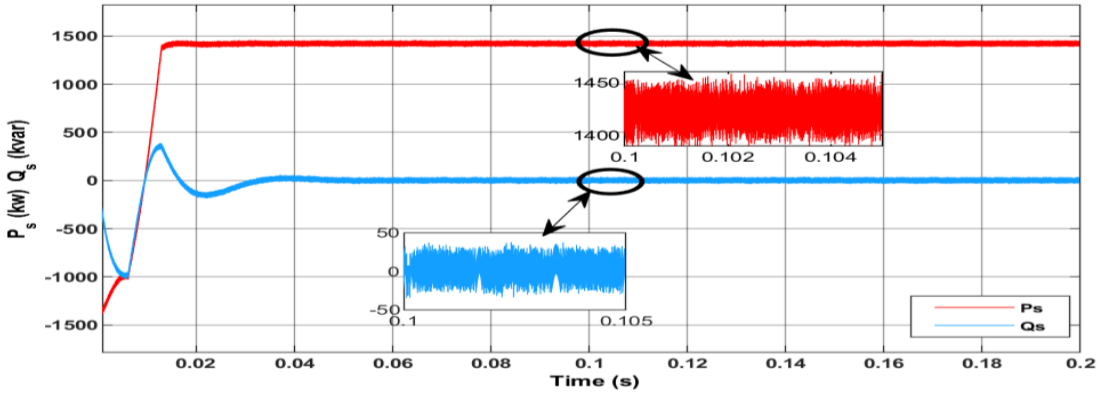

Figure. IV.19 active and reactive power of grid

Figure.IV.19 depicts the results when both the PV generation and the shunt active power filter are controlled using the Third-Order Sliding Mode Control strategy. In this configuration, the system exhibits a fast transient response, with the active power reaching a steady value of approximately 1450 kW within a very short time and maintaining exceptional stability thereafter. The reactive power remains extremely close to zero throughout the operation, with negligible oscillations, as highlighted in the zoomed sections. Compared to the PI-based case, the TOSMC-based control of the filter demonstrates superior ripple suppression, stronger robustness to disturbances, and a more precise compensation of harmonics. This results in a substantial improvement in power quality, ensuring a nearly constant active power delivery to the grid and a complete mitigation of reactive power exchange.

Figure IV.20 places us directly into the DC-link voltage V_{dc} response, where both controllers are tasked with tracking the reference V_{dcref}. At start-up, both curves overshoot the reference, but the TOSMC (blue line) settles faster, with a smaller overshoot. At t≈0.35s, a sudden load change is applied to test robustness. The TOSMC shows only a slight voltage dip and rapidly returns to the reference, while the PI (green line) experiences a larger drop and a slower recovery. This clear contrast demonstrates TOSMC's superior ability to maintain voltage stability and quickly restore performance after load disturbances.

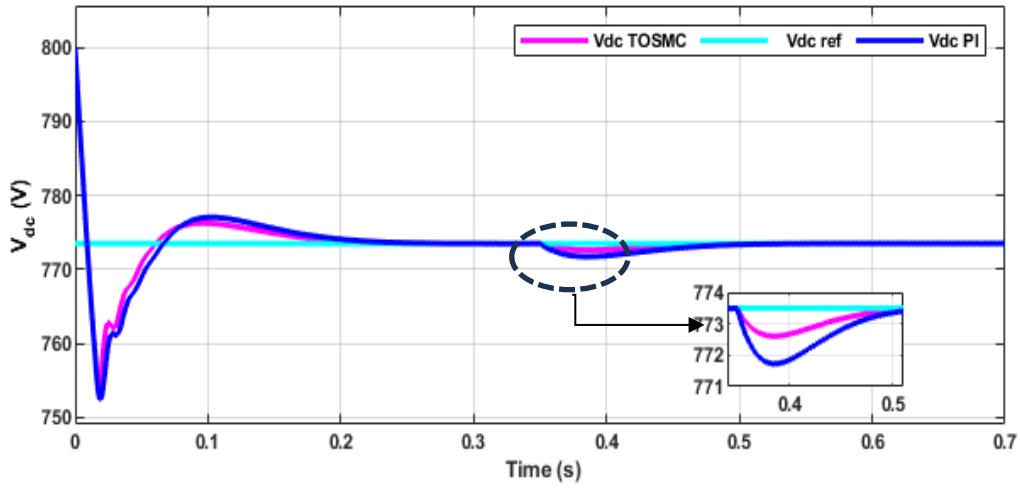

Figure. IV.20 Control of DC-link voltage

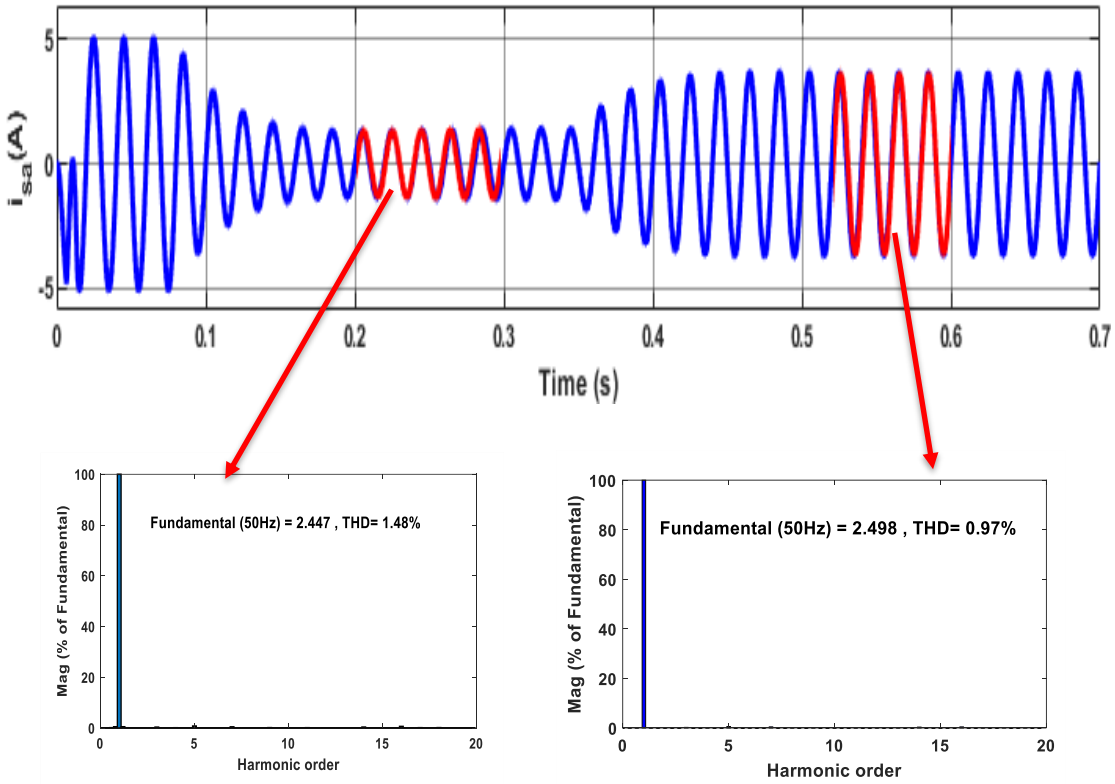

Figure. IV.21 Value of source current THD with variations in nonlinear loads after PI filtering

The figure.IV.21 illustrates the effectiveness of a PI filter in reducing Total Harmonic Distortion (THD) in a source current, even when the load changes. The top graph shows a current waveform with two distinct sections corresponding to different nonlinear loads. The two bar graphs below, labeled as "Value of source current THD with variations in nonlinear loads after PI filtering," analyze the harmonic content of the current at these two points. The left graph shows a fundamental frequency of 50 Hz and a THD of 1.48% for the initial load. After the load changes, the right graph shows a fundamental frequency of 50 Hz and a reduced

THD of 0.97%. This demonstrates that the filter successfully maintains a low THD, actively improving the quality of the current even when a new, potentially more distortive, nonlinear load is introduced. The result highlights the filter's ability to provide a clean and stable power supply under dynamic operating conditions.

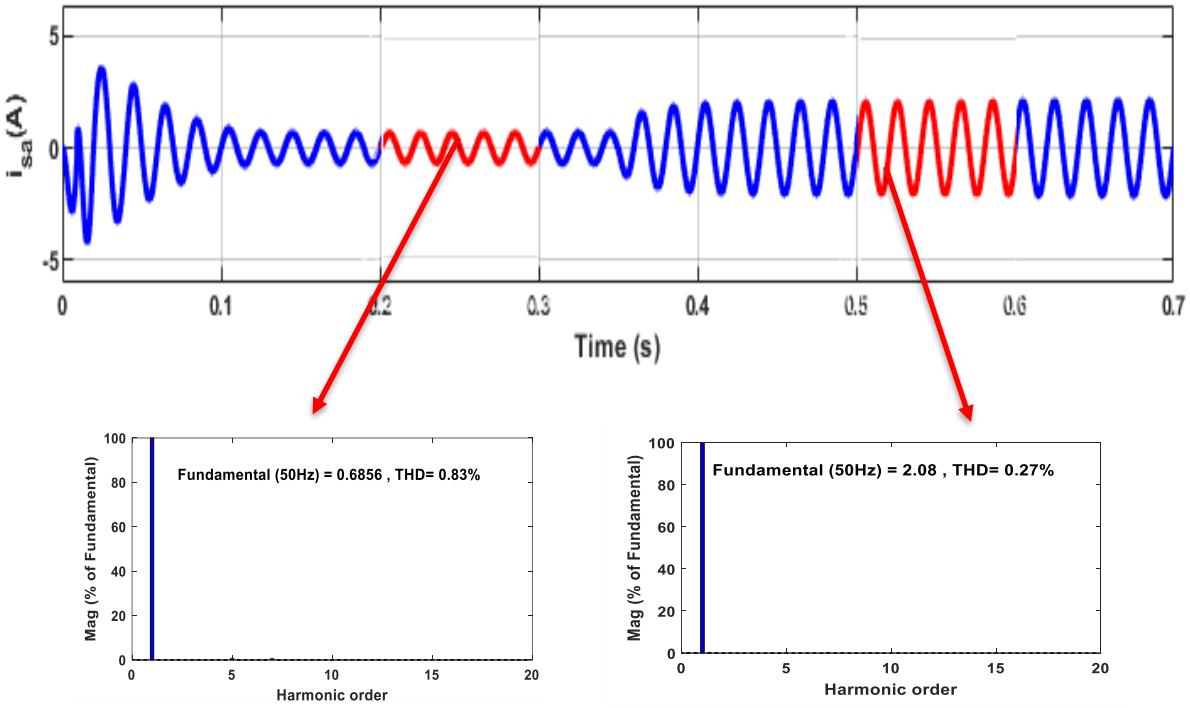

Figure. IV.22 Source current THD value following filtering and load modification using TOSMC

The figure.IV.22 demonstrates the exceptional performance of a TOSMC (Total Order Sliding Mode Control) filter in suppressing Total Harmonic Distortion (THD) in a source current, even under varying load conditions. The top graph displays a current waveform whose amplitude increases significantly, indicating a modification to the load. The two bar graphs below, labeled "Source current THD value following filtering and load modification using TOSMC," provide a detailed analysis. The first graph shows an initial THD of 0.83% for the first load. After the load changes, the second graph shows an even lower THD of 0.27%. This clearly indicates that the TOSMC filter not only effectively maintains a low THD but actively improves it following the load modification, showcasing its robustness and superior ability to mitigate harmonic distortion under dynamic operating conditions.

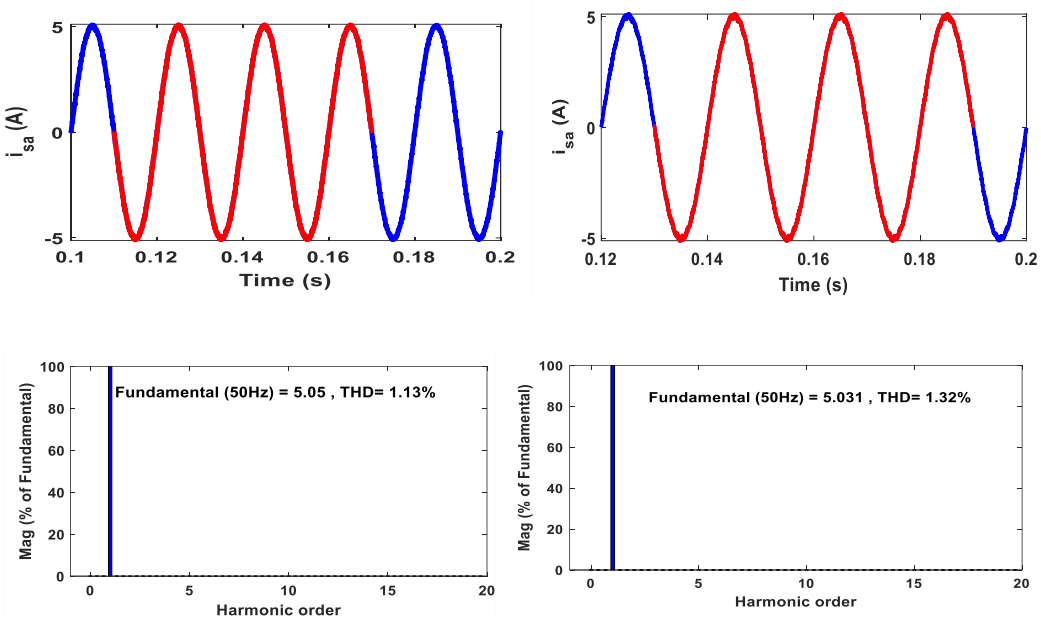

(a) **(b)**

Figure. IV.23 Source current THD at G=0 W/m2 with filtering and no PV system: (a) TOSMC, (b) PI.

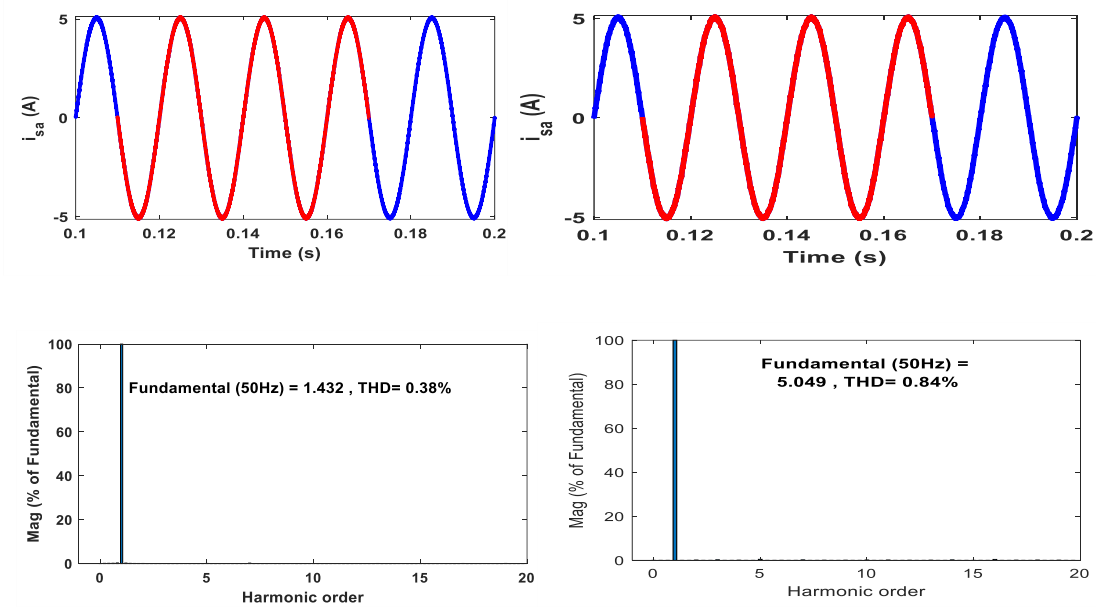

(a) **(b)**

Figure. IV.24 Source current THD at G=1000 W/m2 with filtering and no PV system

The figures (IV.23, IV.24) provide a comparative analysis of the TOSMC and PI filters in reducing Total Harmonic Distortion (THD) under two distinct conditions: without solar irradiance (Figure.IV.23) and with high solar irradiance (Figure.IV.24), both without a PV system. The results consistently show that the TOSMC filter outperforms the PI filter in both

scenarios, achieving a lower THD. Specifically, the TOSMC filter records a THD of 1.13% without solar irradiance, compared to the PI filter's 1.32%. Under high solar irradiance, the performance of both filters improves, with the TOSMC filter further reducing the THD to 0.38%, which is significantly better than the PI filter's 0.83%. This demonstrates the superior effectiveness and adaptability of the TOSMC filter in maintaining a cleaner current waveform under varying environmental conditions.

Table IV. 1 Comparative Analysis of Control Strategies

Case / Controller	THD Before Filtering (%)	THD After Filtering (%)	Response Time (s)	Power Factor	Remarks
PI Controller	27.51	0.70	0.3	0.97	Slight overshoot in transient; slower harmonic suppression
TOSMC Controller	27.51	0.27	0.19	0.99	Fast response; better THD reduction; robust to load changes

The results in Table IV.1 clearly demonstrate the superior performance of the proposed TOSMC strategy compared to the conventional PI controller. Both methods achieve a significant reduction in THD; however, TOSMC achieves a lower final THD (0.27%) compared to PI (0.70%), indicating better harmonic suppression. Additionally, TOSMC exhibits faster transient response and maintains stable power factor close to unity under varying load conditions, while the PI controller shows slower adaptation and slightly higher steady-state error in reactive power compensation.

IV.4 Conclusion

In this chapter, a Third-Order Sliding Mode Control (TOSMC) strategy was proposed and implemented for the control of a three-level NPC-based shunt active power filter integrated with a grid-connected photovoltaic (PV) system. The TOSMC was applied both to the MPPT of the PV generator and to the current control of the active power filter through a Direct Current

Control–PWM scheme. Simulation results were obtained under various operating conditions, including load changes, to evaluate the performance of the proposed control method.

The obtained results demonstrate that the TOSMC strategy offers a significant improvement in dynamic response, harmonic mitigation, and robustness compared to the conventional Proportional–Integral (PI) controller. In particular, TOSMC achieved lower total harmonic distortion (THD), maintained a power factor close to unity, and provided stable operation despite variations in load and irradiance. Furthermore, the PV system under TOSMC control successfully tracked the maximum power point with high precision, ensuring optimal energy extraction.

Overall, the integration of TOSMC with the multilevel shunt active power filter and PV system proves to be an effective solution for enhancing power quality and improving system resilience against disturbances. The comparative analysis confirms that the proposed approach surpasses traditional PI-based control in terms of accuracy, speed, and robustness, making it a promising candidate for advanced power quality applications.

General Conclusion

This thesis has addressed the critical problem of power quality deterioration in electrical networks caused by nonlinear loads, which generate harmonic currents, reactive power demand, and voltage distortions. To overcome the limitations of classical passive solutions, we proposed and developed an advanced framework based on parallel active power filters (APFs) employing the three-level NPC multilevel inverter and controlled through modern sliding mode techniques, while also integrating photovoltaic (PV) generation as a renewable energy source.

The first part of this work reviewed the concepts of power quality, sources of disturbances, and filtering solutions, highlighting the superiority of active filtering in terms of flexibility and adaptability. The second part was dedicated to the modeling of the NPC-based APF, where the power stage and current identification stage were developed, with the Direct Current Control (DCC) method implemented for accurate harmonic current extraction. The third part examined the photovoltaic system, including the PV generator modeling, boost converter, and various MPPT strategies, underlining the importance of renewable integration in modern power systems. Finally, the fourth part introduced advanced sliding mode control, specifically the Third-Order Sliding Mode Control (TOSMC), which was applied both to the MPPT of the PV system and to the dynamic current regulation of the active power filter.

Simulation results have confirmed the effectiveness of the proposed approach. The NPC-based active filter demonstrated its capability to significantly reduce harmonic distortion, achieving source current waveforms close to sinusoidal with low Total Harmonic Distortion (THD). The integration of PV generation not only supplied clean active power to the grid but also enhanced the efficiency and sustainability of the system. The adoption of TOSMC ensured robustness against parameter uncertainties, fast response to load changes, and superior performance compared to conventional control methods. Together, these contributions provide a unified solution that ensures harmonic mitigation, reactive power compensation, and stable renewable power injection.

The main contributions of this thesis can be summarized as follows:

- Development and modeling of a parallel active power filter based on a three-level NPC inverter, combining low harmonic distortion with reliable power conversion.
- Implementation of the DCC method for accurate identification of harmonic currents and reactive components.
- Integration of a photovoltaic generator into the APF structure, including MPPT control through advanced strategies.

- Application of Third-Order Sliding Mode Control (TOSMC) for both PV MPPT and APF current regulation, providing robustness and dynamic adaptability.
- Validation of the proposed system through simulation results, demonstrating improvements in harmonic suppression, reactive power compensation, and renewable energy contribution.

Although the obtained results are promising, several perspectives for future research can be identified. Experimental validation on a laboratory prototype would provide further insight into the practical implementation of the proposed system. Additionally, the extension of this work to other multilevel topologies or hybrid filtering structures could enhance efficiency and scalability. Finally, the combination of advanced control with artificial intelligence and machine learning techniques represents a promising direction for further improvement of adaptability and real-time optimization.

In conclusion, this thesis contributes to the development of robust, efficient, and sustainable power systems by combining multilevel active filtering, renewable energy integration, and advanced nonlinear control. It provides a solid basis for further innovations in the field of power electronics and smart grid technologies.

Bibliographic references

Bibliographic references

[1]. Bollen, M. H. (2000). Understanding power quality problems (Vol. 3). New York: IEEE press.

[2]. Alali, M. A. E. (2002). Contribution à l'Etude des Compensateurs Actifs des Réseaux Electriques Basse Tension:(Automatisation des systèmes de puissance électriques) (Doctoral dissertation, Université Louis Pasteur (Strasbourg)(1971-2008)).

[3]. Klein, J., & Trentin, A. (2020). "Analysis of Voltage Sag Duration and its Effects on Electrical Equipment." IEEE Transactions on Industry Applications, 56(3), 2844-2852.

[4]. Mishra, M. (2019). Power quality disturbance detection and classification using signal processing and soft computing techniques: A comprehensive review. International transactions on electrical energy systems, 29(8), e12008.

[5]. Bajaj, M., & Singh, A. K. (2020). Grid integrated renewable DG systems: A review of power quality challenges and state-of-the-art mitigation techniques. International Journal of Energy Research, 44(1), 26-69.

[6]. Memon, A. A., Koondhar, M. A., Al-Gahtani, S. F., Elbarbary, Z. M. S., & Alaas, Z. M. (2025). Comprehensive review of power quality disturbance detection and classification techniques. Computers and Electrical Engineering, 126, 110512.

[7]. Martinez, R., Castro, P., Arroyo, A., Manana, M., Galan, N., Moreno, F. S., ... & Laso, A. (2022). Techniques to locate the origin of power quality disturbances in a power system: a review. Sustainability, 14(12), 7428.

[8]. Caicedo, J. E., Agudelo-Martínez, D., Rivas-Trujillo, E., & Meyer, J. (2023). A systematic review of real-time detection and classification of power quality disturbances. Protection and Control of Modern Power Systems, 8(1), 1-37.

[9]. Oubrahim, Z., Amirat, Y., Benbouzid, M., & Ouassaid, M. (2023). Power quality disturbances characterization using signal processing and pattern recognition techniques: a comprehensive review. Energies, 16(6), 2685.

[10]. Sankaran, C. (2017). Power quality. CRC press.

[11]. Gundebommu, S. L., Hunko, I., Rubanenko, O., & Kuchanskyy, V. (2020, May). Assessment of the power quality in electric networks with wind power plants. In 2020 IEEE 7th International Conference on Energy Smart Systems (ESS) (pp. 190-194). IEEE.

[12]. Volokhin, V. V., Diahovchenko, I. M., & Derevyanko, B. V. (2017, October). Electric energy accounting and power quality in electric networks with photovoltaic power stations. In 2017 IEEE International Young Scientists Forum on Applied Physics and Engineering (YSF) (pp. 36-39). IEEE.

[13]. Khadkikar, V. (2011). Enhancing electric power quality using UPQC: A comprehensive overview. IEEE transactions on Power Electronics, 27(5), 2284-2297.

[14]. Biryulin, V. I., Kudelina, D. V., & Larin, O. M. (2020, May). Electricity quality problems in the 0.4 kV city electric networks. In 2020 International Conference on Industrial Engineering, Applications and Manufacturing (ICIEAM) (pp. 1-6). IEEE.

[15]. Afonso, J. L., Tanta, M., Pinto, J. G. O., Monteiro, L. F., Machado, L., Sousa, T. J., & Monteiro,V. (2021). A review on power electronics technologies for power quality improvement. Energies, 14(24), 8585.

[16]. BOUHOUTA Ahmed (2022) « Amélioration de la Qualité de l'Énergie Électrique Par des Convertisseurs Statiques Associés Aux Générateurs Photovoltaïques » THÈSE DE DOCTORAT

[17]. Zelloma, Laid (2006) « Filtrage actif parallèle du courant généré par un pont redresseur triphasé non commandé », Thèse de magistère, Département de l'électrotechnique, Université de Annaba.

[18]. H. Sasaki, T. Machida. (1970), A New Method to Elim-inate AC Harmonic by Magnetic Compensation-Considerations on Basic Design, IEEE Trans.on Power Ap-paratus and Syst., vol.90, no.5, pp.2009-2019.

[19]. Schneider Electric (2001)"Guide de la compensation d'énergie réactive et du filtrage des harmoniques" Guides experts basse tension N° 6.

[20]. Schneider Electric (2010)"Guide de l'installation électrique".

[21]. B. SINGH, K. AL-HADDAD et A. CHANDRA, 1999 « A review of active filters for power amélioration de la qualité », Industrial Electronics, IEEE Transactions on, vol. 46, p. 960–971,

[22]. B. Singh and V. Verma. (2006) "An indirect current control of hybrid power filter for varying loads" IEEE Trans. Power Del., Vol. 21, No. 1, pp.178-184.

[23]. Chennai.Salim, (2013). « Etude, Modélisation et Commande des filtres actifs : Apport des techniques de l'intelligence artificielle ». Doctorat en sciences, Université du Biskra,

[24]. Abdelmadjid Chaoui(2010)" Filtrage actif triphasé pour charges non linéaires "Thèse de docteur de l'Université de Poitiers,.

[25]. Compatibility, E. (2002). Electromagnetic Compatibility (EMC)—Part 2–4: Environment—Compatibility Levels in Industrial Plants for Low-Frequency Conducted Disturbances. IEC Standard, 61000-2.

[26]. Mukherjee, S., Saxena, N., & Sharma, A. K. (2014). Power system harmonic compensation using shunt active power filter. Int. Int. Journal of Engineering Research and Applications, 4(7), 60-63.

[27]. Bouhouta, A., Moulahoum, S., Kabache, N., & Colak, I. (2018, October). Simplicity and performance of direct current control dcc compared with other identification algorithms for shunt active power filter. In 2018 7th International Conference on Renewable Energy Research and Applications (ICRERA) (pp. 1352-1357). IEEE.

[28]. Bouhouta, A., Moulahoum, S., Kabache, N., & Colak, I. (2019, November). Experimental investigation of fuzzy logic controller based indirect current control algorithm for shunt active power filter. In 2019 8th International Conference on Renewable Energy Research and Applications (ICRERA) (pp. 309-314). IEEE.

[29]. Bouhouta, A., Moulahoum, S., & Kabache, N. (2022). A novel combined Fuzzy-M5P model tree control applied to grid-tied PV system with power quality consideration. Energy Sources, Part A: Recovery, Utilization, and Environmental Effects, 44(2), 3125-3147.

[30]. Bouhouta, A., Moulahoum, S., Kabache, N., Moualdia, A., & Colak, I. (2023, June). Harmonics compensation of grid-connected PV systems using a novel M5P model tree control. In 2023 11th International Conference on Smart Grid (icSmartGrid) (pp. 1-6). IEEE.

[31]. Bouhouta, A., Moulahoum, S., Kabache, N., & Benyamina, A. (2019, November). Design and real time implementation of three phase shunt active power filter using indirect current control technique. In 2019 International Conference on Advanced Electrical Engineering (ICAEE) (pp. 1-6). IEEE.

[32]. Bouhouta, A., Moulahoum, S., & Kabache, N. (2022). Harmonic Mitigation in Utility Grid with Highly Unbalanced Nonlinear Load Using Intelligent Controller: an Experimental Study. Przeglad Elektrotechniczny, 98(4).

[33]. Bouhouta, A., Moulahoum, S., & Kabache, N. (2022). Hybrid backup energy based on PV/Wind system for marine tugboat: A case study of ASD tug of Arzew port in Algeria. Wind Engineering, 46(5), 1343-1358.

[34]. Ahmed, M., Harbi, I., Kennel, R., Heldwein, M. L., Rodríguez, J., & Abdelrahem, M. (2022). Performance Evaluation of PV Model-Based Maximum Power Point Tracking Techniques. Electronics, 11(16), 2563.

[35]. Ahmed, M., Abdelrahem, M., & Kennel, R. (2020). Highly efficient and robust grid connected photovoltaic system based model predictive control with kalman filtering capability. Sustainability, 12(11), 4542.

[36]. Estévez-Bén, A. A., Alvarez-Diazcomas, A., & Rodríguez-Reséndiz, J. (2020). Transformerless multilevel voltage-source inverter topology comparative study for PV systems. Energies, 13(12), 3261.

[37]. Mosaad, M. I. (2022). Grid-Connected PV System Statistics and Evaluation; Review. Yanbu Journal of Engineering and Science, 19(1), 1-10.

[38]. Debdouche, N., Deffaf, B., Benbouhenni, H., Laid, Z., & Mosaad, M. I. (2023). Direct power control for three-level multifunctional voltage source inverter of PV systems using a simplified super-twisting algorithm. Energies, 16(10), 4103.

[39]. Rafikiran, S., Basha, C. H., & Dhanamjayulu, C. (2024). A Novel Hybrid MPPT Controller for PEMFC Fed High Step-Up Single Switch DC-DC Converter. International Transactions on Electrical Energy Systems, 2024, 1-25.

[40]. Verma, D.; Nema, S.; Agrawal, R.; Sawle, Y.; Kumar, A. A Different Approach for Maximum Power Point Tracking (MPPT) Using Impedance Matching through Non-Isolated DC-DC Converters in Solar Photovoltaic Systems. Electronics 2022, 11, 1053.

[41]. Zaghba, L., Borni, A., Benbiotur, M. K., Fezzani, A., Alwabli, A., Bajaj, M., ... & Ghoneim, S. S. (2024). Enhancing grid-connected photovoltaic system performance with novel hybrid MPPT technique in variable atmospheric conditions. Scientific Reports, 14(1), 8205.

[42]. Şeker, M., Tan, T., & Turan, S. M. (2024). Experimental Analysis of Perturb&Observe and Incremental Conductance Algorithms for Maximum Power Point Tracking in Photovoltaic Systems. European Journal of Science and Technology, (53), 140-149.

[43]. Hussaian Basha, C., Palati, M., Dhanamjayulu, C., Muyeen, S. M. & Venkatareddy, P. A novel on design and implementation of hybrid MPPT controllers for solar PV systems under various partial shading conditions. Sci. Rep. 14, 1609. https://doi.org/10. 1038/s41598-023-49278-9 (2024).

[44]. Nguyen-Duc, T.; Le-Viet, T.; Nguyen-Dang, D.; Dao-Quang, T.; Bui-Quang, M. Photovoltaic Array Reconfiguration under Partial Shading Conditions Based on Short-Circuit Current Estimated by Convolutional Neural Network. Energies 2022, 15, 6341.

[45]. Marroquín-Arreola, R.; Lezama, J.; Hernández-De León, H.R.; Martínez-Romo, J.C.; Hoyo-Montaño, J.A.; Camas-Anzueto, J.L.; Escobar-Gómez, E.N.; Conde-Díaz, J.E.; Ponce-Silva, M.; Santos-Ruiz, I. Design of an MPPT Technique for the Indirect Measurement of the Open-Circuit Voltage Applied to Thermoelectric Generators. Energies 2022, 15, 3833.

[46]. Mosaad, M.I.; Osama abed el-Raouf, M.; Al-Ahmar, M.A.; Banakher, F.A. Maximum Power Point Tracking of PV system Based Cuckoo Search Algorithm; review and comparison. Energy Procedia 2019, 162, 117–126.

[47]. Meddour, S., Rahem, D., Cherif, A. Y., Hachelf, W. & Hichem, L(2019)" A novel approach for PV system based on metaheuristic algorithm connected to the grid using FS-MPC controller." Energy Procedia 162, 57–66. https://doi.org/10.1016/j.egypro.2019.04.007.

[48]. Baishya, C., Naik, M. K., & Premakumari, R. N. (2024). Design and implementation of a sliding mode controller and adaptive sliding mode controller for a novel fractional chaotic class of equations. Results in Control and Optimization, 14, 100338.

[49]. Lin, B., Zheng, M., Han, B., Chu, X., Zhang, M., Zhou, H., ... & Zhang, K. (2024). PSO-Based Predictive PID-Backstepping Controller Design for the Course-Keeping of Ships. Journal of Marine Science and Engineering, 12(2), 202.

[50]. González-Hernández, I., Salazar, S., Lozano, R., & Ramírez-Ayala, O. (2022). Real-time improvement of a trajectory-tracking control based on super-twisting algorithm for a quadrotor aircraft. Drones, 6(2), 36.

[51]. Salameh, T., Hamid, A. K., Farag, M. M., & Abo-Zahhad, E. M. (2023). Energy and exergy assessment for a University of Sharjah's PV grid-connected system based on experimental for harsh terrestrial conditions. Energy Reports, 9, 345-353.

[52]. Manna, S., Singh, D. K., Alsharif, M. H., & Kim, M. K. (2024). Enhanced MPPT approach for grid-integrated solar PV system: Simulation and experimental study. Energy Reports, 12, 3323-3340.

[53]. Shaikh, S., Soomar, A. M., Ullah, K., Ismail, E. A., Awwad, F. A., Kamran, M., ... & Shah, S. H. H. (2024). Modified sliding mode control for seamless integration of PV energy in AC grid. Energy Reports, 12, 673-686. https://doi.org/10.1016/j.egyr.2024.06.062

[54]. Azmi, S. A., Adam, G. P., Williams, B. W., Rahim, N. A., & Rahim, S. R. A. (2023). Grid integration of multiple PV inverters with reduced number of interfacing transformers—A dedicated controller for elimination of DC current injection. Energy Reports, 9, 904-911.

[55]. Bouhadji, F., Bouyakoub, I., Mehedi, F., Kacemi, W. M., & Reguieg, Z. (2024). Optimization of grid power quality using third order sliding mode controller in PV systems with multilevel inverter. Energy Reports, 12, 5177-5193.

[56]. Hussein, I., Çelik, Ö., & Teke, A. (2022). A hybrid random parameters modification to MPPT algorithm to mitigate interharmonics from single-phase grid-connected PV systems. Energy Reports, 8, 6234-6244. https://doi.org/10.1016/j.egyr.2022.04.062

[57]. Fawzy, I. Y., Mossa, M. A., Elsawy, A. M., Suwarno, I., & Diab, A. A. Z. (2024). Deployment of STATCOM with Fuzzy Logic Control for Improving the Performance of Power System under Different Faults Conditions. Journal of Robotics and Control (JRC), 5(3), 636-646.

[58]. Baek, J., & Chen, J. S. (2024). A neural network-based enrichment of reproducing kernel approximation for modeling brittle fracture. Computer Methods in Applied Mechanics and Engineering, 419, 116590.

[59]. Samuel, O. D., Okwu, M. O., Varatharajulu, M., Eseoghene, I. D., & Fayaz, H. (2024). Adaptive neuro-fuzzy inference system for forecasting corrosion rates of automotive parts in biodiesel environment. Heliyon, 10(5).

[60]. Kihal, A., Krim, F., Talbi, B., Laib, A., & Sahli, A. (2018). A robust control of two-stage grid-tied PV systems employing integral sliding mode theory. Energies, 11(10), 2791.

[61]. Imam, A.A.; Sreerama Kumar, R.; Al-Turki, Y.A. 2020 “Modeling and Simulation of a PI Controlled Shunt Active Power Filter for Power Quality Enhancement Based on P-Q Theory.” Electronics, 9, 637.

[62]. Bouhouta, A., Moulahoum, S., Kabache, N., & Colak, I. (2018, October). Simplicity and performance of direct current control dcc compared with other identification algorithms for shunt active power filter. In 2018 7th International Conference on Renewable Energy Research and Applications (ICRERA) (pp. 1352-1357). IEEE.

[63]. Reguieg, Z., Bouyakoub, I., Mehedi, F., & Bouhadji, F. (2024). Optimizing power quality: simulation of UPQC integrated PV with comprehensive reliability and performance analysis. International Journal of Smart Grid, 8(1), 47-52..

[64]. Hoon, Y.; Mohd Radzi, M.A.; Mohd Zainuri, M.A.A.; Zawawi, M.A.M. Shunt Active Power Filter: A Review on Phase Synchronization Control Techniques. Electronics 2019, 8, 791.

[65]. Nyamathulla, S.; Chittathuru, D.; Muyeen, S.M. An Overview of Multilevel Inverters Lifetime Assessment for Grid-Connected Solar Photovoltaic Applications. Electronics 2023, 12, 1944.

[66]. Reguieg, Z., Bouyakoub, I., Mehedi, F., & Bouhadji, F. (2024, May). Enhancing electrical grid stability through power quality optimization via PV-PO-UPQC: An integrated approach. In 2024 2nd International Conference on Electrical Engineering and Automatic Control (ICEEAC) (pp. 1-7). IEEE. Wang, K., Wu, M., Zheng, Z., Pou, J., Rodríguez, J., Li, Y. W., & Li, Y. (2024). A Generalized Derivation Method of Tree-Type Active Neutral-Point-Clamped Multilevel Topologies. IEEE Transactions on Power Electronics.

[67]. Mullali Kunnontakath Puthiyapurayil, M. R., Nadir Nasirudeen, M., Saywan, Y. A., Ahmad, M. W., & Malik, H. (2022). A review of open-circuit switch fault diagnostic methods for neutral point clamped inverter. Electronics, 11(19), 3169.

[68]. Lee, J.S.; Kwak, R.; Lee, K.B. 2018 "Novel discontinuous PWM method for a single-phase three-level neutral point clamped inverter with efficiency improvement and harmonic reduction. IEEE Trans. Power Electron., 33, 9253–9266.

[69]. Reguieg, Z., Bouyakoub, I., Mehedi, F., & Bouhadji, F. (2024). Robust harmonic elimination method for various load conditions. Journal of Renewable Energies, 73-84.

[70]. Kadri, R.; Gaubert, J.-P.; Champenois, G. An improved maximum power point tracking for photovoltaic grid-connected inverter based on voltage-oriented control. IEEE Trans. Ind. Electron. 2011, 58, 66–75.

[71]. Bhatti, M.Z.A.; Siddique, A.; Aslam, W.; Atiq, S.; Khan, H.S. Improved model predictive direct power control for parallel distributed generation in grid-tied microgrids. Energies 2023, 16, 1441.

[72]. Bouhouta, A., Moulahoum, S., & Kabache, N. (2022). Harmonic Mitigation in Utility Grid with Highly Unbalanced Nonlinear Load Using Intelligent Controller: an Experimental Study. Przeglad Elektrotechniczny, 98(4).

[73]. Chen, D., Xu, Z., Xiao, L., Yan, W., & Guo, Y. (2022). A direct current control strategy based on vector resonance controller for shunt active power filter. Energy Reports, 8, 122-130.

[74]. M. Adel,T. Kandil, (2021) "Assessment of Direct and Indirect Current Control Techniques Applied to Active Power Filters," Recent Advances in Electrical & Electronic Engineering, Vol. 13, No. 8, pp. 1256– 1265.

[75]. Ouchen, S., Benbouzid, M., Blaabjerg, F., Betka, A., & Steinhart, H. (2020). Direct power control of shunt active power filter using space vector modulation based on supertwisting sliding mode control. IEEE Journal of Emerging and Selected Topics in Power Electronics, 9(3), 3243-3253.

[76]. Ouchen, S., Steinhart, H., Blaabjerg, F., Benbouzid, M., Betka, A., & Gaubert, J. P. (2019, October). Performance analysis of direct power control with space vector modulation for shunt active power filter. In IECON 2019-45th Annual Conference of the IEEE Industrial Electronics Society (Vol. 1, pp. 467-472). IEEE.

[77]. Benbouhenni, H., Bizon, N., 2021. Third-order sliding mode applied to the direct field-oriented control of the asynchronous generator for variablespeed contra-rotating wind turbine generation systems. Energies 14, 5877.

[78]. Akbari, E., & Seyyedi, A. Z. G. (2023). Power quality enhancement of distribution grid using a photovoltaic based hybrid active power filter with three level converter. Energy Reports, 9, 5432-5448.

[79]. Debdouche, N., Zarour, L., Chebabhi, A., Deffaf, B., & Ouchen, S. (2022, October). Super Twisting Sliding Mode Direct Power Control of SAPF with Space Vector Modulation for Power Quality improvement. In 2022 2nd International Conference on Advanced Electrical Engineering (ICAEE) (pp. 1-6). IEEE.

[80]. Boujmil, M. H., Badis, A., & Nejib Mansouri, M. (2018). Nonlinear robust backstepping control for three-phase grid-connected PV systems. Mathematical Problems in Engineering, 2018(1), 3824628.

[81]. Kadem, M., Semmah, A., Wira, P., & Dahmani, S. (2020). Fuzzy logic-based instantaneous power ripple minimization for direct power control applied in a shunt active power filter. Electrical Engineering, 102(3), 1327-1338.

[82]. Govindharaj, A., Mariappan, A., Ambikapathy, A., Bhadoria, V.S., Alhelou, H.H., 2021. Real-time implementation of adaptive neuro backstepping controller for maximum power point tracking in photo voltaic systems. IEEE Access 9, 105859–105875.

[83]. Ahmed, M., Abdelrahem, M., & Kennel, R. (2020). Highly efficient and robust grid connected photovoltaic system based model predictive control with kalman filtering capability. Sustainability, 12(11), 4542.

[84]. Gursoy, M., Zhuo, G., Lozowski, A. G., & Wang, X. (2021). Photovoltaic energy conversion systems with sliding mode control. Energies, 14(19), 6071.

[85]. Khan, R., Khan, L., Ullah, S., Sami, I., Ro, J.-S., (2020). Backstepping based super-twisting sliding mode MPPT control with differential flatness oriented observer design for photovoltaic system. Electronics 9, 1543.

[86]. Maaruf, M., Khan, K., & Khalid, M. (2022). Robust control for optimized islanded and grid-connected operation of solar/wind/battery hybrid energy. Sustainability, 14(9), 5673.

[87]. Seyedmahmoudian, M., Rahmani, R., Mekhilef, S., Maung Than Oo, A., Stojcevski, A., Soon, T.K., Ghandhari, A.S., 2015. Simulation and hardware implementation of new maximum power point tracking technique for partially shaded PV system using hybrid DEPSO method. IEEE Trans. Sustain. Energy 6, 850–862.

[88]. Walid, K., Sofiane, M., Benbouhenni, H., Hamza, G., Es-saadi, T., 2023. Application of third-order sliding mode controller to improve the maximum power point for the photovoltaic system (December). Energy Rep. 9, 5372–5383.

[89]. Debdouche, N., Zarour, L., Chebabhi, A., Bessous, N., Benbouhenni, H., Colak, I., 2023c. Genetic algorithm-super-twisting technique for grid-connected PV system associate with filter. Energy Rep. 10, 4231–4252.

[90]. Debdouche, N., Zarour, L., Benbouhenni, H., Mehazzem, F., Deffaf, B., 2023d. Robust integral backstepping control microgrid connected photovoltaic System with battery energy storage through

multi-functional voltage source inverter using direct power control SVM strategies. Energy Rep. 10, 565–580.

[91]. Hoon, Y., Mohd Radzi, M. A., Hassan, M. K., & Mailah, N. F. (2017). Control algorithms of shunt active power filter for harmonics mitigation: A review. Energies, 10(12), 2038.

[92]. C. Khomsi, M. Bouzid, K. Jelassi, "Power Quality Improvement in a Three-Phase Grid Tied Photovoltaic System Supplying Unbalanced and Non-Linera Loads," International Journal Of Renewable Energy Research (IJRER), Vol.8, No.2, June,2018.

[93]. Govind, A., Jayaswal, K., Tayal, V. K., & Kumar, P. (2024). Simulation and real time implementation of shunt active power filter for power quality enhancement using adaptive neural network topology. Electric Power Systems Research, 228, 110042

[94]. Popescu, M., Bitoleanu, A., Suru, C. V., Linca, M., & Subtirelu, G. E. (2020). Adaptive control of DC voltage in three-phase three-wire shunt active power filters systems. Energies, 13(12), 3147.

[95]. Rahman, N. A., Nasir, N. M., & Baharom, R. (2019, July). Comparative Study of Direct and Indirect Current Control Algorithms for Shunt Active Power Filter. In 2019 International Conference on Electrical Engineering and Informatics (ICEEI) (pp. 324-329). IEEE.

[96]. Alahmad, A., Kaçar, F., Farsakoğlu, Ö. F., & Uzunoğlu, C. P. (2023, March). Medium-voltage drives (MVD)-pulse width modulation (PWM) techniques. In 2023 Second International Conference on Electronics and Renewable Systems (ICEARS) (pp. 91-94). IEEE.

[97]. Maklakov, A. S., & Erdakov, I. N. (2023). Study of Behavior of Voltage and Current Spectra of Three-Level Neutral Point Clamped Converter at Selected Harmonic Elimination Programmed Pulse Pattern Pulse-Width Modulation. Energies, 16(13), 5183.

[98]. Mohiuddin, M., Maricar, N., Kadir, K. A., Roslan, N. F., Islam, M., Khan, S., & Aboadla, E. H. (2023). Mitigation of Harmonics Using Novel Sector-Based Switching Pattern Space Vector Pulse Width Modulation. IEEE Access, 11, 51465-51479.

[99]. Eroğlu, F., & Kurtoğlu, M. (2023). Trapezoidal reference-based single carrier pulse width modulation method for multilevel converters with novel FPGA implementation. Computers and Electrical Engineering, 107, 108650.

[100]. Naamane, D., Laid, Z., & Fateh, M. (2023). Power quality improvement based on third-order sliding mode direct power control of microgrid-connected photovoltaic system with battery storage and nonlinear load. Iranian Journal of Science and Technology, Transactions of Electrical Engineering, 47(4), 1473-1490.

[101]. Boiko, I., Fridman, L., Pisano, A., Usai, E., 2007. Analysis of chattering in systems with second-order sliding modes. IEEE Trans. Automat. Control 52, 2085–2102.

[102]. Gasmi, H., Mendaci, S., Laifa, S., Kantas, W., Benbouhenni, H., 2022. Fractionalorder proportional-integral super twisting sliding mode controller for wind energy conversion system equipped with doubly fed induction generator. J. Power Electron. 22 (8), 1–17

[103]. Kchaou, A., Naamane, A., Koubaa, Y., M'sirdi, N., 2017. Second order sliding mode-based MPPT control for photovoltaic applications. Sol. Energy 155, 758–769

[104]. Debdouche, N., Chebabhi, A., Ouchen, S., & Zarour, L. (2022, May). Direct power control of three-level SAPF with space vector modulation for power quality improvement. In 2022 19th International Multi-Conference on Systems, Signals & Devices (SSD) (pp. 103-108). IEEE.

[105]. Koganti, S., Koganti, K. J., & Salkuti, S. R. (2022). Design of multi-objective-based artificial intelligence controller for wind/battery-connected shunt active power filter. Algorithms, 15(8), 256.

[106]. Asadi, Y., Eskandari, M., Mansouri, M., Chaharmahali, S., Moradi, M. H., & Tahriri, M. S. (2022). Adaptive neural network for a stabilizing shunt active power filter in distorted weak grids. Applied Sciences, 12(16), 8060.

[107]. Nikkhah Kashani, H., Rouhi Ardeshiri, R., Gheisarnejad, M., & Khooban, M. H. (2022). Optimal cascade non-integer controller for shunt active power filter: real-time implementation. Designs, 6(2), 32.

[108]. Gao, H., Zhang, W., Ren, M., & Liu, X. (2022). Three-level active power filter based on model predictive control. Electronics, 11(9), 1291.

[109]. Musa, S., Mohd Radzi, M. A., Hizam, H., Abdul Wahab, N. I., Hoon, Y., & Mohd Zainuri, M. A. A. (2017). Modified synchronous reference frame based shunt active power filter with fuzzy logic control pulse width modulation inverter. Energies, 10(6), 758.

[110]. Mohamed Cherif Daia Eddine Oussama ,2025 « Commandes Avancées Des Systèmes Photovoltaïques Dédiées A L'amélioration De La Qualité De L'énergie Dans Les Réseaux Electriques » Doctoral thesis from the University of Mohamed El Bachir El Ibrahimi de Bordj Bou Arréridj.

[111]. Senouci Meriem ,2025 « Intégration des énergies renouvelables dispersées dans les réseaux électriques de distribution » Doctoral thesis from the University of Mohamed Boudiaf.

[112]. Rokaia Sh. Habeeb Al-Joubori ,2001« Tuning of Fuzzy Logic Controller Using Genetic Algorithms" Doctoral thesis from the University of Al-Mustansiriyah University.

[113]. Adel DAHDOUH ,2024 "Contribution to the Study and Control of the Multilevel PVG-UPQC System for Power Quality Improvement" Doctoral thesis from the University of Ziane Achour Djelfa.

[114]. Rabia BEHLOUL , 2025 "Contribution to the intelligent control of a wind conversion chain" Doctoral thesis from the University of Ziane Achour Djelfa.

[115]. SLAMA Fateh,2012« Modélisation d'un système multi générateurs photovoltaïques interconnectés au réseau électrique » Doctoral Magister from the University FERHAT ABBAS - SETIF.

[116]. MABROUK Younes Abdelbadie, 2025 « Contribution à l'Analyse Harmonique d'une Commande DTC Appliquée à un MAS Alimenté par Onduleur Multiniveau » Doctoral thesis from the University of Amar Telidji de Laghouat.

[117]. Boutouta Fatima , 2025 "Control Technique Development for Inverters Used in Grid Connected Applications" Doctoral thesis from the University of Ziane Achour Djelfa.

[118]. Zoubida AMRANI, 2025 “Advanced Control of Grid-Connected Photovoltaic Generation Systems” Doctoral thesis from the University of Ziane Achour Djelfa.

[119]. Zakaria LAALA , 2024 « Contribution à l'amélioration de la qualité d'énergie dans les systèmes électriques embarqués » Doctoral thesis from the University of Ziane Achour Djelfa.

[120]. CHEBABHI Ali , 2015“Contribution à la dépollution harmonique et à la compensation de l’énergie réactive par l’étude et la commande avancée de filtres actifs parallèles.” Doctoral thesis from the University of Djillali Liabes Sidi-Bel-Abbes.

[121]. Tidjani MAHNI , 2017 « Étude et conception d'un filtre actif parallèleTriphasé quatre fils en vue de sa commande par des méthodes d'intelligence artificielle » Doctoral thesis from the University of Mohamed Khider Biskra.

[122]. ELBAR Mohamed , 2022 “Power Quality Enhancement Techniques In Smart Grid” Doctoral thesis from the University of Ziane Achour Djelfa.

[123]. Sana OTHMAN ,2021 « Modélisation et commande à base d’une représentation par réseau de Pétri d’un filtre actif parallèle avec un onduleur multicellulaire série » Doctoral thesis from the University of L’École Nationale d’Ingénieurs de Gabès.

Annexes

Table 1 Simulation Parameters

Characteristic	Value
Voltage and frequency at grid	230V, 50Hz
Impedance of coupling Rf, L f	0.1 mΩ, 3.5mH
Impedance of the source Rs, Ls	0.1 Ω, 0.1mH
impedance to load R_d, L_d	70 Ω, 4mH
Impedance of line RL, LL	0.1 mΩ, 2mH
DC bus capacitors total C_{dc}	12μF
Reference for the total DC bus voltage	773V
Maximum Power Pmp	150 Watt
Open circuit voltage V_{oc}	43.6 V
Voltage at maximum power point V_{mp}	34.6 V
Short-circuit current Isc	4.76 A
Current at maximum power point Imp	4.36 A
PV panel series number (Ns)	20
PV panel parallel number (Np)	5
Photovoltaic capacitor C_{PV}	470 μF
Inductor boost L	10mH

Table 2 Control Gain Values Used in This Work

Controller	PI Parameters	TOSMC Parameters
DCC-PWM	Kp= 15 Ki=100	λ_a=2 λ_b=50 λ_c=100
PV	Kp= 0.5 Ki=50	λ_{pv1}=0.1707 λ_{pv2}=0.0426 λ_{pv3}=0.3303
DC-Link voltage	Kp= 5 Ki=15	λ_{vdc1}= 110 λ_{vdc2} = 305 λ_{vdc3}= 200

Simulink Blocks for Harmonic Identification Using DCC

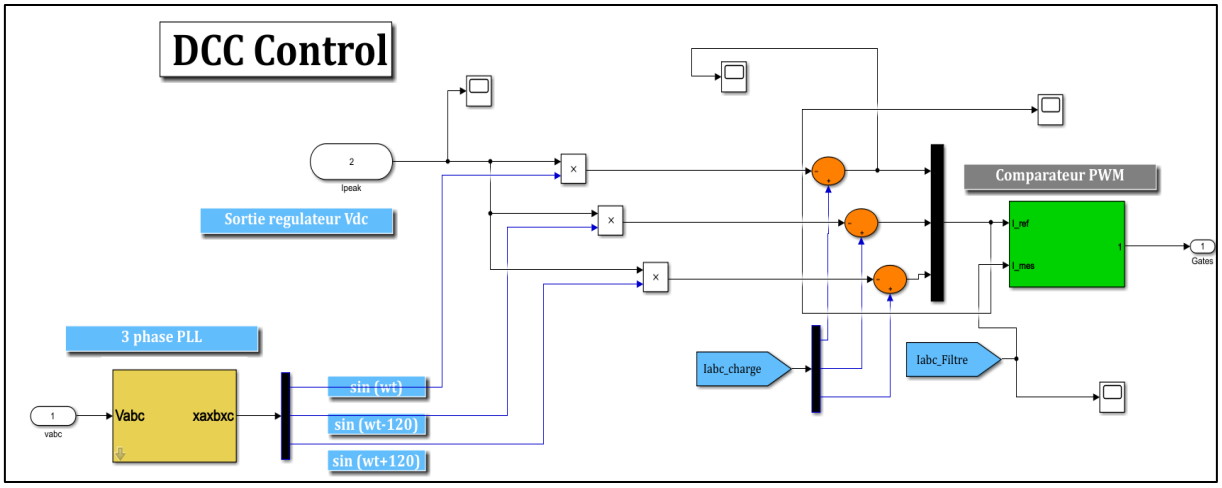

MATLAB/Simulink block of the DCC method


الحمد لله
الذي بنعمته تتم الصالحات